Bio-molecular impedance biosensing in Nanofluidic devices

Thesis submitted to the school of Chemical and Physical Sciences,

Faculty of Science and Engineering, The Flinders University of South Australia,

in partial fulfillment of the requirements for the degree of

Doctor of Philosophy

May 2014

Krishna Kant

Supervisors:

Prof. Joseph G. Shapter, Prof. Dusan Losic and Dr. Craig Priest

Table of Contents

List of Figures

Chapter 1

Chapter 3

Chapter 4

Chapter 5

Chapter 6

Chapter 7

Chapter 8

List of Tables

Abstract

A small chip for biomedical analysis connected to our home computer or smart mobile, which would be capable of diagnosing illnesses, a lack of vitamins, or the over-presence of substances from samples of blood, urine or saliva would be a great advance. Such a system could give advice to the user about the optimal medicines to take or provide information to a specialist for effective treatment. Of course this system will take some time to develop but this thesis aims to provide some key understandings to help make such systems a reality and bring some new biosensing elements to this exciting project by investigating the molecular sensing of proteins in well-defined nanometer-sized confined areas. The understanding of molecular dynamics in nano-confined volumes is fundamental for designing the appropriate lab-on-a-chip devices able to transport and sense biomolecules. However, the advantages and problems occurring at the nanoscale are still to be discovered and currently, there is a lack of accurate sensing devices for proteins in nanofluidics. One limitation for performing these studies and biosensing device developments is to have a low-cost and simple nanopore biosensing platform. To address these limitations this thesis focuses on exploration on nanoporous alumina (NPA) with perfectly ordered nanoporous or nanochannels prepared by unique self-ordering electrochemical process with the aim of developing new nanofluidic biosensing platform with new functionalities that are not accessible to microfluidics. Based on measurements performed in 20-70 nm nanochannels, where proteins were binding on the internal surface of the nanochannel and its interactions with antigens were investigated using electrochemical impedance spectroscopy measurements. The size of prepared nanofluidic channels is comparable to the length scale for electrostatic interactions in aqueous solutions

and the binding of proteins in the various dimensions and shape of nanochannels were modeled theoretically and verified experimentally with impedance spectroscopy. As a result of electrostatic interactions, surface charge can govern ionic concentrations in nanofluidic channels. On the other hand, it has been shown that protein charges directly influence the nanochannel conductance giving a better understanding of how the protein's counter-ions modify the surface charges inside the nanochannels. A direct measurement inside the nanochannels has allowed the identification of different systems of interacting proteins, depending on the thickness of the electrical double layer. Due to the small channel size, surface binding of protein and a generated electrostatic conduction effect inside the nanochannel due to the charge of the proteins and ionic strength of the solution have important role in the impedance biosensing. An understanding of the properties and advantages of the nanoporous alumina nanochannels lead to the various other applications including the extraction of DNA and proteins, and measurement of the activities of bacterial nanowires. Finally, a novel microchip biosensing device with an NPA platform is designed and demonstrated for impedance biosensing to measure the changes inside the nanochannel due to the binding of proteins. The results showed that changes in the impedance can indicate target binding and sample surface morphology is responsible for changes in the sensing ability of the developed device.

The work described in this thesis details significant research in the nascent field of nanofluidic biosensing. The work points out novel, important, experimentally-verified complements to define theoretical models as well as practical approach to go forward with the design of complex nanofluidic systems applied to biomedical and biological applications.

Declaration

'I certify that this thesis does not incorporate without acknowledgment any material previously submitted for a degree or diploma in any university; and that to the best of my knowledge and belief it does not contain any material previously published or written by another person except where due reference is made in the text'.

Krishna Kant

Acknowledgements

I have been fortunate to be surrounded by loving people. It is their love, nourishing, help, goodwill and blessings that have given me the strength to forge ahead in life. This research is a milestone that would not have been possible without their support. First of all, I would like to thank Prof. Dusan Losic for being a great advisor and mentor. I came to him as a Master's student and he gave me the opportunity to work with him and come into new realm of nanotechnology. It was in his nano-engineering laboratory that I found a foothold and learned to navigate the landscapes of research. He encouraged me by giving me the freedom to try new ideas and trust my opinions. During my life as a graduate student at Adelaide, I had the opportunity to work with a number of collaborators and all the three Universities in Adelaide, South Australia. I would like to express my gratitude Prof. Joe G. Shapter and Dr. Craig Priest who always been with me not only as supervisors but also as caring people throughout my good and bad times. I am very thankful to them for giving me priority over their busy schedule to help me in each and every aspect of learning. I would like to deeply acknowledge Mr. Len Green at Adelaide Microscopy. Len helped me to learn the FIB instrument which was one of the major parts of my work and we both enjoyed the work and conversations that we had together. I also like the thank Dr. Mahaveer Kurkuri for his help discussion and motivation.

The environment in the Nanotechnology Lab at Adelaide University with Tariq other lab members Tushar, Karan, Shervin, Mohammad, Sheena, Manpreet and Dr. Abel Santos was conducive for exchange of ideas, and chatting sessions covered topics ranging from science philosophy to history and arts. At the end of the day when I went home, I had the support and company of Avishek (*Bondhu*),

Akash (*bhai*), Raj *bhaiya*, Vikram, and Yatin. Living with them was fun and gave me a sense of belonging. Raj (*bhaiya*) become very close to me in very short time and we have many long discussions over weekends. I like to thank him for all the support and encouragement at all times. Yatin was good support in the final year of my PhD and become good friend of mine. I was lucky that I had the company of all these intellectual guys in one place doing PhD and all living at same place. Our diverse personalities, outlooks and areas of work made sure that time spent at home was far from boring! I also like to give my special thanks to Shaurya Badsar and Gurvinder Singh who help me in the starting phase of my life in Adelaide and made me feel at home. At the end I like to thank my dear friend Yogesh who always stood by me and encouraged me. I also made many friends at my hostel as well as work place – Thana, Anirudh, Sophie, Amanda, Ophelia, Cuong and others. I will always cherish the time we spent at Aroma Café or in the office.

My parents, Er. Jai Prakash Yadav and Kunti Yadav who was a constant source of love, encouragement and support during the course of my life with their strength. They shielded me from many worries and at the same time allowed me to express myself and realize my potential. No words are sufficient to thank them here. Finally, I would like to thank The School of Chemical Engineering where I spent many long hours during the work. I also thank all funding sources – Australian Research Council, Inphaze Pty. Ltd. Sydney and Flinders University for financial support to my research work and scholarship.

The source of this life is the Mystery that I do not understand. To that One I owe everything.

Krishna Kant

List of Publications

Invited Book Chapter

1. **K. Kant**, D. Losic, Focused Ion Beam (FIB) technology for micro and nanoscale fabrications Book: "*Lecture notes in Nanoscale Science and Nanotechnology*", Eds. Z.M. Wang, A. Wang, G. Salamo, K. Kishimito, S. Belluci, Y.I. Park, Springer, 2013. (Invited)

Refereed journal publications

1. **K. Kant**, C. Priest, J. G. Shapter, D. Losic, "*Microbial cell lysis and nucleic acid extraction through focused ion beam milled nanofluidic channel*" Lab on Chip, 2014. (Under review)
2. **K. Kant**, C. Priest, J. G. Shapter, D. Losic, "*Influence of nanopore dimensions on electrochemical properties of nanopore arrays studied by impedance spectroscopy"* Sensors, 2014 (under review)
3. S. Chandrasekaran, M. J. Sweetman, **K. Kant**, W. Skinner, D. Losic, T. Nann and N. H. Voelcker, "*Silicon diatom frustules as nanostructured photoelectrodes*", Chemical Communications , (2014)
4. **K. Kant**, C. Priest, J. G. Shapter, D. Losic, "*Characterization of impedance biosensing performance of single and nanopore arrays of anodic porous alumina fabricated by focused ion beam (FIB) milling*" Electrochemica Acta 139 (2014) 225–231.
5. S. Simovic, K. R. Diener, A. Bachhuka, **K. Kant**, D. Losic, J. D. Hayball, M.P. Brownc, and K.Vasilev, *"Controlled release and bioactivity of the monoclonal antibody rituximab from a porous matrix: a potential in situ therapeutic device"* Materials Letters 130 (2014) 210–214.
6. **K. Kant**, J. Yu, C. Priest, J. G. Shapter and Dusan Losic *"Impedance nanopore biosensor: influence of pore dimensions on biosensing performance*" Analyst, (RSC), 139 (2014) 1134-1140.
7. **K. Kant,** M. Kurkuri, J. Yu, J. G. Shapter, C. Priest, D. Losic, *"Impedance spectroscopy study of nanopore arrays for biosensing applications"* Science of Advanced Materials, 6, (2014) 1375-1381.

8. Y. Yu, **K. Kant,** J. G. Shapter, J. Addai-Mensah, D. Losic, "*Characterisation of catalytic properties of gold nanotube membranes"*, Microporous and Mesoporous Materials, 153 (2012) 131-136.

Conferences presentation/Abstracts

1. **K. Kant**, S. Amos, M. Erkelens, C. Priest, J. G. Shapter, D. Losic, '*Microchip nanofludic channel for microbial cell lysis and nucleic acids extraction'* RACI National Congress 7-12 Dec. 2014, Adelaide, Australia.
2. M. Alsawat, **K. Kant**, T. Altalhi and D. Losic, *"Tuning of electrochemical properties of carbon nanotube membranes by chemical modification"* ICONN-2014 International conference on Nanoscience and Nanotechnology, 2-6 Feb. 2014 Adelaide.
3. **K. Kant**, J. G. Shapter, C. Priest, D. Losic, *"Impedance spectroscopy study on focused ion beam (FIB) milled nanopore arrays of alumina membrane"* Nanotoday, 8-12 Dec. 2013 Singapore P1-308.
4. **K. Kant**, J. Rochow, C. Priest, J. G. Mitchell, J. G. Shapter, D. Losic, *"Growth of conducting microbial nanowires through nanofluidic membrane"* 4th Australia and New Zealand Micro/Nanofluidics Symposium (ANZMNF) 22-23 April 2013 Adelaide, Australia.
5. **K. Kant**, M. Kurkuri, J. Yu, J. G. Shapter, C. Priest, D. Losic, *"Impedance spectroscopy study of nanopore arrays for biosensing applications"* 1st International Conference on Emerging Advanced Nanomaterials (ICEAN), 22-25 October 2012 Brisbane, Australia.
6. K. Gulati, **K. Kant**, D. Losic, *"Enhanced drug storage and elution characteristics of geometrically tailored Titania nanotubes"* Thirteenth International Conference on Science and Application of Nanotubes (NT12), 24–29 June 2012 Brisbane, Australia.
7. Y. Yu, **K. Kant,** J. G. Shapter, J. Addai-Mensah, D. Losic, *"Study of catalytic properties of gold nanotube membranes",* Chemeca 2011 proceeding , Sydney 18-21 Sept. 2011.

Chapter 1

INTRODUCTION

1.1. Biosensors: principle and concept

A biosensor is an independent receptor or transducing device, which has capacity to provide quantitative evidence using a biological element [1]. Sensor contains a recognition element that enables the selective response to a particular target molecules or analyte, and minimizes interferences from other foreign components available in sample (Figure 1.1).

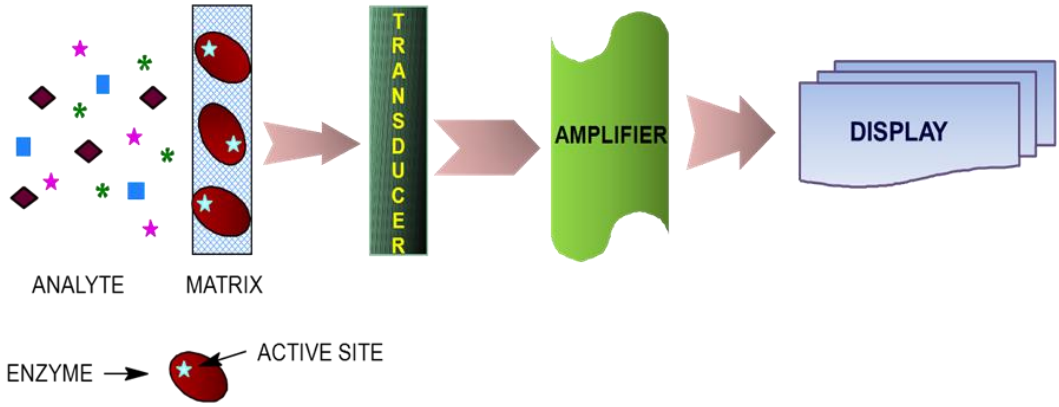

Figure 1.1: *Generalized concept of biosensor device, showing the working components of the sensor and their physical arrangement.*

Biosensors constitute an interdisciplinary field that is currently one of the most active and attractive areas of research. Using biosensors typically eliminates the need for sample preparation. The biosensor's performance is usually evaluated experimentally, which is based on its sensitivity, limit of detection (LOD), linear and dynamic ranges of sensing, reproducibility or precision of the response, selectivity, linear range and its response to interferences [2, 3]. Many other parameters that are often included in the sensor's response time (i.e. the time after adding the analyte for the sensor response to reach 95 % of its final value), operational and storage stability, ease of use and portability. In an ideal case, the sensing surface should be re-generable so that it can be used in several

consecutive measurements. For many clinical, food, environmental, and national defense applications, the sensor should be capable of continuously monitoring the analyte on-line. However, disposable, single-use biosensors are satisfactory for some important applications such as personal blood glucose monitoring by diabetics [4-6]. The bio-elements and sensing detection principles for various kinds of biosensors are presented in Figure 1.2.

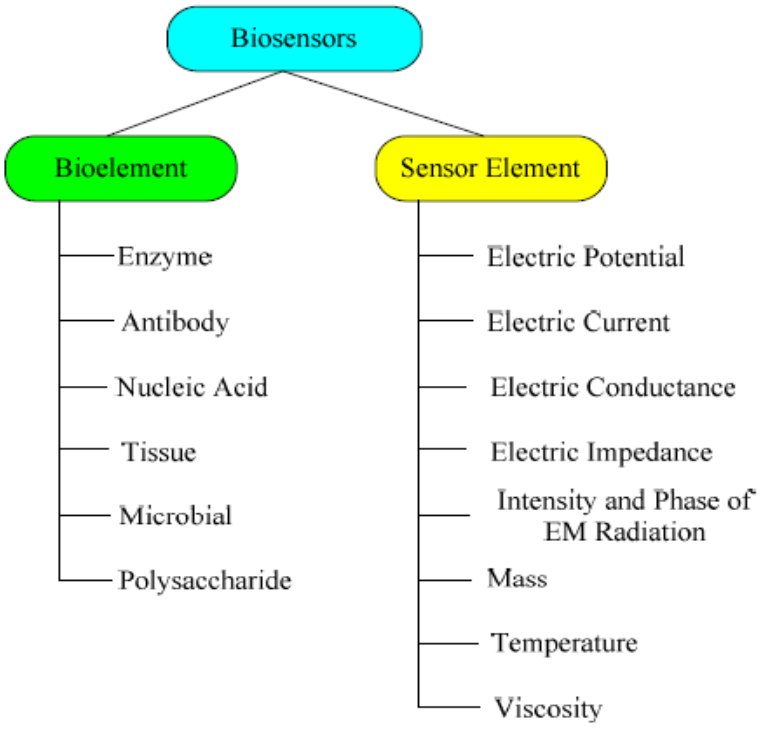

***Figure 1.2**: Scheme showing typical bio-elements and detection principles of biosensor [1].*

1.1.1. Label or non-labelled biosensors

Most biosensors are designed to have a marker or label which is immobilized to the target site. In the sensing experiments the amount of these labels detected corresponds to the number of bound target molecules. These labels can be fluorescent, magnetic or bio-active (reactive) molecules with an easily detectable product. Redox-active labels are commonly used in various types of electrochemical biosensors. Along with many advantages, labelling of analytes is

sometime undesirable for several reasons. It increases the amount of sample required and its preparation. Addition of a label can also change the binding properties of the biomolecule. As a result, the yield of the target-label in the coupling reaction of analyte can be variable [7]. In the case of DNA sensors, labelling is not an issue because of chemical homogeneity of DNA and ease of labelling during its amplification. On the other hand labelling is serious problem for protein targets. Thus, a sandwich assay is mostly used for protein or enzyme recognition [8]. This type of assay requires two different probes to bind on two different sites of the target, this yields enhanced selectivity of the system but limits its use in research. The ELISA (Enzyme-Linked Immuno Sorbent Assay) is a good example of a sandwich assay [9].

1.1.2. Label-free operation of biosensors

A current major driving force is to develop biosensors that can perform label-free detection. The reaction between target biomolecule and the bio-functionalized surface produces the changes in the sample surface electrical properties (e.g. resistance, capacitance etc.) and detects the existence of only the target molecule. There is no labelling required for biosensing. The use of a label offers selectivity and sensitivity but can also greatly change the impedance of the system. Besides the benefit of sample preparation, label-free operation enables recognition for real time target-probe binding, which is ability that label-based systems generally do not possess [10]. There are two advantages in the real-time sensing, one is time of binding or unbinding of molecules improves its measurement accuracy and other one is determination of affinity constants of the sensor, which is very close to the response of surface plasmon resonance (SPR) [11, 12].

1.1.3. Limitations of label-free biosensor performance

The limits of label-free affinity biosensor performance are mostly due to the affinity step in the binding reaction. Previous studies claimed that most of the electrochemical impedance techniques do not have very high sensitivity and their LOD is often low as compared with optical methods, but others disagree [13, 14]. Label-free biosensors are useful when moderate sensitivity in the sample is required. However, it is not yet explained and observed that label-free affinity impedance biosensors can also perform at the same level of sensitivity as of label-based techniques.

1.2. The electrochemical biosensors: concepts

The electrochemical detection method is used in most of the biosensors due to its sensitivity, portability and simple handling. The cost effectiveness of the electrochemical biosensors is another advantage for their use [1, 15]. The electrochemical techniques can be defined into three main categories of measurement: current, potential and impedance. To measure the resistance of chemical reactants in the biosensing system; impedance is commonly used technique. This type of measurement is not dependent on the reaction volume, so a very small sample volume can be used for measurement [16, 17]. The lowest detection limits down to zeptomoles were detected without the conventional sample preparation [18]. In other words electrochemical detection did not require any special sample preparation while being used in sensing device [18, 19]. It can easily be used to do measurements on the samples like colored or whole blood samples without interference from globules and blood cells [5, 20]. In some type of immunoassays no separation step is performed to isolate the antibody–antigen

complex from the sample. There is no effect on the electrochemical detection by sample components (e.g. chromophores or fluorophores) and other types of foreign material which can interfere with electrochemical detection. Further subdivision in electrochemical biosensors can be achieved on the basis of their nature for the recognition of a biological sample and its process of recognition. The biocatalytic and affinity based detection are two main recognition methods which are commonly used in sensor devices [15]. There has been lot of attention in past years on the biocatalytic type of sensing which has mainly been used for the incorporation of enzymes, cells, tissue and glucose. [21]. On the other hand affinity based sensors were dependent on the selective binding and interaction between the analyte. In a biological component such as an antibody, nucleic acid, affinity based sensing devices were very useful [5, 21]. The surface charge effect in controlling ionic conductance has also been investigated for its application in the detection of unlabeled DNA as shown in Figure 1.3 [22, 23].

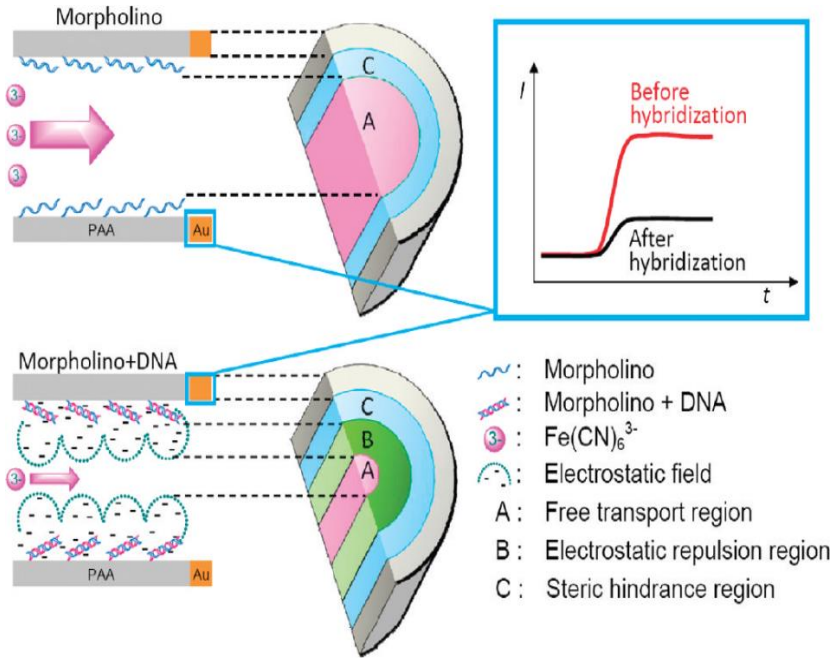

Figure 1.3: *Schematic representation of the principle for the label-free DNA detection system using an electrochemical detector [23].*

1.2.1. Impedance biosensor

Impedance biosensors mostly provide measurement for the electrical impedance of an AC state interface with DC bias environments. Impedance biosensors have one working electrode and one counter electrode to collect the signals and analyte samples are either attached to one of the electrode surfaces or in very close contact with both the electrodes (Figure 1.4). Basically impedance is measured by applying a small voltage of a particular frequency and measuring the resulting current. This can be done at a range of frequencies. Taking the current-voltage ratio at each frequency yields an impedance spectrum. This methodology is known as Electrochemical Impedance Spectroscopy (EIS) [24]. When the target analytes are captured by the sensing substrate, EIS will show a change in the impedance value. The impedance measurement does not require any special reagents or probes to enhance the strength of signals. In other words, it is label-free detection. Through impedance biosensing a variety of target analytes can be detected by changing the surface of the substrates for detection. In previous studies target analytes were used for detection of proteins though impedance sensing [25, 26]. Impedance biosensing has also been used for the detection of small biological molecules [27-29]. It has proven useful in monitoring cellular state with change in environmental conditions of the cells and can monitor the cell membrane proteins [30-33]. Apart from biosensing, researchers have used EIS in physical and material science to characterize coatings, track corrosion processes and to study charge transfer in fuel cells. This type of use of EIS sensing makes it a technique with wide variety applications [34]. These qualities make EIS biosensing stand close to the traditional field-effect sensors [35]. In an example of whole cell detection by EIS, where impedance sensing was used on nanoporous

membranes having poly ethylene glycol (PEG) hydrogel microwells as shown in Figure 1.4. The PEG was used to make a small area for the cells and electrolytes were flowing through the nanopores to cancer cells. Two electrodes (working and counter) were used for the impedance signals [36].

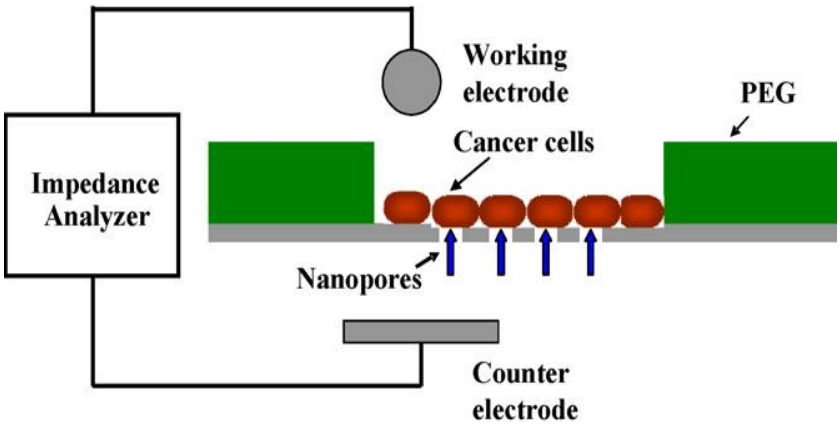

Figure 1.4: *Schematic diagram for impedance sensing using nanoporous membrane with PEG hydrogel microwell [36].*

Several studies have been reported on the affinity based impedance sensing for biomolecules as well as non-affinity biosensing. The affinity is only the mechanism of binding the biomolecules and used to identify the bonding of affinity molecules on the target surface than other foreign molecules in the reaction. However non-affinity measurements in impedance sensing lack specificity in the target bonding. Some labelling may be required to identify the reaction completion and target sample quantification [37-39]. Dielectric spectroscopy in biosensing has the same limitations as non-affinity biosensing [40, 41]. The most important question is this: Can impedance biosensors have potential to solve these limitations of non-affinity and labelling of the analyte samples. In real-life applications, biological samples typically contain a large amount of foreign molecules which may challenge the selectivity of the biosensor.

The detailed reviews by Macdonald, Bard and Faulkner on Impedance technique and electrochemistry are useful in developing the basic understanding about the impedance sensing [24, 42]. In previous years, protein detection by use of electrical sensors was reviewed by many authors [43]. There are many articles which focused on Faradaic and non-Faradaic techniques and also on the impedance amplification using labels [44-46]. A more recent review of impedance biosensors presented different approaches, but was broader in scope [47]. Capacitive biosensing has been described in detail and the use of semiconductor substrates for capacitive type of biosensing is another way to get field-effect contributions. This type of biosensing is very important in the field of impedance biosensing [48]. Various electrochemical DNA detection approaches, including impedance techniques, were reviewed by Gooding and others [49, 50]. Thévenot has recommended the certain criteria's for electrical biosensors in his articles [51]. Overall an impedance biosensor is a simple, rapid, label free, low cost detection method for biological molecules. It also does not require special reagents in most of its applications and handling [21].

1.2.2. Affinity impedance biosensor: Concepts

The Faradaic type of impedance biosensors mostly monitor changes in the affinity binding of target molecules in the sensor. The affinity impedance biosensor has some specific active sites for biomolecules; the analytes have affinity towards the active site to complete the recognition such as biotin has strong binding affinity for streptavidin as shown in Figure 1.5. Most of the reported DNA sensors are based on Faradaic impedance spectroscopy and were easily able to detect 1 nM of 15mer target [52]. Researchers have published many

papers about DNA matching by use of a Faradic technique [53, 54]. A decrease in impedance takes place by a small change in concentration of biotin exposed to an avidin-functionalized gold electrode [55]. This decrease was explained as the target surface had positive charge but at the same time probe has negative charge, thus target molecules binding decreased the electrostatic forces for the redox species. Mirsky et al. presented a non-Faradaic type of biosensing by using anti-HSA antibodies attached to a tightly packed SAM via a linker and the data was collected by impedance spectroscopy at 20 Hz [56, 57]. It was observed that the capacitance changes when probe molecules are immobilized to estimate probe density and tried to improve response time and reproducibility (10–30 % over several trials). Although the reported limit of detection is 1 μg/mL. There are many other research groups who have used low frequency non-Faradaic measurements to detect DNA [52-54, 58, 59]. The non-Faradaic impedance measurement for biotin and streptavidin at low frequencies was also been performed by Lasseter et al. at flat surface substrates [55, 60].

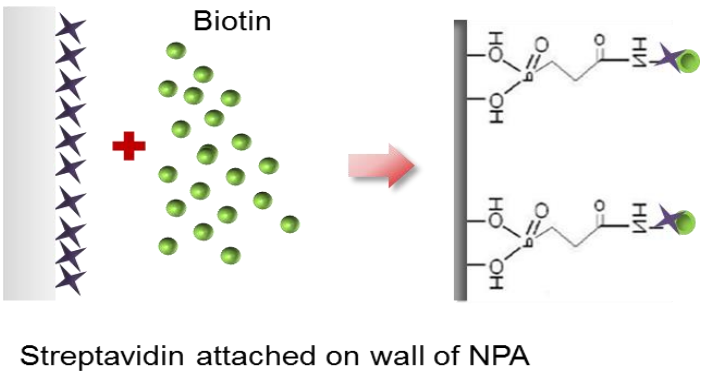

Figure 1.5: *Schematics for affinity impedance biosensing, where NPA surface modified with streptavidin and biotin molecules are binding on streptavidin.*

Other investigators used a flow cell to monitor and introduce controlled amount of antigen in the system, which was further followed by several buffer

washes. Although it was been reported that there was large scale non-specific binding at target surface and can be avoided by washing samples. In recent studies these results have been confirmed using signal-to-noise ratios at the required optimal frequency for measurements [57, 61]. Determining the target molecule binding by signal-to-noise ratio at different frequencies became a powerful concept but still the reproducibility and non-specific response in measurement is big disadvantage in the measurements.

1.2.3. Practical issues in impedance biosensors

There were many strategies and models (theoretical) have been explained by many previous researchers, which explain the reasons behind the change in impedance upon target binding. An understanding about target binding mechanism and impedance change will be important to improve biosensor devices and its sensitivity. It was observed that a label-free measurement can have significant changes in impedance data if we keep the target surface larger than used sensing probe [62]. Most of the charged surfaces of the sample either exert an attractive or repulsive force on the ions near the electrode. This applies for the Faradaic type of sensors because they have the interaction of redox species and target probe which reduces the resistance of the system and enhance the sensitivity of the sensor [63, 64]. This type of non-Faradic effect has been generally used for self-assembled monolayers (SAMs), DNA sensors, and protein sensors [65-67]. Sometimes surface charge is also dependent on temperature, electrolyte pH and other factors which can impact impedance measurements greatly [68]. The impact of pH and ion generated capacitance in the system can be controlled by increasing the ionic strength of the solution and generate a high

electrode potential by the charged ions to the target surface because most of the time they are pH dependent [69, 70]. In studies it was also noted that abnormal behaviour of impedance at low frequencies may be the resultant of dipole effects [71].

It was reported that applying a small voltage between the electrodes can change the thickness of electrical double layer due to the electrostatic interaction with the charged target molecules [72]. This has be termed as dielectric spectroscopy in the field of impedance sensing but not many people put their attention on it for biosensing [41, 73]. The dielectric impedance spectroscopy was important in the measurement of bulk solution properties at high range (MHz) frequencies [74]. The frequencies which are related to the dielectric relaxation times between free and bound target molecules may give us specific binding information to understand the change in impedance measurement. In general, these effects do not have any importance in surface-sensitivity or specificity. So it was used to study the behaviour of biomolecules or concentration of target molecules in the sample [39, 75, 76].

1.3. Impedance biosensors designs and electrode surfaces

The surface geometry and area are two major components which are mainly responsible for the performance of electrochemical biosensors. Most of the time biological elements were immobilized on the electrode surface, so a larger the surface increases the number of binding sites for target molecules. The chemical composition or substrate material and its electrochemical properties are also considered as most important parameters. Most of the experiments nanoparticles were largely used to enhance the surface area of the electrode. It also affects the

sensitivity of the device. Gold nanoparticles are the most commonly used nanoparticles on the electrode surface for immobilization of antibodies [77]. In some other strategies the electrochemical deposition of gold was used rather than using gold nanoparticles [78]. One of the Faradaic EIS studies where allergen probe was immobilized on an electrode and coated with gold nanoparticles for detection of antibodies [79]. Some other work using thin films of platinum coated with an antibody have been used as the probe surface for the sensor [80]. Silver nanoparticles have also been used in similar approach to detect DNA [81, 82].

Interdigitated electrodes are very important type of methods for electrodes to be considered. Most of the modified type of electrode surface been used in the capacitive type of impedance biosensors [27]. They are easy to fabricate by conventional methods and largely been used for various sensors [83]. The impedance measurements generally took place between two (identical) electrodes and have no direct electrical connection. The flow of charge is always made through the solution. The geometry of the target surface can alter the capacitance in the system and affect the sensitivity of the device [84, 85].

1.3.1. Impedance biosensors with interdigitated electrodes

In early studies, it was reported that interdigitated electrodes were the most commonly used electrodes for sensing. The electrodes were covered by target molecules and work as probes [86, 87]. Interdigitated electrodes were either coated with gold films or nanoparticles, along with polymer with or without the receptor for target molecules. The impedimetric sensors for small molecule like neurotransmitter acetylcholine and a related neurotoxin using protein receptors isolated from animal tissue has also been reported [27]. F. Lisdat & D. Schäfer

suggested that the recognition element can be immobilized on a single working electrode to construct an interdigitated electrode (Figure 1.6) [47].

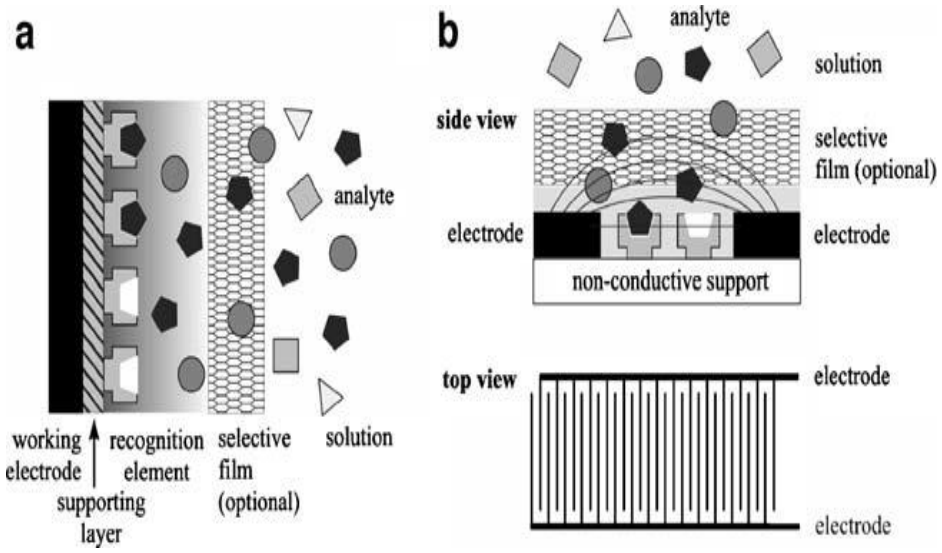

Figure 1.6: *Schemes of impedimetric biosensors using a modified working electrode as sensor (a) or an in-plane arrangement of two electrodes (interdigitated electrodes, IDE) (b). Immobilisation of the biocomponent occurs on the electrode in (a) and between and/or on the electrodes in (b) [47].*

In general, interdigitated electrodes in impedance biosensors are either based on the metal or semiconductor, which were coated with target molecules. In case of semiconducting material a thin native oxide film is used for making the connection for the electrodes assuming that field effects is negligible. Researchers were unable to determine the reason behind changes in impedance measurement using a silane-antibody coupling on semiconductor substrate but significant changes were observed in the impedance of a polymer-antibody film when exposed to alpha-fetoprotein target [88, 89]. It been reported that the platinum electrodes functionalized with antibody for impedance measurement at low frequency (1.5 kHz) are a poor sensor but a high detection limit [90].

1.3.2. Impedance biosensing with nanopores as electrode

In a new strategy, nanopore based impedance biosensing where biomolecules are present inside the nanopores approaches the direct sensing of target molecule inside the nanopore [90, 91].

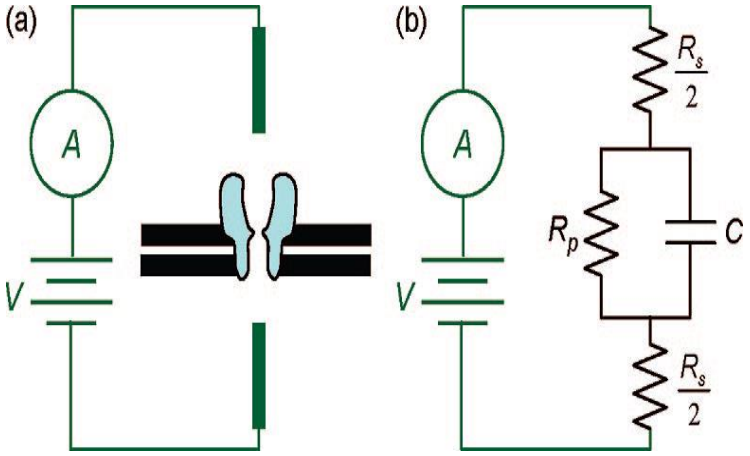

Figure 1.7: *(a) Schematic diagram of the nanopore biosensing device. A voltage is applied across the electrodes via an external circuit, and the ionic current flowing through the nanopore is monitored. The presence of an analyte near the entrance or inside the nanopore causes this current to decrease. (b) Equivalent circuit for the ionic part of this system. R_s, R_p, and C represent the resistance of the solution, the resistance of the pore, and the capacitance of the lipid bilayer in which the nanopore is embedded, respectively. Molecular-scale events at the pore correspond to temporary changes in the value of R_p [92].*

As illustrated in Figure 1.7, a nanopore which is opened at both ends is sandwiched between two reservoirs containing an electrolyte. The voltage difference is been applied between both reservoirs using two electrodes through the nanopore, resulting in an ionic current flowing between the two reservoirs. The nanopore, which is the main resistance in the flow of ions, system magnitude can be essentially determined by the size of the nanopore. Any change in the size of the nanopore or other obstacles will affect the flow of ions through the nanopore, which results in change in the current. The researcher defined that if the pore size is in nano dimensions then it can be comparable to the size of molecule

present in the system. Any passage of molecules through that nano hole can be detected by the sensing device. Such type of detection where molecules are driven through the pore and biosensing through nanopores is called as nanofluidic biosensing [91].

1.4. Impedance biosensing by nanopores and nanofluidics

The study of fluid in nanoscale objects or its flow/application in nano dimensions known as nanofluidics [93]. The term "nanofluidics" its most commonly used in field of membrane science and colloid science. The recent developments of tools which are capable of manipulation and fabrication (ion beam, e-beam lithography, etc.) at the nanoscale make it possible to work in field of nanofluidics [94]. The structure of the nanopore and the target molecules in or outside it has to be taken into account to understand transport mechanism as well as the binding of molecules inside the nanopores. The nanoporous membranes have always been of interest for researchers to use its exceptional properties for biosensing platform due to high surface area in nano dimensions. There are many studies reported which uses the porous alumina membranes as a platform substrate in biosensing [95]. In some of the studies nanopores were open at one or both ends, e.g. an immune-sensor developed in porous membrane where one end of the nanopore works as an electrode for virus antibody detection (Figure 1.8) [95]. The electrical impedance biosensors in nanofluidics are not very well explored yet due to the lack of technologies for fabrication as well as the characterization of nanofludic devices. This nascent interdisciplinary field of impedimetric nanofluidic biosensing includes a combination of different major fields such as biology, electrochemistry, chemistry, and physics [21, 96].

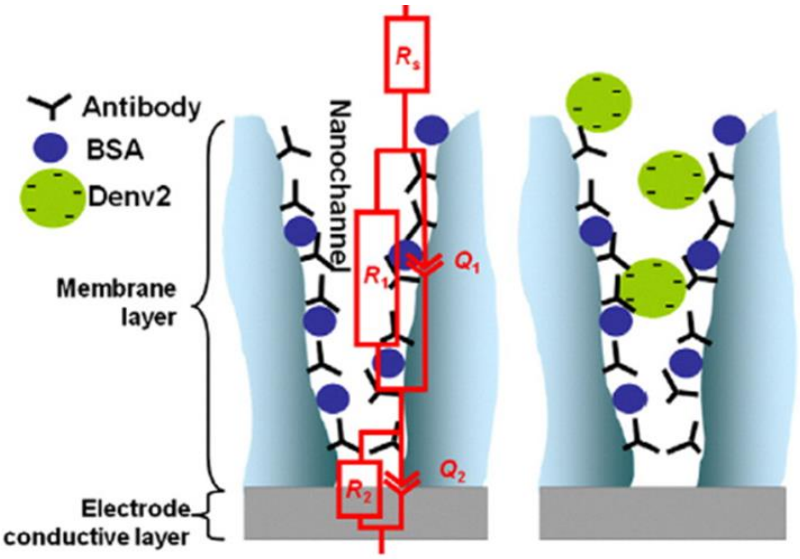

Figure 1.8: *Schematics of the porous alumina nano-biosensor for Denv2 virus detection by specific binding to immunoglobulin G antibody 3H5 positioned along the walls of the alumina nanochannels. The equivalent circuit model is inserted [95].*

Nanoporous alumina (NPA) based DNA biosensor was presented by Chee Seng Toh et al. which uses thermo-stated complementary target solution at 45 ^{o}C. In this biosensor the target molecules were rinsed with DI water to remove target molecules which were not bonded with target DNA molecule. The electrochemical measurements were taken at room temperature (Figure 1.9). This immobilization and hybridization of DNA molecules inside NPA pores led to a significant decrease in resistance measured by EIS on a control sample which has no modification on surfaces. In another approach, Wang et al. detected DNA hybridization using a dynamic polymerase-extending method. In which a combined cyclic voltammetry and EIS measurement was carried out on NPA membranes. The immobilization of single stranded DNA molecules as a recognition element for detection of hybridized DNA molecules on APTES-glutaraldehyde functionalized NPA surface by research group of Takmakov et al. [98, 99]. Nanofluidic membranes have been used as a bridge substrate between multilayered microfluidic channels by Kuo et al. [100].

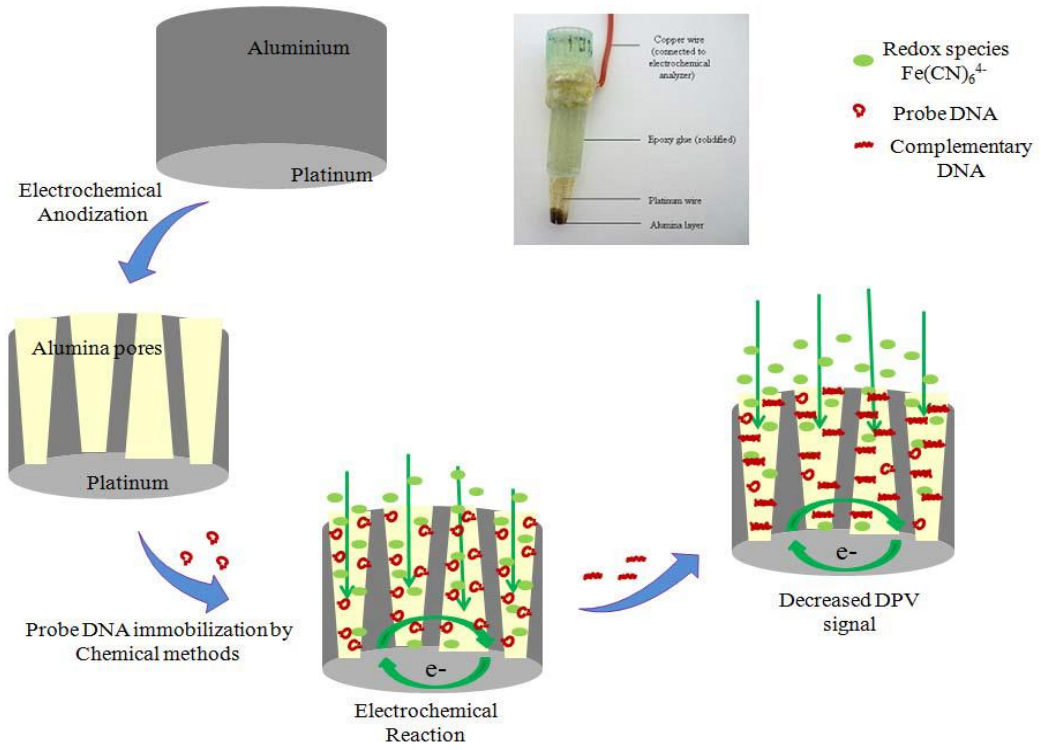

Figure 1.9: *Scheme of construction and operation for nanoporous alumina membrane based electrochemical label free DNA biosensor [97].*

The research group of Pu et al. worked on the controlled transfer of analytes in between two microfluidic channel and observed concentration enhancement in one side of reservoir when a high voltage was applied across a nanofluidic channel [101]. Merkoci et al. presented a nanochannel/nanoparticle-Based direct detection and filtering platform for cancer biomarker in blood. A protein sensing technology using an NPA platform in which cells present in the sample remain at the outer surface of the pores and proteins are recognized by specific antibodies. The sensing principle works to detect specific proteins in the sample by using AuNP tags [102]. The fabrication of gold nanotube membranes by electro-deposition of gold on commercially available polycarbonate membranes has also been investigated using various approaches which can control the nanopore size up to 0.8 nm [103, 104]. The investigators recognized the

method as an attractive approach for biosensing where alumina membranes were used as nanofluidic channels and antibodies specific to a drug molecule can be easily load inside alumina template membranes [105].

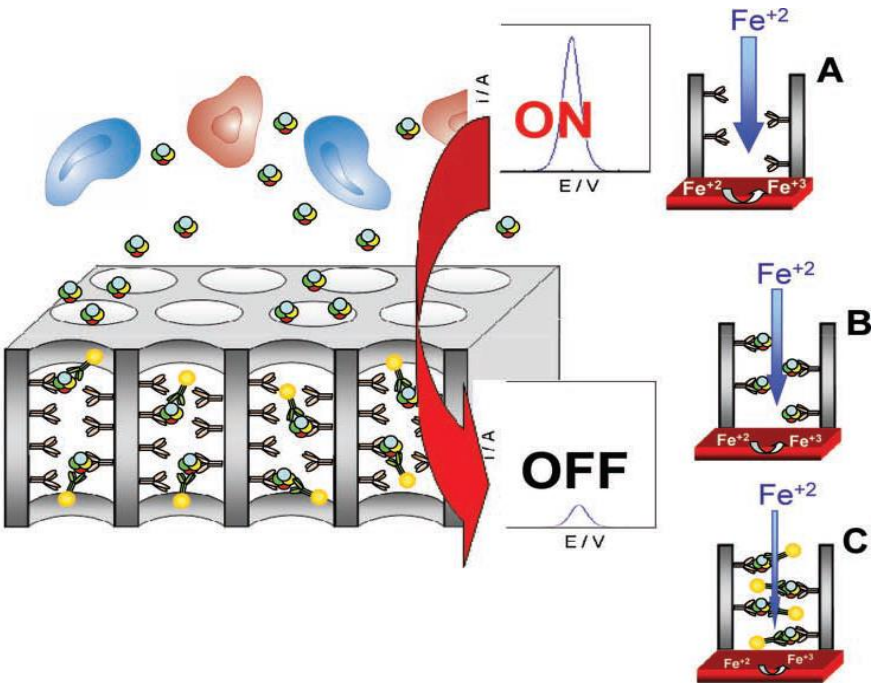

Figure 1.10: *A protein sensing technology using an NPA. The cells in the sample remain outside the pores and the proteins enter inside and are recognized by specific antibodies. Sensing principle in the absence (a) and presence (b) of the specific protein in the sample and in the case of the sandwich assay using AuNP tags (c) [102].*

These membranes have the properties of ionic selectivity which could be controlled either by chemically controlling the surface charge or a small potential can be applied with respect to the electrolyte solution. These properties of alumina membranes can be used as molecular filters [106]. This property has already been investigated by some research groups for single molecule detection and field-effect control [107-109]. NPA with nanofluidic channels with controlled geometry were fabricated using electrochemical techniques which will be discussed later in this thesis.

Table 1 summarizes selected label-free affinity impedance biosensors published in recent literature utilizing porous alumina and other types of nano channels:

Nanopore/ Nanochannel	Single / array	Material/fabrication	Detection	Analyte	Ref.
biological ion channel	Single	α-hemolysin nanopore	Electrical sensing	Proteins enzymes Peptides	50,57, 59,60, 61,62,64
	Array		electrical sensing	DNA	74
solid-state nanochannel	Single	SiN-SiO_2 membranes	Electrical sensing	DNA Proteins	185-189, 191, 192, 197, 198
		Porous alumina / Polymeric membranes	Electrical sensing	DNA Proteins	79, 190 183, 199-205
		Glass nanopore	Electrical sensing	ions	206-208
	Array	Porous alumina membranes	Electrical electrode	Proteins DNA	209-212 214-216
		Porous silicon	Optical	Proteins	130, 226, 228

Table 1.1: *Summary of the various nanopores/nanochannels based affinity biosensors and their applications.*

1.5. Fabrication of nanoporous alumina (NPA)

1.5.1. Basic concept of NPA

NPA with controlled dimensions and geometry of nanopore can be fabricated using electrochemical techniques [110, 111]. This fabrication technique consists of alumina oxide nanopore array generation on aluminum. The anodization of aluminum took place in an electrolytic solution by applying a voltage or current. The oxide of aluminum is generated with surface irregularities

or defects due to irregular electric field concentration over the surface of aluminum during anodization. In the anodization process, the applied electric field started the acidic dissolution of the oxide at the bottom of the pores and leaving nanopore walls intact, which results in fabrication of nano dimensional channels. The oxide layer produced at the bottom of the nanopore can be removed by chemical etching to achieve free standing membrane with both ends open. Masuda's group established a two-step anodization process for fabricating self-ordered NPA templates [112]. These nanoporous alumina membranes have a very high pore density and controlled pore diameters. This kind of substrate with high surface area can be used in biosensing [113].

The structure of NPA has been described by many research groups as a close-packed hexagonal array of cylindrical nanopores (Figure 1.11). The morphology, diameter, inter-pore distance, wall thickness, length and barrier layer thickness are the most important parts of the nanopore to characterize and can be controlled by tuning anodization conditions. The nanopore structures range from about 20 - 300 nm in diameter, 50 - 400 nm for inter-pore distance and thickness of the porous layer from 10 nm to 150 μm. The density from 10^9 to 10^{11} cm^{-2} and porosity from 5 to 50 % can be controlled [114-116]. Over the long period of research on Al anodization it was observed that the applied potential, electrolyte, electrolyte concentration, temperature and pre-patterning of the surface have crucial roles in achieving control over the self-ordering process and NPA structures [112, 117-119]. The porosity (P) of the NPA can be estimated assuming an ideal hexagonal arrangement of the pores;

$$P = \left(\frac{\pi}{2\sqrt{3}}\right)\left(\frac{D_p}{D_{int}}\right)^2 \qquad (1.1)$$

Where D_p and D_{int} are pore diameter and the inter-pore distance respectively [112]. A typical cross-sectional structure of the prepared NPA is shown in Figure 1.11. There are three different electrolytes which are commonly used for anodization of Al. They are sulfuric, oxalic and phosphoric acids [120]. Each of these electrolytes gives the different anodization rate (pore diameter, length) under controlled conditions. The anodization conditions can be classified in two major subdivisions one is conventional anodization conditions, which is sometimes called as 'mild' anodization (MA) and the other one is fast anodization or hard anodization (HA). The ordered alumina nanopore array can be obtained with both types of anodization. The use of different electrolytes will have different impacts on anodization of Al. For sulphuric acid, the electrolyte anodization condition is optimal at 25 V to achieve an inter-pore distance (D_{int}) = 63 nm. For oxalic acid at 40 V, it is D_{int} = 100 nm. For phosphoric acid at 195 V, it is very high (D_{int} = 500 nm). In other studies researchers has used other acids such as chromic, boric, citric and tartaric acid, but pore ordering and growth in comparison with the three commonly used electrolytes are not good [117, 121].

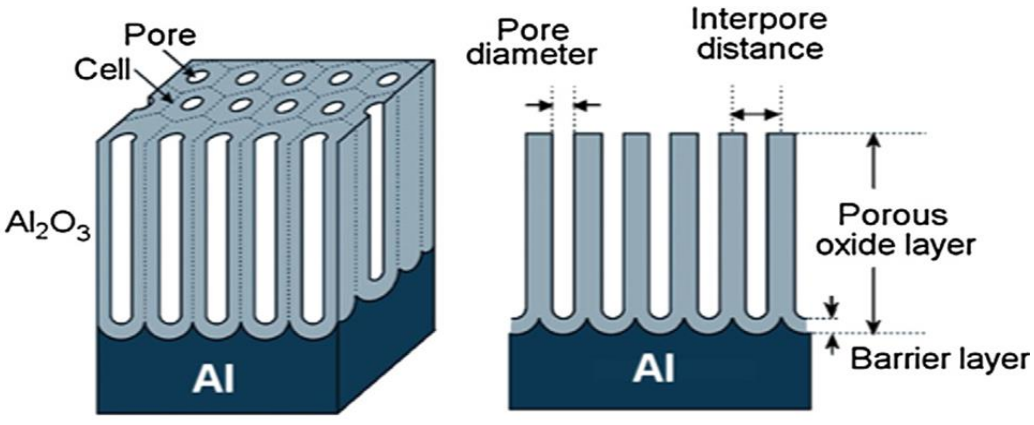

Figure 1.11: *(a) Schematic drawing of NPA structure prepared by electrochemical anodization of Al. (b) Summary of self-ordering voltage and corresponding inter-pore distance of NPA produced within three well-known regimes of electrolytes (sulfuric, oxalic and phosphoric) [121].*

The first generated porous layer after first anodization step was removed by use of oxide removing chemicals. This provides a pre-structured Al surface and facilitates the propagation of pores in the following anodization step. The difficulty in this process is slow fabrication of alumina membrane. Hard anodization has been presented by the Gösele group to solve this problem [122]. By this method the anodization rate is considerably higher compare to MA. The HA has been used in all the conditions and electrolytes and provides more control on nanopore characterization parameters such as pore diameters and inter-pore distance [123-125].

1.5.2. Self-ordering electrochemistry for nanopore formation

The self-ordering process of nanopores is mainly influenced by the type of electrolyte used; its concentration, pH, temperature, applied voltage and current. The nanotube morphology has been demonstrated by many previous research groups by changing these anodization parameters [126, 127]. At the start of the anodization process under controlled and constant voltage conditions, the metal surface has an oxide layer, as shown in Figure 1.12. Once this oxide layer forms on the metal surface, the current density drops (Step I). The distribution of the electric field is strongly dependent on the homogeneity and surface irregularity of the oxide layer, which generates a local electric field on the surface of oxide–electrolyte interface (Step II). The electric field assisted oxidation and dissolution takes place and localized pore like structures are formed and start further growth of pores (Step III). The pore growth is not uniform at this stage, but it leads to uniformity in structure with long period of anodization [128]. The long anodization time create a competition between oxide growth at the bottom of the pore and oxide dissolution at the barrier layer interfaces of nanopore. At the end

the pore growth, a stable and uniformly distributed pore array is formed (Step IV). Researchers are still not certain of the mechanism behind the pore growth and its generation but most of the researchers accepted that, "*the driving force for the self-ordering process can be attributed to a stress driven interface caused by the repulsive forces between neighboring pores that lead to ideal self-organization"* [129-131].

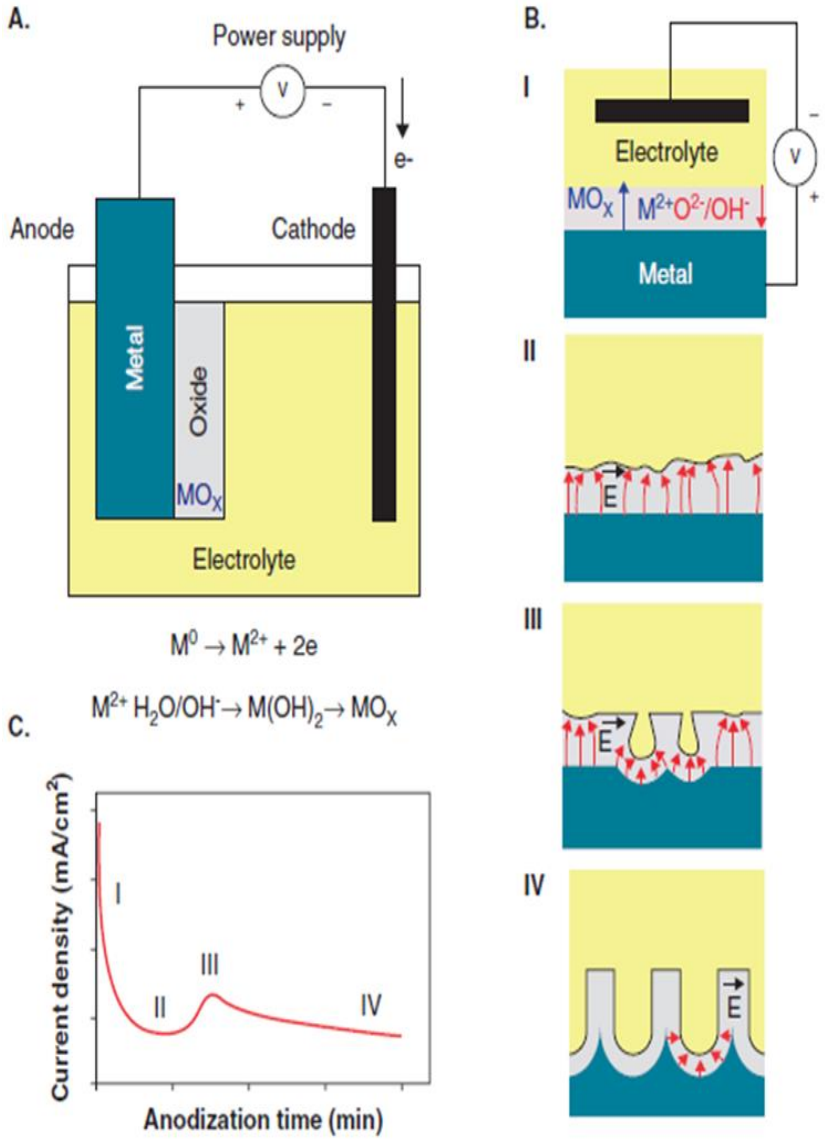

Figure 1.12: *Schematic diagram of the self-ordering process of pore formation by electrochemical anodization including electrochemical cell set-up and typical current density curve of electrochemical anodization. Stages of pore growth: (I) formation of oxide layer; (II) formation of pits by local electric field heterogeneities; (III) initial pore formation; (IV) pore growth under steady-state conditions [126].*

1.5.3. Challenges with nanopores for biosensing applications

The understanding of physical and chemical interaction for the molecules and ions inside these nanopores is driving the development of new kinds of nano-scale biosensing devices. Previous studies have shown that transportation or bio-functionalization of molecules inside nanopores is mostly affected by the steric and electrostatic effects. This is a long-range effect which caused by interaction of the surface immobilized molecules and ions involved in transportation. This transport of ions is dependent on the pore size and number of pores. It can be modulated by altering the surface charge of nanopore or ionic strength of the electrolyte.

This thesis presents the fabrication of NPA with nanopore arrays of highly ordered pore structures with controlled pore dimensions and its application as the electrochemical impedance sensing platform for the detection of biomolecules. Development of nanochannel or nanopore array biosensing devices has proven to be an excellent approach toward the development of simple, inexpensive and highly sensitive biomolecule detection. The sensitivity, low cost, simplicity, and easy miniaturization of electrochemical detection is particularly suited to the development of highly sensitive nanopore based biosensor. However, to improve and optimize the performance of nanopore biosensors, it is essential to understand the electrical and electrochemical properties of the nanopores. The dependence of these properties is on nanopore dimensions, diffusion and molecular transport of analyte molecules inside the nanopores and their physical and chemical interactions. In particular, their interactions and specific binding with the immobilized probe confined in a nanoscale volume are critical parameters which determine the performance of biosensing devices, e.g. sensitivity, response time

and detection limit. Surprisingly there are only few electrochemical studies on nanopores that address these questions.

1.6. Challenges in fabrication of an integrated NPA nanofluidic device

Fabrication of nanofluidic channels in the 10-100 nm diameter range can be achieved using sophisticated micro-fabrication techniques. It is known that majority of current nanofluidic research for their use in bioengineering and biotechnology applications. This thesis covers some of the significant progress in fabrication of nanofluidic devices, and methods for fabricating such devices [132-136]. The fabrication can be divided into two categories. First category includes top-down methods which start with patterns already in use and reduce their lateral dimensions to form nanostructures. Second category includes bottom-up methods which begin with one or two atoms or molecules to build up entire nanostructures [137]. The commonly used 2D nanochannels can be defined as nanochannels which have their dimensions in the nanometer range. These are mostly fabricated using of deep reactive ion etching (DRIE), electron-beam lithography (EBL) and focused ion beam (FIB) lithography [138, 139]. Previous researchers developed a nanofluidic separation device for DNA molecules which works on the size of DNA [140-143]. In biomedical diagnostics the major issue is target molecules which are generally not concentrated enough in sample solutions, e.g. in blood, saliva or urine, for direct detection. This is an important obstacle in protein biosensing on a nanofluidic device. This concentration issue of protein detection was also demonstrated using porous silica membranes [144, 145]. A device containing functionalized micro-tubules in nanofluidic device has also been reported, which contains highly concentrated target molecules to reduce the

analysis time and foreign molecule binding effects [146]. Several strategies were reported to create integrated circuits to perform the impedance measurements. The implementation of this technique on a nanofluidic device shows significant changes in biosensing capabilities [147, 148]. In most of these studies, scientists used very high concentrations of target molecules but the reproducibility in the system was very poor. An integrated electrochemical sensor with electrochemical bio-molecular detection has been offered recently [149, 150]. In this thesis, implementation of impedance spectroscopy measurement on a nanoporous alumina surface in a nanofluidic device will be examined, to address some of these limitations.

1.7. Objectives and aims

Impedance biosensors are traditionally used as a single functionalized electrode which required a large substrate surface. Reducing the size and cost of the measurement system enables new applications. On the other hand the semiconductor technology creates compact and inexpensive biosensors. CMOS biosensor arrays have recently been used to detect labelled biomolecules by electrical method [147, 151, 152], optical method [153] and magnetic detection method [154, 155]. Label-free impedance biosensors reduced the extra cost and complexity of using labels but to date a completely integrated impedance biosensor analyser has not been demonstrated in this field. Qualitative methods, such as the use of biomarkers, staining, and western blotting analysis are used for detection. These methods are time consuming and labor intensive. Impedance spectroscopy in quantitative measurements can be used to refine or design qualitative device for day to day use.

The principal goal of this work is to demonstrate an integrated nanoporous array for impedance biosensing application. The successful development of the integrated nanofluidic impedance biosensor will provide a means to use of nanopore substrate as an electrically detecting device for various biological molecules (antibody, enzyme, protein etc.) and quantify their presence in solution. Impedance measurements can also aid in obtaining fundamental information about cellular responses and behaviors. Therefore, this work aims to address these problems through porous alumina nanopore fabrication and nanofluidic device design optimization, designing multi-electrode devices, and automating data collection and analysis for large data sets.

Through the fabrication of a nanofluidic substrate and an impedance measurement system, the dependence of the electrode-solution interface impedance will be investigated and demonstrated changes can be used to interpret analyte capture at a functionalized surface. This thesis will describe new label free nanofluidic impedance biosensing. This would provide a means to explore the feasibility of electrically characterization with greater accuracy and enhanced sensitivity. The specific objectives include:

1. Investigate the effect of geometry (diameter and length) of NPA as a biosensing substrate on bio-impedance measurements.
2. Explore FIB methods to make precise (size/number) of nanopore to enhance the EIS measurement and sensitivity for development of optimized impedance microchip device.
3. Fabrication of nanofluidic device on quartz using FIB milling approach for application of single cell detection and manipulation.

4. Application of nanopore substrate for growth and separation of bacterial nanowires.

1.7.1. Thesis organization

Chapter 2 provides details about the experimental techniques used in this work including anodization of NPA, impedance spectroscopy, FIB and photolithography for fabrication of nanofluidic chip.

Chapter 3 describes the fabrication of NPA membranes by use of electrochemical anodization. To make it more specific and provide a precise area for biosensing, photolithographic patterning is done to achieve small 20 x 20 μm^2 area for further biosensing applications. The nanofluidic alumina array was used to define the properties of nanopores and effect on impedance measurement due to the change in their morphology. The studies of morphological effects help us to understand their biosensing abilities. Measurements using NaCl with nanoporous membrane was applied to confirm that changes in surface impedance correspond to the structure of the sample surface.

Chapter 4 explains the measurements using a four electrode measurement system and revealed target binding change inside the nanopores. A small change in the concentration of target molecule inside the nanofluidic nanopores was detected by impedance measurement over the range of frequencies. Surface modification inside the nanopores was successfully achieved by use of plasma cleaning step, which removed the excess amount of binding site from the sample surface. This label free biosensing on the small area of nanopore array was achieved.

For further improvement in the biosensing performance of the nanopore array and to achieve precise single nanopore biosensing we used focused ion beam milling on an alumina nanopore array as described in Chapter 5. The focused ion beam technology provides the ability to remove the barrier layer precisely leaving a few (2-3) nanopores available on sample surface. In focused ion beam milling patterns were made to compare the effect of change number of nanopores on their biosensing ability. It was found that reducing the number of nanopore enhances the impedance sensing ability with a limited number of pores. A large number of nanopores in an array are affected by the bulk properties of the solution and the sample morphology.

Chapter 6 describes the newly designed and implemented two and four electrode device which includes nanopore array fabrication, surface chemistry, measurement and data processing. First the operational impedance system for two electrodes and four electrodes which is the impedance-measuring circuit is discussed and the potential impact of reducing the device size is explored. The second half of the chapter explains the concept and advantages and disadvantages of two electrode and multi electrode systems and summarizes the measured performance of both the systems.

Chapter 7 describes the photolithographic fabrication of nanofluidic chip on quartz and fabrication of nanofluidic channel by use of focused ion beam technology. The fabricated nanofluidic chip had a nanofluidic channel connecting two micro channels. The application of this nanofluidic chip for the DNA extraction form cells is demonstrated.

Chapter 8 describes the application of nanoporous alumina membrane for the growth of conductive bacterial nanowires and their separation form the

bacterial cell for application in making electrodes. This type of growth of microbial bacteria is also used in the microbial fuel cells. NPA was used as the anode connecting channel for bacteria to donate electrons in the system, which forces them to grow their flagella through the nanochannels. Those grown flagella's are worked as the nanowires.

Chapter 9 concludes by summarizing both the contributions and achievement in this work. The concluding points for major outcomes by use of NPA and its use in the impedance biosensing. It also provides information for further improvements in this area and aspects for future research.

1.8. References

1. Eggins, B. R., *Chemical sensors and biosensors*. John Wiley & Sons: 2008; Vol. 28.
2. Pänke, O.; Balkenhohl, T.; Kafka, J.; Schäfer, D.; Lisdat, F., Impedance Spectroscopy and Biosensing. In *Biosensing for the 21st Century*, Renneberg, R.; Lisdat, F., Eds. Springer Berlin Heidelberg: 2008; Vol. 109, pp 195-237.
3. Berdat, D.; Marin, A.; Herrera, F.; Gijs, M. A. M., DNA biosensor using fluorescence microscopy and impedance spectroscopy. *Sensors and Actuators B: Chemical* **2006,** 118, (1–2), 53-59.
4. Yu, X.; Lv, R.; Ma, Z.; Liu, Z.; Hao, Y.; Li, Q.; Xu, D., An impedance array biosensor for detection of multiple antibody-antigen interactions. *Analyst* **2006,** 131, (6), 745-750.
5. Ronkainen, N. J.; Halsall, H. B.; Heineman, W. R., Electrochemical biosensors. *Chemical Society Reviews* **2010,** 39, (5), 1747-1763.
6. Zhang, J.; Zhu, J., A novel amperometric biosensor based on gold nanoparticles-mesoporous silica composite for biosensing glucose. *Sci. China Ser. B-Chem.* **2009,** 52, (6), 815-820.
7. Haab, B. B., Methods and applications of antibody microarrays in cancer research. *Proteomics* **2003,** 3, (11), 2116-2122.

8. Bilitewski, U., Protein-sensing assay formats and devices. *Analytica Chimica Acta* **2006,** 568, (1), 232-247.
9. Kindt, T. J.; Kuby, J., *Kuby immunology*. Macmillan: 2007.
10. Pohanka, M.; Skladal, P., Electrochemical biosensors principles and applications. *J Appl Biomed* **2008,** 6, (2), 57-64.
11. Rich, R. L.; Papalia, G. A.; Flynn, P. J.; Furneisen, J.; Quinn, J.; Klein, J. S.; Katsamba, P. S.; Waddell, M. B.; Scott, M.; Thompson, J., A global benchmark study using affinity-based biosensors. *Analytical biochemistry* **2009,** 386, (2), 194-216.
12. Cooper, M. A., Label-free screening of bio-molecular interactions. *Anal Bioanal Chem* **2003,** 377, (5), 834-842.
13. Jiang, D.; Tang, J.; Liu, B.; Yang, P.; Shen, X.; Kong, J., Covalently coupling the antibody on an amine-self-assembled gold surface to probe hyaluronan-binding protein with capacitance measurement. *Biosensors and Bioelectronics* **2003,** 18, (9), 1183-1191.
14. Sadik, O.; Xu, H.; Gheorghiu, E.; Andreescu, D.; Balut, C.; Gheorghiu, M.; Bratu, D., Differential impedance spectroscopy for monitoring protein immobilization and antibody-antigen reactions. *Analytical Chemistry* **2002,** 74, (13), 3142-3150.
15. Wang, J., *Analytical electrochemistry*. John Wiley & Sons: 2006.
16. Grieshaber, D.; MacKenzie, R.; Vörös, J.; Reimhult, E., Electrochemical biosensors-Sensor principles and architectures. *Sensors* **2008,** 8, (3), 1400-1458.
17. Ronkainen-Matsuno, N. J.; Thomas, J. H.; Halsall, H. B.; Heineman, W. R., Electrochemical immunoassay moving into the fast lane. *TrAC Trends in Analytical Chemistry* **2002,** 21, (4), 213-225.
18. Bauer, C. G.; Eremenko, A. V.; Ehrentreich-Förster, E.; Bier, F. F.; Makower, A.; Halsall, H. B.; Heineman, W. R.; Scheller, F. W., Zeptomole-detecting biosensor for alkaline phosphatase in an electrochemical immunoassay for 2, 4-dichlorophenoxyacetic acid. *Analytical Chemistry* **1996,** 68, (15), 2453-2458.
19. Jenkins, S. H.; Heineman, W. R.; Halsall, H. B., Extending the detection limit of solid-phase electrochemical enzyme immunoassay to the attomole level. *Analytical biochemistry* **1988,** 168, (2), 292-299.

20. Wijayawardhana, C. A.; Halsall, H. B.; Heineman, W. R., Electrochemical immunoassay. *Encyclopedia of Electrochemistry* **2002**.
21. Daniels, J. S.; Pourmand, N., Label-Free Impedance Biosensors: Opportunities and Challenges. *Electroanalysis* **2007,** 19, (12), 1239-1257.
22. Vlassiouk, I.; Takmakov, P.; Smirnov, S., Sensing DNA Hybridization via Ionic Conductance through a Nanoporous Electrode. *Langmuir* **2005,** 21, (11), 4776-4778.
23. Li, S. J.; Li, J.; Wang, K.; Wang, C.; Xu, J. J.; Chen, H. Y.; Xia, X. H.; Huo, Q., A nanochannel array-based electrochemical device for quantitative label-free DNA analysis. *ACS Nano* **2010,** 4, (11), 6417-6424.
24. Macdonald, J. R., Impedance spectroscopy. *Annals of biomedical engineering* **1992,** 20, (3), 289-305.
25. Lazcka, O.; Campo, F.; Munoz, F. X., Pathogen detection: a perspective of traditional methods and biosensors. *Biosensors and Bioelectronics* **2007,** 22, (7), 1205-1217.
26. Stelzle, M.; Weissmüller, G.; Sackmann, E., On the application of supported bilayers as receptive layers for biosensors with electrical detection. *The Journal of Physical Chemistry* **1993,** 97, (12), 2974-2981.
27. Taylor, R. F.; Marenchic, I. G.; Cook, E. J., An acetylcholine receptor-based biosensor for the detection of cholinergic agents. *Analytica Chimica Acta* **1988,** 213, 131-138.
28. Yin, F., A novel capacitive sensor based on human serum albumin–chelant complex as heavy metal ions chelating proteins. *Analytical letters* **2004,** 37, (7), 1269-1284.
29. Hleli, S.; Martelet, C.; Abdelghani, A.; Burais, N.; Jaffrezic-Renault, N., Atrazine analysis using an impedimetric immunosensor based on mixed biotinylated self-assembled monolayer. *Sensors and Actuators B: Chemical* **2006,** 113, (2), 711-717.
30. Arndt, S.; Seebach, J.; Psathaki, K.; Galla, H. J.; Wegener, J., Bioelectrical impedance assay to monitor changes in cell shape during apoptosis. *Biosensors and Bioelectronics* **2004,** 19, (6), 583-594.
31. Asphahani, F.; Zhang, M., Cellular impedance biosensors for drug screening and toxin detection. *Analyst* **2007,** 132, (9), 835-841.

32. Radke, S. M.; Alocilja, E. C., A microfabricated biosensor for detecting foodborne bioterrorism agents. *Sensors Journal, IEEE* **2005,** 5, (4), 744-750.
33. Mishra, N. N.; Retterer, S.; Zieziulewicz, T. J.; Isaacson, M.; Szarowski, D.; Mousseau, D. E.; Lawrence, D. A.; Turner, J. N., On-chip micro-biosensor for the detection of human CD^{4+} cells based on AC impedance and optical analysis. *Biosensors and Bioelectronics* **2005,** 21, (5), 696-704.
34. Anderson, E. P.; Daniels, J. S.; Yu, H.; Karhanek, M.; Lee, T. H.; Davis, R. W.; Pourmand, N., A system for multiplexed direct electrical detection of DNA synthesis. *Sensors and Actuators B: Chemical* **2008,** 129, (1), 79-86.
35. Poghossian, A.; Ingebrandt, S.; Abouzar, M.; Schöning, M., Label-free detection of charged macromolecules by using a field-effect-based sensor platform: Experiments and possible mechanisms of signal generation. *Applied Physics A* **2007,** 87, (3), 517-524.
36. Yu, J.; Liu, Z.; Yang, M.; Mak, A., Nanoporous membrane-based cell chip for the study of anti-cancer drug effect of retinoic acid with impedance spectroscopy. *Talanta* **2009,** 80, (1), 189-194.
37. Sanabria, H.; Miller Jr, J. H.; Mershin, A.; Luduena, R. F.; Kolomenski, A. A.; Schuessler, H. A.; Nanopoulos, D. V., Impedance Spectroscopy of alfa, beta Tubulin Heterodimer Suspensions. *Biophysical Journal* **2006,** 90, (12), 4644-4650.
38. Krommenhoek, E.; Gardeniers, J.; Bomer, J.; Van den Berg, A.; Li, X.; Ottens, M.; Van der Wielen, L.; Van Dedem, G.; Van Leeuwen, M.; Van Gulik, W., Monitoring of yeast cell concentration using a micromachined impedance sensor. *Sensors and Actuators B: Chemical* **2006,** 115, (1), 384-389.
39. Liu, Y. S.; Banada, P. P.; Bhattacharya, S.; Bhunia, A. K.; Bashir, R., Electrical characterization of DNA molecules in solution using impedance measurements. *Applied Physics Letters* **2008,** 92, (14), 143902-143902-3.
40. Feldman, Y.; Ermolina, I.; Hayashi, Y., Time domain dielectric spectroscopy study of biological systems. *Dielectrics and Electrical Insulation, IEEE Transactions on* **2003,** 10, (5), 728-753.

41. Facer, G.; Notterman, D.; Sohn, L., Dielectric spectroscopy for bioanalysis: From 40 Hz to 26.5 GHz in a microfabricated wave guide. *Applied Physics Letters* **2001,** 78, (7), 996-998.
42. Bard, A. J., *Electrogenerated chemiluminescence*. CRC Press: 2004.
43. Bergveld, P., A critical evaluation of direct electrical protein detection methods. *Biosensors and Bioelectronics* **1991,** 6, (1), 55-72.
44. Katz, E.; Willner, I.; Wang, J., Electroanalytical and bioelectroanalytical systems based on metal and semiconductor nanoparticles. *Electroanalysis* **2004,** 16, (1-2), 19-44.
45. Guan, J. G.; Miao, Y. Q.; Zhang, Q. J., Impedimetric biosensors. *Journal of bioscience and bioengineering* **2004,** 97, (4), 219-226.
46. Katz, E.; Willner, I., Probing biomolecular interactions at conductive and semiconductive surfaces by impedance spectroscopy: routes to impedimetric immunosensors, DNA-sensors, and enzyme biosensors. *Electroanalysis* **2003,** 15, (11), 913-947.
47. Lisdat, F.; Schäfer, D., The use of electrochemical impedance spectroscopy for biosensing. *Anal Bioanal Chem* **2008,** 391, (5), 1555-1567.
48. Limbut, W.; Kanatharana, P.; Mattiasson, B.; Asawatreratanakul, P.; Thavarungkul, P., A comparative study of capacitive immunosensors based on self-assembled monolayers formed from thiourea, thioctic acid, and 3-mercaptopropionic acid. *Biosensors and Bioelectronics* **2006,** 22, (2), 233-240.
49. Wong, E. L.; Erohkin, P.; Gooding, J. J., A comparison of cationic and anionic intercalators for the electrochemical transduction of DNA hybridization via long range electron transfer. *Electrochemistry Communications* **2004,** 6, (7), 648-654.
50. Velusamy, V.; Arshak, K.; Korostynska, O.; Oliwa, K.; Adley, C. In *Design of a real time biorecognition system to detect foodborne pathogens-DNA Biosensor*, Sensors Applications Symposium, SAS; IEEE **2009;** pp 38-42.
51. Thévenot, D. R.; Toth, K.; Durst, R. A.; Wilson, G. S., Electrochemical biosensors: recommended definitions and classification. *Biosensors and Bioelectronics* **2001,** 16, (1), 121-131.
52. Gebala, M.; Stoica, L.; Neugebauer, S.; Schuhmann, W., Label-Free Detection of DNA Hybridization in Presence of Intercalators Using

Electrochemical Impedance Spectroscopy. *Electroanalysis* **2009,** 21, (3-5), 325-331.

53. Gong, H.; Zhong, T.; Gao, L.; Li, X.; Bi, L.; Kraatz, H. B., Unlabeled hairpin DNA probe for electrochemical detection of single-nucleotide mismatches based on MutS− DNA interactions. *Analytical Chemistry* **2009,** 81, (20), 8639-8643.
54. Long, Y. T.; Li, C. Z.; Sutherland, T. C.; Kraatz, H. B.; Lee, J. S., Electrochemical detection of single-nucleotide mismatches: application of M-DNA. *Analytical Chemistry* **2004,** 76, (14), 4059-4065.
55. Ding, S. J.; Chang, B. W.; Wu, C. C.; Lai, M. F.; Chang, H. C., Electrochemical evaluation of avidin–biotin interaction on self-assembled gold electrodes. *Electrochimica Acta* **2005,** 50, (18), 3660-3666.
56. Mirsky, V. M.; Riepl, M.; Wolfbeis, O. S., Capacitive monitoring of protein immobilization and antigen–antibody reactions on monomolecular alkylthiol films on gold electrodes. *Biosensors and Bioelectronics* **1997,** 12, (9), 977-989.
57. Huang, Y.; Bell, M. C.; Suni, I. I., Impedance biosensor for peanut protein Ara h 1. *Analytical Chemistry* **2008,** 80, (23), 9157-9161.
58. Bonanni, A.; Pumera, M.; Miyahara, Y., Rapid, sensitive, and label-free impedimetric detection of a single-nucleotide polymorphism correlated to kidney disease. *Analytical Chemistry* **2010,** 82, (9), 3772-3779.
59. Cosnier, S.; Mailley, P., Recent advances in DNA sensors. *Analyst* **2008,** 133, (8), 984-991.
60. Lasseter, T. L.; Cai, W.; Hamers, R. J., Frequency-dependent electrical detection of protein binding events. *Analyst* **2004,** 129, (1), 3-8.
61. Ramón-Azcón, J.; Valera, E.; Rodríguez, Á.; Barranco, A.; Alfaro, B.; Sanchez-Baeza, F.; Marco, M., An impedimetric immunosensor based on interdigitated microelectrodes (IDμE) for the determination of atrazine residues in food samples. *Biosensors and Bioelectronics* **2008,** 23, (9), 1367-1373.
62. Numnuam, A.; Kanatharana, P.; Mattiasson, B.; Asawatreratanakul, P.; Wongkittisuksa, B.; Limsakul, C.; Thavarungkul, P., Capacitive biosensor for quantification of trace amounts of DNA. *Biosensors and Bioelectronics* **2009,** 24, (8), 2559-2565.

63. Shen, G.; Tercero, N.; Gaspar, M. A.; Varughese, B.; Shepard, K.; Levicky, R., Charging behavior of single-stranded DNA polyelectrolyte brushes. *Journal of the American Chemical Society* **2006,** 128, (26), 8427-8433.
64. Komura, T.; Yamaguchi, T.; Shimatani, H.; Okushio, R., Interfacial charge-transfer resistance at ionizable thiol monolayer-modified gold electrodes as studied by impedance spectroscopy. *Electrochimica Acta* **2004,** 49, (4), 597-606.
65. Li, C.; Li, X.; Liu, X.; Kraatz, H. B., Exploiting the Interaction of Metal Ions and Peptide Nucleic Acids− DNA Duplexes for the Detection of a Single Nucleotide Mismatch by Electrochemical Impedance Spectroscopy. *Analytical Chemistry* **2010,** 82, (3), 1166-1169.
66. Lee, J. A.; Hwang, S.; Kwak, J.; Park, S. I.; Lee, S. S.; Lee, K.-C., An electrochemical impedance biosensor with aptamer-modified pyrolyzed carbon electrode for label-free protein detection. *Sensors and Actuators B: Chemical* **2008,** 129, (1), 372-379.
67. Cai, H.; Lee, T. M.-H.; Hsing, I., Label-free protein recognition using an aptamer-based impedance measurement assay. *Sensors and Actuators B: Chemical* **2006,** 114, (1), 433-437.
68. Schweiss, R.; Werner, C.; Knoll, W., Impedance spectroscopy studies of interfacial acid–base reactions of self-assembled monolayers. *Journal of Electroanalytical Chemistry* **2003,** 540, 145-151.
69. Burgess, I.; Seivewright, B.; Lennox, R. B., Electric field driven protonation/deprotonation of self-assembled monolayers of acid-terminated thiols. *Langmuir* **2006,** 22, (9), 4420-4428.
70. Schweiss, R.; Pleul, D.; Simon, F.; Janke, A.; Welzel, P. B.; Voit, B.; Knoll, W.; Werner, C., Electrokinetic potentials of binary self-assembled monolayers on gold: acid-base reactions and double layer structure. *The Journal of Physical Chemistry B* **2004,** 108, (9), 2910-2917.
71. Pei, R.; Cheng, Z.; Wang, E.; Yang, X., Amplification of antigen–antibody interactions based on biotin labeled protein–streptavidin network complex using impedance spectroscopy. *Biosensors and Bioelectronics* **2001,** 16, (6), 355-361.

72. Kelley, S. O.; Barton, J. K.; Jackson, N. M.; McPherson, L. D.; Potter, A. B.; Spain, E. M.; Allen, M. J.; Hill, M. G., Orienting DNA helices on gold using applied electric fields. *Langmuir* **1998,** 14, (24), 6781-6784.
73. Kremer, F.; Schönhals, A., *Broadband dielectric spectroscopy*. Springer: 2003.
74. Bordi, F.; Cametti, C.; Colby, R., Dielectric spectroscopy and conductivity of polyelectrolyte solutions. *Journal of Physics: Condensed Matter* **2004,** 16, (49), R1423.
75. Hayashi, Y.; Miura, N.; Isobe, J.; Shinyashiki, N.; Yagihara, S., Molecular dynamics of hinge-bending motion of IgG vanishing with hydrolysis by papain. *Biophysical Journal* **2000,** 79, (2), 1023-1029.
76. Gebbert, A.; Alvarez Icaza, M.; Stoecklein, W.; Schmid, R. D., Real-time monitoring of immunochemical interactions with a tantalum capacitance flow-through cell. *Analytical Chemistry* **1992,** 64, (9), 997-1003.
77. Hu, S. Q.; Xie, Z. M.; Lei, C. X.; Shen, G. L.; Yu, R. Q., The integration of gold nanoparticles with semi-conductive oligomer layer for development of capacitive immunosensor. *Sensors and Actuators B: Chemical* **2005,** 106, (2), 641-647.
78. Wei, D.; Bailey, M. J.; Andrew, P.; Ryhänen, T., Electrochemical biosensors at the nanoscale. *Lab on a Chip* **2009,** 9, (15), 2123-2131.
79. Yang, M.; Kostov, Y.; Bruck, H. A.; Rasooly, A., Gold nanoparticle-based enhanced chemiluminescence immunosensor for detection of Staphylococcal Enterotoxin B (SEB) in food. *International journal of food microbiology* **2009,** 133, (3), 265-271.
80. DeSilva, M. S.; Zhang, Y.; Hesketh, P. J.; Maclay, G. J.; Gendel, S. M.; Stetter, J. R., Impedance based sensing of the specific binding reaction between *Staphylococcus* enterotoxin B and its antibody on an ultra-thin platinum film. *Biosensors and Bioelectronics* **1995,** 10, (8), 675-682.
81. Xu, K.; Huang, J.; Ye, Z.; Ying, Y.; Li, Y., Recent development of nano-materials used in DNA biosensors. *Sensors* **2009,** 9, (7), 5534-5557.
82. Jiang, D.; Tang, J.; Liu, B.; Yang, P.; Kong, J., Ultrathin alumina sol-gel-derived films: allowing direct detection of the liver fibrosis markers by capacitance measurement. *Analytical Chemistry* **2003,** 75, (17), 4578-4584.

83. Syaifudin, A.; Mukhopadhyay, S. C.; Yu, P. L.; Haji-Sheikh, M. J.; Chuang, C. H.; Vanderford, J. D.; Huang, Y. W., Measurements and Performance Evaluation of Novel Interdigital Sensors for Different Chemicals Related to Food Poisoning. *Sensors Journal, IEEE* **2011,** 11, (11), 2957-2965.
84. Hang, T. C.; Guiseppi-Elie, A., Frequency dependent and surface characterization of DNA immobilization and hybridization. *Biosensors and Bioelectronics* **2004,** 19, (11), 1537-1548.
85. Laureyn, W.; Nelis, D.; Van Gerwen, P.; Baert, K.; Hermans, L.; Magnee, R.; Pireaux, J.-J.; Maes, G., Nanoscaled interdigitated titanium electrodes for impedimetric biosensing. *Sensors and Actuators B: Chemical* **2000,** 68, (1), 360-370.
86. Zou, Z.; Kai, J.; Rust, M. J.; Han, J.; Ahn, C. H., Functionalized nano interdigitated electrodes arrays on polymer with integrated microfluidics for direct bio-affinity sensing using impedimetric measurement. *Sensors and Actuators A: Physical* **2007,** 136, (2), 518-526.
87. Roxana Varlan, A.; Suls, J.; Sansen, W.; Veelaert, D.; De Loof, A., Capacitive sensor for the allatostatin direct immunoassay. *Sensors and Actuators B: Chemical* **1997,** 44, (1), 334-340.
88. Maupas, H.; Saby, C.; Martelet, C.; Jaffrezic-Renault, N.; Soldatkin, A. P.; Charles, M. H.; Delair, T.; Mandrand, B., Impedance analysis of Si/SiO_2 heterostructures grafted with antibodies: an approach for immunosensor development. *Journal of Electroanalytical Chemistry* **1996,** 406, (1), 53-58.
89. Kim, J.; Gonzalez-Martin, A., Nanopore membrane-based electrochemical immunoassay. *J Solid State Electrochem* **2009,** 13, (7), 1037-1042.
90. Maupas, H.; Soldatkin, A.; Martelet, C.; Jaffrezic-Renault, N.; Mandrand, B., Direct immunosensing using differential electrochemical measurements of impedimetric variations. *Journal of Electroanalytical Chemistry* **1997,** 421, (1), 165-171.
91. Wang, K. G.; Niu, H., Nanofluidic Channel Fabrication and Manipulation of DNA Molecules. In *Micro and Nano Technologies in Bioanalysis*, Foote, R. S.; Lee, J. W., Eds. Humana Press: 2009; Vol. 544, pp 17-27.
92. Lemay, S. G., Nanopore-based biosensors: the interface between ionics and electronics. *ACS Nano* **2009,** 3, (4), 775-779.

93. Eijkel, J. C.; Van Den Berg, A., Nanofluidics: what is it and what can we expect from it? *Microfluidics and Nanofluidics* **2005,** 1, (3), 249-267.
94. Subramani, A.; Kim, S.; Hoek, E., Pressure, flow, and concentration profiles in open and spacer-filled membrane channels. *Journal of Membrane Science* **2006,** 277, (1), 7-17.
95. Nguyen, B. T. T.; Peh, A. E. K.; Chee, C. Y. L.; Fink, K.; Chow, V. T.; Ng, M. M.; Toh, C. S., Electrochemical impedance spectroscopy characterization of nanoporous alumina dengue virus biosensor. *Bioelectrochemistry* **2012,** 88, 15-21.
96. de la Escosura-Muñiz, A.; Merkoçi, A., Label-free voltammetric immunosensor using a nanoporous membrane based platform. *Electrochemistry Communications* **2010,** 12, (6), 859-863.
97. Rai, V.; Deng, J.; Toh, C. S., Electrochemical nanoporous alumina membrane-based label-free DNA biosensor for the detection of *Legionella sp*. *Talanta* **2012,** 98, 112-117.
98. Wang, L.; Liu, Q.; Hu, Z.; Zhang, Y.; Wu, C.; Yang, M.; Wang, P., A novel electrochemical biosensor based on dynamic polymerase-extending hybridization for *E. coli O157: H7* DNA detection. *Talanta* **2009,** 78, (3), 647-652.
99. Takmakov, P.; Vlassiouk, I.; Smirnov, S., Hydrothermally shrunk alumina nanopores and their application to DNA sensing. *Analyst* **2006,** 131, (11), 1248-1253.
100. Kuo, T. C.; Cannon, D. M.; Chen, Y.; Tulock, J. J.; Shannon, M. A.; Sweedler, J. V.; Bohn, P. W., Gateable nanofluidic interconnects for multilayered microfluidic separation systems. *Analytical Chemistry* **2003,** 75, (8), 1861-1867.
101. Pu, Q.; Yun, J.; Temkin, H.; Liu, S., Ion-enrichment and ion-depletion effect of nanochannel structures. *Nano Letters* **2004,** 4, (6), 1099-1103.
102. de la Escosura-Muñiz, A.; Merkoçi, A., A Nanochannel/Nanoparticle-Based Filtering and Sensing Platform for Direct Detection of a Cancer Biomarker in Blood. *Small* **2011,** 7, (5), 675-682.
103. Siwy, Z.; Heins, E.; Harrell, C. C.; Kohli, P.; Martin, C. R., Conical-nanotube ion-current rectifiers: the role of surface charge. *Journal of the American Chemical Society* **2004,** 126, (35), 10850-10851.

104. Lee, S. B.; Martin, C. R., Electromodulated molecular transport in gold-nanotube membranes. *Journal of the American Chemical Society* **2002,** 124, (40), 11850-11851.
105. Lee, S. B.; Mitchell, D. T.; Trofin, L.; Nevanen, T. K.; Söderlund, H.; Martin, C. R., Antibody-based bio-nanotube membranes for enantiomeric drug separations. *Science* **2002,** 296, (5576), 2198-2200.
106. Yu, S.; Lee, S. B.; Kang, M.; Martin, C. R., Size-based protein separations in poly (ethylene glycol)-derivatized gold nanotubule membranes. *Nano Letters* **2001,** 1, (9), 495-498.
107. Fan, R.; Yue, M.; Karnik, R.; Majumdar, A.; Yang, P., Polarity switching and transient responses in single nanotube nanofluidic transistors. *Physical Review Letters* **2005,** 95, (8), 086607.
108. Karnik, R.; Fan, R.; Yue, M.; Li, D.; Yang, P.; Majumdar, A., Electrostatic control of ions and molecules in nanofluidic transistors. *Nano Letters* **2005,** 5, (5), 943-948.
109. Masuda, H.; Yamada, H.; Satoh, M.; Asoh, H.; Nakao, M.; Tamamura, T., Highly ordered nanochannel-array architecture in anodic alumina. *Applied Physics Letters* **1997,** 71, (19), 2770-2772.
110. Losic, D.; Velleman, L.; Kant, K.; Kumeria, T.; Gulati, K.; Shapter, J. G.; Beattie, D. A.; Simovic, S., Self-ordering Electrochemistry: A Simple Approach for Engineering Nanopore and Nanotube Arrays for Emerging Applications. *Australian Journal of Chemistry* **2011,** 64, (3), 294-301.
111. Nguyen, B. T. T.; Peh, A. E. K.; Chee, C. Y. L.; Fink, K.; Chow, V. T. K.; Ng, M. M. L.; Toh, C. S., Electrochemical impedance spectroscopy characterization of nanoporous alumina dengue virus biosensor. *Bioelectrochemistry* **2012,** 88, (0), 15-21.
112. Masuda, H.; Fukuda, K., Ordered Metal Nanohole Arrays Made by a Two-Step Replication of Honeycomb Structures of Anodic Alumina. *Science* **1995,** 268, (5216), 1466-1468.
113. Zhang, J.; Li, C. M., Nanoporous metals: fabrication strategies and advanced electrochemical applications in catalysis, sensing and energy systems. *Chemical Society Reviews* **2012,** 41, (21), 7016-7031.

114. Li, A.; Müller, F.; Birner, A.; Nielsch, K.; Gösele, U., Hexagonal pore arrays with a 50–420 nm interpore distance formed by self-organization in anodic alumina. *Journal of Applied Physics* **1998,** 84, (11), 6023-6026.
115. Losic, D.; Losic Jr, D., Preparation of porous anodic alumina with periodically perforated pores. *Langmuir* **2009,** 25, (10), 5426-5431.
116. Furneaux, R.; Rigby, W.; Davidson, A., The formation of controlled-porosity membranes from anodically oxidized aluminium. *Nature* **1989,** 337, (6203), 147-149.
117. Lee, W.; Kim, J. C., Highly ordered porous alumina with tailor-made pore structures fabricated by pulse anodization. *Nanotechnology* **2010,** 21, (48), 485304.
118. Lee, W.; Kim, J. C.; Gösele, U., Spontaneous current oscillations during hard anodization of aluminum under potentiostatic conditions. *Advanced Functional Materials* **2010,** 20, (1), 21-27.
119. Lee, K.; Tang, Y.; Ouyang, M., Self-ordered, controlled structure nanoporous membranes using constant current anodization. *Nano Letters* **2008,** 8, (12), 4624-4629.
120. Choi, J.; Wehrspohn, R. B.; Gösele, U., Mechanism of guided self-organization producing quasi-monodomain porous alumina. *Electrochimica Acta* **2005,** 50, (13), 2591-2595.
121. Md Jani, A. M.; Losic, D.; Voelcker, N. H., Nanoporous anodic aluminium oxide: Advances in surface engineering and emerging applications. *Progress in Materials Science* **2013,** 58, (5), 636-704.
122. Li, A.; Müller, F.; Gösele, U., Polycrystalline and monocrystalline pore arrays with large interpore distance in anodic alumina. *Electrochemical and Solid-State Letters* **2000,** 3, (3), 131-134.
123. Berger, S.; Tsuchiya, H.; Schmuki, P., Transition from nanopores to nanotubes: self-ordered anodic oxide structures on titanium− aluminides. *Chemistry of Materials* **2008,** 20, (10), 3245-3247.
124. Lee, W.; Ji, R.; Gösele, U.; Nielsch, K., Fast fabrication of long-range ordered porous alumina membranes by hard anodization. *Nature materials* **2006,** 5, (9), 741-747.

125. Lee, W.; Schwirn, K.; Steinhart, M.; Pippel, E.; Scholz, R.; Gösele, U., Structural engineering of nanoporous anodic aluminium oxide by pulse anodization of aluminium. *Nature Nanotechnology* **2008,** 3, (4), 234-239.
126. Losic, D.; Simovic, S., Self-ordered nanopore and nanotube platforms for drug delivery applications. *Expert opinion on drug delivery* **2009,** 6, (12), 1363-1381.
127. Adiga, S. P.; Jin, C.; Curtiss, L. A.; Monteiro-Riviere, N. A.; Narayan, R. J., Nanoporous membranes for medical and biological applications. *Wiley Interdisciplinary Reviews: Nanomedicine and Nanobiotechnology* **2009,** 1, (5), 568-581.
128. Ghicov, A.; Schmuki, P., Self-ordering electrochemistry: a review on growth and functionality of TiO2 nanotubes and other self-aligned MOx structures. *Chemical Communications* **2009**, (20), 2791-2808.
129. Hebert, K. R.; Albu, S. P.; Paramasivam, I.; Schmuki, P., Morphological instability leading to formation of porous anodic oxide films. *Nature materials* **2012,** 11, (2), 162-166.
130. Su, Z.; Hähner, G.; Zhou, W., Investigation of the pore formation in anodic aluminium oxide. *Journal of Materials Chemistry* **2008,** 18, (47), 5787-5795.
131. Houser, J. E.; Hebert, K. R., The role of viscous flow of oxide in the growth of self-ordered porous anodic alumina films. *Nature materials* **2009,** 8, (5), 415-420.
132. Abgrall, P.; Nguyen, N. T., Nanofluidic devices and their applications. *Analytical Chemistry* **2008,** 80, (7), 2326-2341.
133. Han, A.; de Rooij, N. F.; Staufer, U., Design and fabrication of nanofluidic devices by surface micromachining. *Nanotechnology* **2006,** 17, (10), 2498.
134. Goldberger, J.; Fan, R.; Yang, P., Inorganic nanotubes: a novel platform for nanofluidics. *Accounts of chemical research* **2006,** 39, (4), 239-248.
135. Kong, Y.; Fan, X.; Zhang, M.; Hou, X.; Liu, Z.; Zhai, J.; Jiang, L., Nanofluidic diode based on branched alumina nanochannels with tunable ionic rectification. *ACS Applied Materials and Interfaces* **2013,** 5, (16), 7931-7936.
136. Santra, T.; Tseng, F., Recent Trends on Micro/Nanofluidic Single Cell Electroporation. *Micromachines* **2013,** 4, (3), 333-356.

137. Mijatovic, D.; Eijkel, J. C. T.; van den Berg, A., Technologies for nanofluidic systems: top-down vs. bottom-up-a review. *Lab on a Chip* **2005,** 5, (5), 492-500.
138. Kim, C. S.; Ahn, S. H.; Jang, D. Y., Review: Developments in micro/nanoscale fabrication by focused ion beams. *Vacuum* **2012,** 86, (8), 1014-1035.
139. Sievila, P.; Chekurov, N.; Tittonen, I., The fabrication of silicon nanostructures by focused-ion-beam implantation and TMAH wet etching. *Nanotechnology* **2010,** 21, (14).
140. Cross, J.; Craighead, H., Micro- and Nanofluidics for Biological Separations. In *CMOS Biotechnology*, Lee, H.; Westervelt, R.; Ham, D., Eds. Springer US: 2007; pp 31-75.
141. Salieb-Beugelaar, G. B.; Dorfman, K. D.; van den Berg, A.; Eijkel, J. C. T., Electrophoretic separation of DNA in gels and nanostructures. *Lab on a Chip* **2009,** 9, (17), 2508-2523.
142. Fu, J.; Mao, P.; Han, J., Nanofilter array chip for fast gel-free biomolecule separation. *Applied Physics Letters* **2005,** 87, (26), -.
143. Lopez, G. P.; Brueck, S. R.; Ista, L. K., Nanostructured separation and analysis devices for biological membranes. In Google Patents: 2005.
144. Khandurina, J.; Jacobson, S. C.; Waters, L. C.; Foote, R. S.; Ramsey, J. M., Microfabricated porous membrane structure for sample concentration and electrophoretic analysis. *Analytical Chemistry* **1999,** 71, (9), 1815-1819.
145. Foote, R. S.; Khandurina, J.; Jacobson, S. C.; Ramsey, J. M., Preconcentration of proteins on microfluidic devices using porous silica membranes. *Analytical Chemistry* **2005,** 77, (1), 57-63.
146. Kim, T.; Meyhöfer, E., Nanofluidic concentration of selectively extracted biomolecule analytes by microtubules. *Analytical Chemistry* **2008,** 80, (14), 5383-5390.
147. Stagni, C.; Guiducci, C.; Benini, L.; Riccò, B.; Carrara, S.; Samorí, B.; Paulus, C.; Schienle, M.; Augustyniak, M.; Thewes, R., CMOS DNA sensor array with integrated A/D conversion based on label-free capacitance measurement. *Solid-State Circuits, IEEE Journal of* **2006,** 41, (12), 2956-2964.

148. Wang, S. W.; Lin, C. H.; Yang, Y. S.; Lu, M. C. In *A CMOS capacitive dopamine sensor with Sub-nM detection resolution*, Sensors, IEEE, **2009**; pp 400-404.
149. Carrara, S., Nano-bio-technology and sensing chips: new systems for detection in personalized therapies and cell biology. *Sensors* **2010,** 10, (1), 526-543.
150. Carrara, S.; Cavallini, A.; Leblebici, Y.; De Micheli, G.; Bhalla, V.; Valle, F.; Samorì, B.; Benini, L.; Riccò, B.; Vikholm-Lundin, I., Capacitance DNA bio-chips improved by new probe immobilization strategies. *Microelectronics Journal* **2010,** 41, (11), 711-717.
151. Schienle, M.; Paulus, C.; Frey, A.; Hofmann, F.; Holzapfl, B.; Schindler-Bauer, P.; Thewes, R., A fully electronic DNA sensor with 128 positions and in-pixel A/D conversion. *Solid-State Circuits, IEEE Journal of* **2004,** 39, (12), 2438-2445.
152. Tokuda, T.; Noda, T.; Sasagawa, K.; Ohta, J., Optical and electric multifunctional CMOS image sensors for on-chip biosensing applications. *Materials* **2010,** 4, (1), 84-102.
153. Manickam, A.; Chevalier, A.; McDermott, M.; Ellington, A. D.; Hassibi, A. In *A CMOS electrochemical impedance spectroscopy biosensor array for label-free biomolecular detection*, IEEE **2010;** pp 130-131.
154. Wang, H.; Chen, Y.; Hassibi, A.; Scherer, A.; Hajimiri, A. In *A frequency-shift CMOS magnetic biosensor array with single-bead sensitivity and no external magnet*, Solid-State Circuits Conference-Digest of Technical Papers (ISSCC), IEEE International, **2009**; pp 438-439,439 a.
155. Manickam, A.; Chevalier, A.; McDermott, M.; Ellington, A. D.; Hassibi, A. In *A CMOS electrochemical impedance spectroscopy biosensor array for label-free biomolecular detection*, Solid-State Circuits Conference Digest of Technical Papers (ISSCC), IEEE International, IEEE **2010;** pp 130-131.

Chapter 2

EXPERIMENTAL TECHNIQUES

Book Chapter:

K. Kant, D. Losic, *Focused Ion Beam (FIB) technology for micro and nanoscale fabrications Book:* "Lecture notes in Nanoscale Science and Nanotechnology", Eds. Z.M. Wang, A. Wang, G. Salamo, K. Kishimito, S. Belluci, Y.I. Park, Springer, 2013. (Invited)

2.1 Electrochemical Impedance spectroscopy: practical considerations

The ratio between the changes in voltage to its resulting incremental variation in current can be defined as impedance. It is also termed as the reciprocal slope of the current and voltage (I-V) curve. It can be defined mathematically in an equation, if applied voltage (V) and current is written as:

$$V = V_{DC} + V_{AC}\sin(\omega t) \qquad (2.1)$$

$$I = I_{DC} + I_{AC}\sin(\omega t - \phi) \qquad (2.2)$$

The impedance can be defined as $Z(\omega)$ and has magnitude of V_{AC}/I_{AC} and phase angle (ϕ) as defined in Eq-1. Impedance also depends on both applied (V) and the frequency (ω) of measurement. Impedance spectroscopy is not the measurement at one frequency but the repeating measurement process at different frequencies which generate a combined impedance $Z(\omega)$. The applied voltage in EIS measurements is small and it causes imaginary impedances in the system (through the solution) and work in parallel in the impedance measurement. The applied frequencies are important in the measurement as the electrode to electrolyte interface is strongly dependent on ω rather than the applied voltage [1].

However, while taking the impedance measurements on the biosensing device the applied voltage V should be small. There are many reasons explained previously by the investigators. Sometime current and voltage relationship in the system shows linear response for a small region [2, 3]. When impedance signal is based on the change in the V then the impedance of that system cannot be defined uniquely. In case of Faradaic measurements it is been defined in Section 2.1.2 of this chapter, always show nonlinearity because the electron transfer generally

depends on the oxidation on the sample surface and applied potential [4, 5]. The sample surface is another reason for not applying very high *V* because it is not good idea to create any changes on the sample surface due to high voltage. In some of the surface modification target molecules are covalent bonded on the surface and the covalent bonding energies in order of 1–3 eV or much less than the applied voltages, which can generate a force on charged molecules in the system. It also applies to the electrode-solution interface. To perform a good electrochemical measurement on the sample it is always important to keep in account that bio-molecular sensing layer is not damaged or disturbed. This is an important advantage of impedance spectroscopy over voltammetry or amperometry methods [6-8].

2.1.1. Instrumentation and electrodes used in this work

A minimum of two electrodes are required to measure the impedance of any electrolyte solution or sample. Many researchers also used three or more electrodes to avoid signal to noise ratio while measurement. Usually bio-functionalized electrode is the working electrode or electrode with the molecules of interest. The current is always measured at the working electrode. The electrical contact is generally made by the electrolyte solution in between the two electrodes (working and counter). Most of the investigators used a reference electrode for the reproducible electrical signal between electrode and electrolyte solution. Silver-silver chloride electrodes are the most common type of reference electrodes used in such type of measurements because built-in potential of the Ag/AgCl interface is almost constant and not make any further interruption in signal [9, 10]. In the impedance measurement it is important to keep in mind that the counter electrode should have higher surface area than the working electrode

so that it can easily supply the required current. The integration of counter and reference electrodes is possible if reference electrode is capable of supplying required current through it in the system [11]. If we combine the electrodes the 3-electrode measurement can be a 2-electrode measurement. In this case, the combined impedance of both electrodes and solution is measured, but in a 3 or 4 electrode impedance measurements only the impedance between the working electrode and reference electrode been measured. In this work the Inphaze impedance spectroscope is been used, developed and provided by Australian company Inphaze Pyt. Ltd. (Figure 2.1).

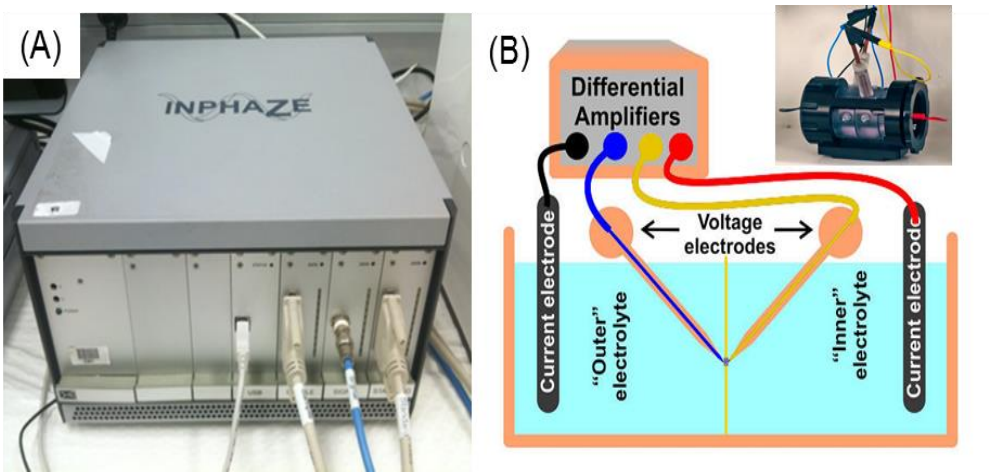

***Figure 2.1**: (a) Inphaze impedance spectroscope (b) four electrode cell designed for impedance measurement.*

Impedance spectroscopy is a complete circuit that applies voltage between the solution and electrode and at the same time it measures the current flowing between electrodes. The working electrode is just to provide connection for the impedance amplifier system and the applied voltage across the electrode-electrolyte measures the resulting current in the system as response of impedance data. It works as a simple potentiostat, which is used to measure AC impedance

over a range of frequencies from 10^{-2} - 10^{6} Hz. Computer controlled software of EIS analyser provides digital signals for further processing of generated data.

2.1.2. Faradaic vs. non-Faradaic impedance biosensing

In a real system of electrode-solution interfaces there exists both Faradaic and non-Faradaic components at same time; however impedance spectroscopy only represents them one at a time. A non-Faradaic interface is available if the measurement changes are due to capacitance in the system and Faradaic interface if measurement is based on resistance. It is essential to distinguish between non-Faradaic and Faradaic type of biosensors, if sensing is dependent on the impedance. The Faradaic process can be termed as one process where charge is transported across an interface in form of an electron transfer in between, either from the electrode to an ion solution or from solution to electrodes. In case of Faradaic process a redox probe is used to oxidize and reduce one of the electrodes by the transfer of an electron from the surface of metal electrode. In the case of Faradaic EIS, it requires a redox-active species rather than the marker reagent which are required for non-Faradaic impedance spectroscopy. The non-Faradaic types of measurements are more useful for point-of-care applications and easy for commercial use. Capacitive biosensors always work as non-Faradaic sensors which are capable of taking measurements at a single point of frequency.

2.1.3. Modeling and EIS Data fitting

The impedance data can be interpreted in many different ways on the basis of their measured impedance spectrum which can be used to extract values of capacitance and resistance without any particular defined model [6, 12]. In Figure 2.2 a typical circuit model shows the equivalent circuit for impedance data, and

Figure 2.3 shows an example of impedance data after modelling. It is not always an exact equivalent circuit for the impedance data, even though sometimes the best models for the system does not fit measurements for some points of frequency and require other fitting parameters.

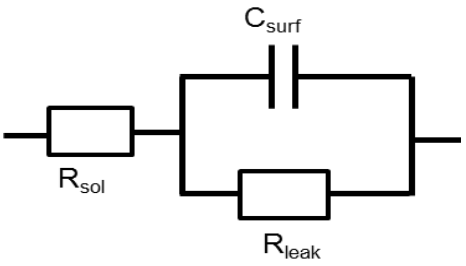

Figure 2.2*: Typical circuit model used for the impedance measurements.*

The raw data of the impedance measurement is used to extract the graph by fitting with the equivalent circuit model. The sensing signal of the system depends on the changes in a particular model element. The fitting of the impedance data some time incorporate both magnitude and phase angle of the measurement in the fitting, which is done mostly by the instrument inbuilt software. In previous studies many researchers had interpreted the data according to their own way, there is not any particular guide line for interpretation of impedance spectra, it is sometimes more art than science [13]. There are two common ways of representing the impedance data either impedance data as magnitude/phase plots vs. frequency (e.g. Figure 2.3b) or Nyquist plots in which the impedance values are plotted as a complex of impedance and phase angle and each data point represent the impedance at a different frequency (Figure 2.3a) [14]. In an equivalent circuit the circuit elements and actual system processes is often experimental and different from any other physical effects into a single model element [14]. If the solution resistance is written as (R_{sol}), which represent

the ions of bulk solution and is responsible for the applied voltage in the system not affected by any target binding molecules.

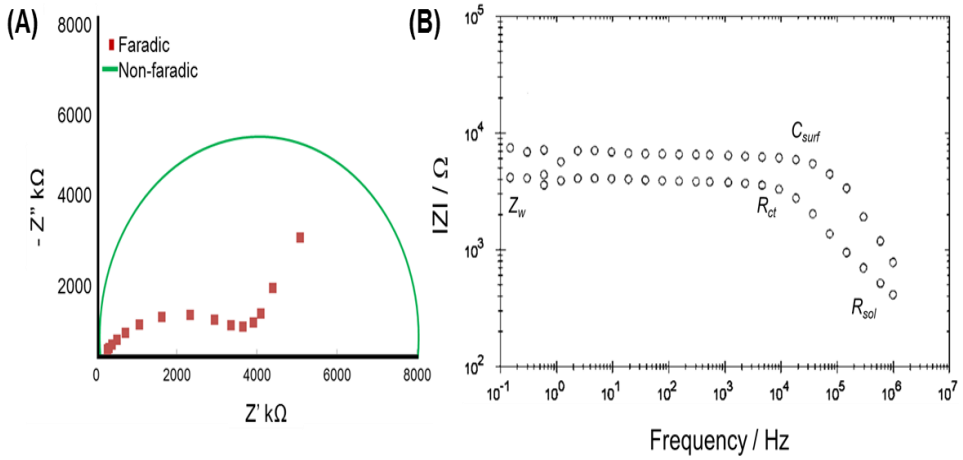

Figure 2.3: *(a) An example of typical Nyquist plots generated by the simulation of impedance data either non-Faradaic or Faradaic. (b) Plot of Impedance IZI with frequency.*

The generated capacitance by applying voltage between the ions in solution and metal electrodes can be modelled by use of equivalent circuit as capacitance, ionic double layer capacitance and surface modification. The sensor geometry and solution conductivity is key point in the measurement. The prediction of solution resistance which is calculable from diffusion coefficients of constituent ions and these calculated values are treated as a fitting parameter in modelling. The ionic double layer capacitance generated from the electrostatic attraction of ions in solution to a charged electrode. The surface capacitance (C_{surf}) is often modelled by a constant phase element (CPE) rather than a real system capacitance. The surface resistive path (R_{leak}) has also been modelled along with the surface capacitance for non-Faradaic sensors. Although R_{leak} is theoretically infinite if no redox species are present. In Faradaic type of EIS the *Warburg impedance* (Z_w) is only of physical significance in the system. The *charge transfer resistance*, R_{ct}, encodes the resistance corresponding to the

electron transfer between electrode and the relevant redox species. Its value is an expression of energy potential which is directly related with the oxidation or reduction happened on the electrode surface. There are two types of circuit elements used to indicate affinity binding of target molecules in impedance biosensors are surface capacitance for non-Faradaic biosensors and charge transfer resistance in case of Faradaic biosensors.

2.1.4. Constant phase element (CPE)

It's been observed that the impedance measurement for solid electrodes are usually differs from its real capacitive behaviour. The actual behaviour is modelled as a *CPE* which is given as:

$$Z_{CPE} = \frac{1}{I\omega} mA \qquad (2.3)$$

A is analogous to a capacitance and (ω) is expressed as frequency in rad/sec, and *m* is the so-called constant phase element (CPE) parameter. A CPE can be thought of as a frequency-dependent resistor against a pure capacitor and can be modelled as a network of resistors and capacitors over a range of frequencies. CPE for solid electrodes can be explained mathematically by modelling the experimental values as dispersion in capacitance values. The surface roughness at microscopic level can cause CPE effect, but some researchers suggested that a small change in ion adsorption or alteration in chemical concentration can make big changes [15]. A recent article summarizes these effects and demonstrates that the composite electrode impedance can have a CPE character even if the localized impedance is strictly capacitive [16]. Most of the solid electrodes are probable to have a certain level of CPE behaviour, and thus modelling of electrode-solution interface can help in reducing this effect.

2.1.5. Double-layer capacitance in EIS

When a charged surface is in contact with an electrolyte, it attracts ions of opposite polarity. This attractive tendency is opposed by the randomized thermal motion of the ions, resulting in a build-up of ions with opposite charge near the surface. This local charge imbalance prevents the electric field emanating from the charged surface from penetrating very far into solution. The characteristic length of this spatial decay of the electric field is called as *Debye length*. It was observed that the locally-enhanced population of ions acts like second plate of a capacitor, and the charge-voltage ratio is termed as double layer capacitance.

2.1.6. Biosensor response and time curves

The response curve in affinity biosensor arises from two separate relations of sensor output and the sample target concentration. One of it is related to the affinity step of target molecules, which leads towards the sample surface coverage in bulk target concentration and other one is resembles to the final impedance. Till now most of literature has predicted the change in impedance as ΔZ. It is expected that the sensor output is related to the concentration of target molecules. It has been observed that the response curve is logarithmic in *Target* concentration until saturation [17]. The Langmuir isotherm was also been used to get good fits of experimental data into the model circuit [18, 19]. There is always a question about the binding of target molecules whether is it controlled kinetically or it achieves the equilibrium in the reaction. The understanding of this binding nature of the target molecules can improve the sensing capacity of affinity biosensors. After long period of research still there is no standard method to determine response curves for biosensors [20]. It is expected that there might be some methods which

may introduce some variation in sensing by regenerating the layer of probe molecule in the system. These types of methods of regeneration are expected to represent biosensor in the day to day life [21].

The time scale of response is approximately given by the square of the Debye length divided by the diffusion constant of the ions. For ions with $D = 2\times10^{-5}$ cm^2/sec and Debye length of 1 nm, the time scale is about 0.5 ns, corresponding to RF frequencies. These time scales can be significantly longer and depend on the thickness of the Stern layer, electrode geometry, and electrode spacing. However, for frequencies of interest in impedance biosensors it is safe to assume that the ionic double layer responds instantaneously to the applied voltage [22].

2.1.7. Scaling electrode size

The size of the electrode directly impacts on the magnitude of measured impedance, and it should be chosen with extra care. While measuring over range of frequencies generated data which is more reliable and useful. It is also important to have frequency range accordingly. Sometime measurements at higher frequencies are good as there is very less chances to be effected by the drift and noise during measurements, but on other hand it also complicates the measured data and increase the chances of errors from other parasitic capacitances and inductances. It is not yet defined about the biomolecules whether they are frequency dependent or not [23]. There are some contradiction in the measurements in impedance as investigators reported unexplained impedance drift at frequency range 100 Hz or lower but at same time other investigators did their measurements successfully. The capacitive impedance can be altered by making

change in the electrode area or insulator thickness at higher frequencies. The impedance can also be altered by making variation in the concentration of the electrolyte, such as salt concentration increases the R_{sol} decreases. This mainly affects measurements taking place at high frequencies. So reducing the size of the biosensor may more likely shift impedance curve towards the high frequency measurement. However, it will also affect the surface capacitance over the frequencies

Madou et al, described a concept of biosensor miniaturization and scaling up other various kinds of electrical and impedance biosensors [23]. There is another important thing to keep in mind while reducing size of biosensors that, it also reduces the surface area for probe molecules and number of sites for target molecules to bind. It is always expected that target binding remain constant in measurements otherwise it will be very difficult to measure the changes which are dependent on the signal to noise ratio or impedance drift [24]. Also, decreasing the number of probes will increase the stochastic noise of probe-target binding. However, small geometries may be beneficial for reducing diffusion times and increasing the density of multiplexed biosensors [25]. This lack of knowledge currently inhibits the identification of optimum parameters for sensor design.

2.2. Focused Ion Beam (FIB)

2.2.1. Principle of FIB system

A FIB system is consist of an ion source, ion optics, a sample stage and a vacuum chamber with high power turbo motor to generate high end vacuum (Figure 2.4) [26]. A FIB system is similar to the SEM as both of these instruments are based on a focused electron beam for imaging and an ion beam for the FIB

fabrications. The operating ion beam in FIB is based on liquid metal ion source (LMIS) of gallium (Ga^+) which is positioned in close contact with Tungsten (W) needle. When an electric field of ($>10^8$ V/cm) is applied the Ga^+ started to get in liquid the needle and flows towards the tip (5-10 nm) of the needle. The use of Ga^+ has several advantages: (i) Ga^+ low melting point so it almost in the liquid state lose to room temperature (ii) it can also be forced to flow through very small pore size in nano dimension.

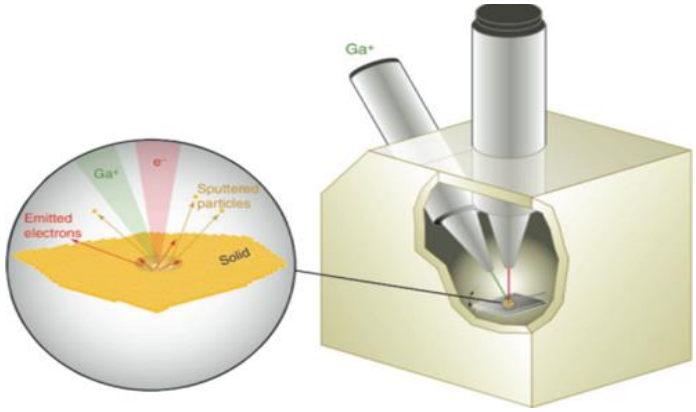

Figure 2.4: *Schematic illustration of a dual-beam FIB–SEM instrument. Expanded view shows the electron and ion beam sample interaction [26].*

The accelerating voltage for FIB generally lies between 5 to 50 keV. The controlling of the electrostatic lenses and adjusting its effective aperture sizes, the ion current density can be changed from some pA to the several nA. The ion of the beam collides with the surface atoms and transfers its energy to the surface electrons. The physical effect due to this collision of ions are known as sputtering of ionized atoms from substrates surface which lead to the substrate milling, the electrons which are emitted as secondary electrons provide the imaging of surface and also make sample charged. In the presence of gases chemical interactions between the surface and breaking of their chemical bonds helps in the deposition process of ion milling.

2.2.2. The FIB instrument description

FIB (FEI Helios NanoLab) have a high vacuum system, a chamber with sample stage, LMIS source, neutral or reactive gas jet and a computer to run the complete instrument [27]. The configuration is similar to an SEM and the only difference is the use of a gallium ion (Ga^{+}) beam rather than normal ion source. The operating extraction current is 2 μA and extraction voltage is up to 7000 V. The sample stage is a motorized stage inside the vacuum chamber. The chamber is divided in two parts with the valve, one is beam line chamber and other one is working chamber for sample loading and unloading. Under normal operating conditions chamber vacuum is up to 10^{-7} mbar.

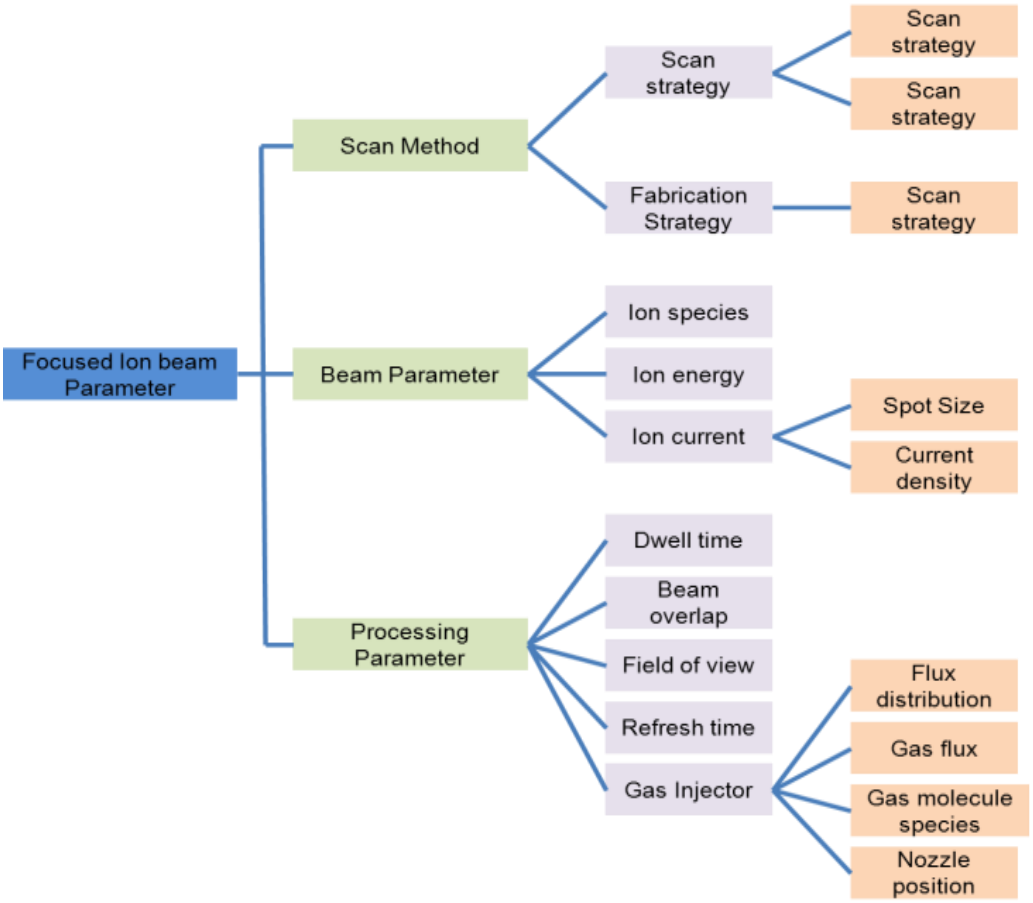

Table: 2.1: *Classification of FIB parameters [27].*

To maintain the vacuum inside the beam chamber the valve gets closed while loading or unloading the sample. The ion source column is separated with one pump to create high vacuum. Most of FIB systems can deliver a variety of gases in working stage to help milling of the sample surface. The gas containers are directly connected to a gas jet which is available inside the chamber. Most of the gases are used for fast and selective etching on the sample surface, as well as for the deposition of metal [27]. There are number of parameters responsible for efficiency and structural stability, investigated by many authors, as shown in Table 2.1.

2.2.3. Imaging, milling and deposition by FIB

The FIB is used to scan over a substrate, and secondary electrons are generated form the surface of the sample and used for imaging purpose (Figure 2.5a) [28]. The detector for collecting secondary ion scan is positive or negative depending on the sample surface. These secondary electrons are also used in the secondary ion mass spectroscopy (SIMS). In FIB imaging small amount of Ga^+ ions collision with sample surface leads to the huge numbers of secondary electrons to leave the sample surface which helps to generate a high resolution image. The resolution of images also depends on the spot size of the ion beam which is generally below 10 nm. The removal of sample material and making patterns and structures can be achieved by using a high current ion beam. The result of high current FIB is that the high mass atoms of material come out and leave empty space at the site as shown in schematic Figure 2.5 b. By scanning over the sample in a particular manner it is possible to produce any type of shape or structure in surface. The angle of incidence ion beam is very important in

sputtering yield. The angle of ion beam increases by 1/ cos (θ), where θ is the angle of incidence beam and ion beam direction [28].

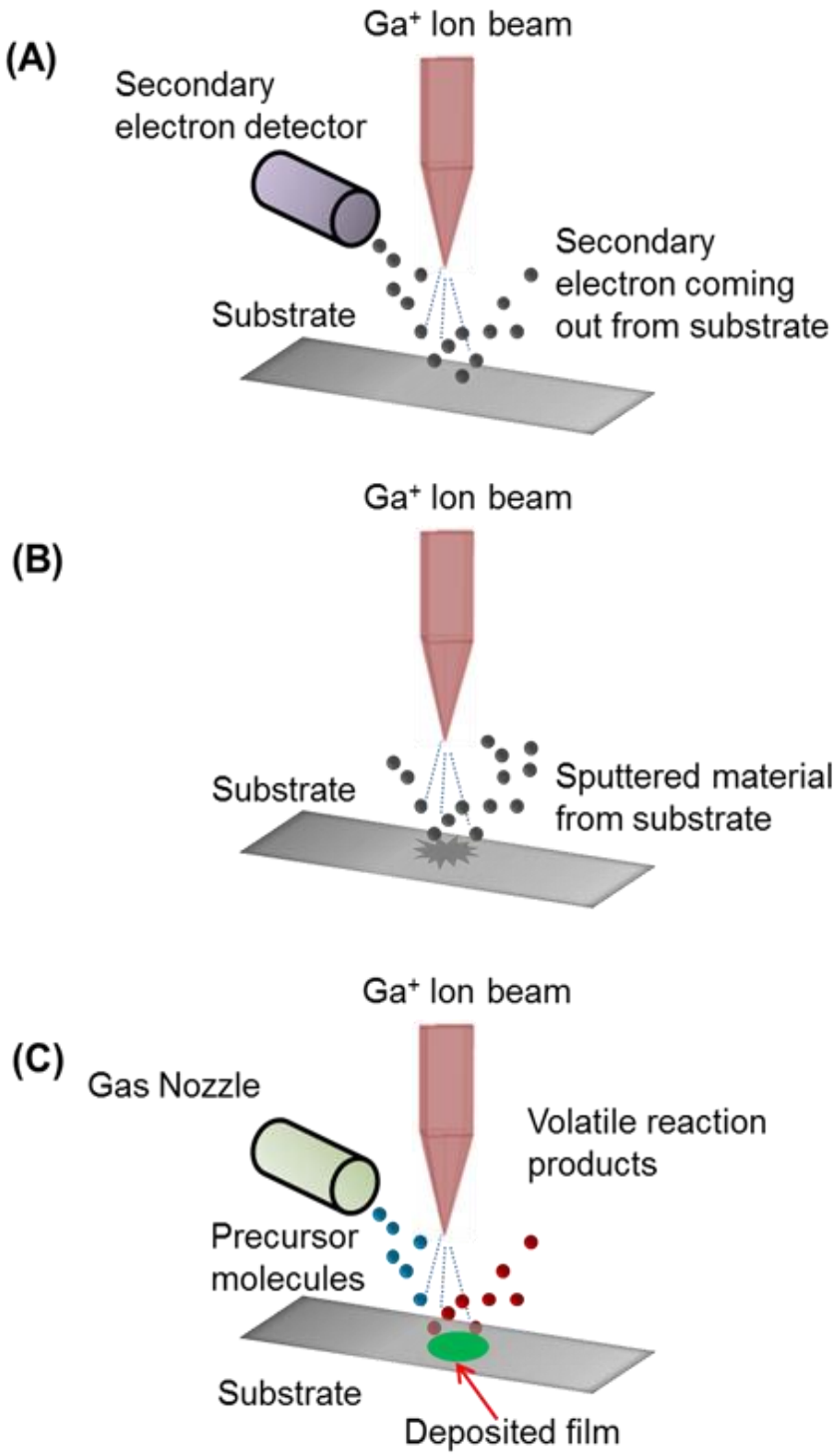

Figure 2.5: *Principle of FIB (a) imaging, (b) milling and (c) deposition [28].*

At the end of the milling process an insulator will appear dark in the SEM image than a conductor because conductor loses secondary electrons readily. The resolution of imaging during the milling process only few nanometers with aspect ratio of the milled holes is up to 10–20 nm. The etching gas can be useful to increase the rate of milling or selectivity of ion beam towards materials by chemical removal of reaction products. This is called as gas-assisted etching (GAE). FIB provides the capability of localized mask-free deposition of metal and insulator materials. It works on the chemical vapor deposition (CVD) technique or is similar to laser induced CVD. But in FIB a higher resolution with lower deposition rate can be achieved. Generally Pt and tungsten is used for deposition in FIB system. The deposition process is shown schematically in Figure 2.5c.

2.2.4. FIB patterning on nanopore alumina (NPA) arrays

In recent years, NPA fabrication by self-organized electrochemical anodization process, which produces nanopores of hexagonal arrangement, has been developed. This has created huge potential to be used for many applications including molecular separations, biosensing, energy storage, photonics, drug delivery and template synthesis. However this fabrication process has limitations related to pores diameter, pore inter-distance, pore patterns and shapes. To address this problem FIB based lithography combined with the anodization process has been developed. FIB lithography on silicon has been demonstrated to produce patterns of ordered NPA with controlled inter-pore distances and patterns. The depths of the FIB patterns are from 5 - 20 nm for pore growth during anodization. With the FIB, gradation in the size and shape (rectangle, square, and circle) can be easily achieved with the array of the nano patterns [29-32]. Therefore the

fabrication of pores with different pores sizes, inter-pore distances, shapes and patterns is possible by combining FIB and anodization method [33, 34]. The oxide wall thickness between two nanopores is counted as 2 d_w and the barrier layer thickness for the same can be define as d_B and controlled by the anodization voltage (Figure 2.6). The implantation of Ga^+ into the Al plays important role in growth of nanopore.

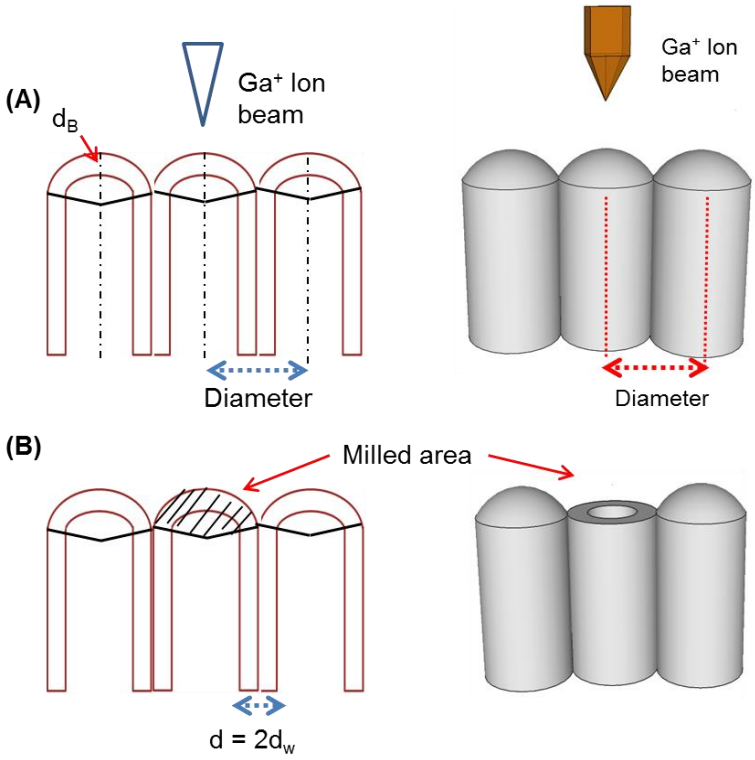

Figure 2.6: *Schematic diagram of the concept of using focused ion-beam technique (FIB) for fabrication of single nanopore and nanopore arrays using NPA as substrate (a) inter-pore distance and diameter of the nanopore (b) FIB milled barrier layer of alumina nanopores by removing of barrier.*

The FIB patterned Al foils get anodized in 0.3 M oxalic acid at 60-80 V for 5 min and characterized by SEM. In FIB guided anodization oxide walls of the nanopores make different large and small concaves which restrict the growth of other nanopore. The higher diameter represents the large amount of Ga^+ ion implantation. Based on this concept the FIB has been combined with other

synthetic approaches including chemical vapor, atomic layer and electrochemical deposition to grow nanotubes pattern on a substrate [35]. In addition to the FIB guided anodization method there is another approach to use FIB for fabrication of NPA with single or nanopore arrays. This method is based on the pore opening from the bottom side of NPA by FIB milling and presented in Figure 2.6. To obtain a single nanopore opening on NPA the ion-beam milling carrier out at the middle of a single NPA cell using a 30 keV Ga^{+} ion beam at low beam current of 1.5 pA for a very short duration of time. The milling of a single nanopore is very challenging and needs high precision and very fine position adjustments of ion beam.

2.3. Photolithography for microchannel fabrication

Nanofabrication techniques include top-down and bottom-up approaches and various hybrids. Top-down approaches refer to the conventional or new techniques, such as conventional photolithography, focused ion beam lithography (FIB), e-beam lithography (EBL), nanoimprint lithography and atomic force microscopy (AFM) lithography. Bottom-up approaches make use of materials, such as nanoparticles, DNA to directly assemble and make patterns. A new hybrid approach is the integration of top-down and bottom-up approaches which provides an alternative approach to reduce cost and create complex architectures. Photolithography is generally refers to a process which is used in micro fabrication to selectively remove parts in thin film. It uses a light source projected through a patterned mask onto a substrate. First, a substrate is spin-coated with a thin film of photoresist and an ultraviolet (UV) light is projected onto the photoresist film through a mask. The exposed area of photoresist is chemically

changed due to reaction with UV light. Therefore, the exposed/unexposed area of the photoresist film can be removed leaving a positive/negative pattern (depending on type of photoresist) on the substrate after a development process. The photoresist patterns are used as protective layer in the fabrication process. Resolution of the pattern is an important factor to determine the performance of a lithography process, which is defined as the ability to separate closely spaced patterns on the substrate. In an optical exposure system, resolution is determined by the diffraction phenomenon of light. The formula for resolution, R, is [36].

$$R = \frac{k\lambda}{NA} \tag{2.4}$$

Where k is the factor that represents specific applications, with a range between 0.6 and 0.8, λ is the wavelength of the radiation source and NA presents the numerical aperture of lens. From equation (1), it should be obvious that a decrease in λ will improve the resolution capability of the lithography system and increasing NA of the projection lens also improves resolution. But, increasing NA needs a larger diameter lens, which can be costly. Therefore, an alternative way to improve resolution is by decreasing the wavelengthλ. However, the requirements of higher resolution and higher throughput mean current lithography tools are no longer able to meet the industry's need.

2.3.1. Materials and methods for photolithography

Photoresists can be of two types: positive and negative photoresist. Positive photoresists are commonly used because they give better resolution in patterning even though they are more expensive than negative photoresists. Photoresists are made up of three components: a polymer which is base material of photoresist, a solvent to keep it in solution, and a Photo Active Compound

(PAC). In case of negative photoresist the PAC makes bonding in between the polymer molecules when it is exposed to the UV light. This bonding of molecules or cross linking keep it attached to the substrate and remains unreactive while development of the sample takes place.

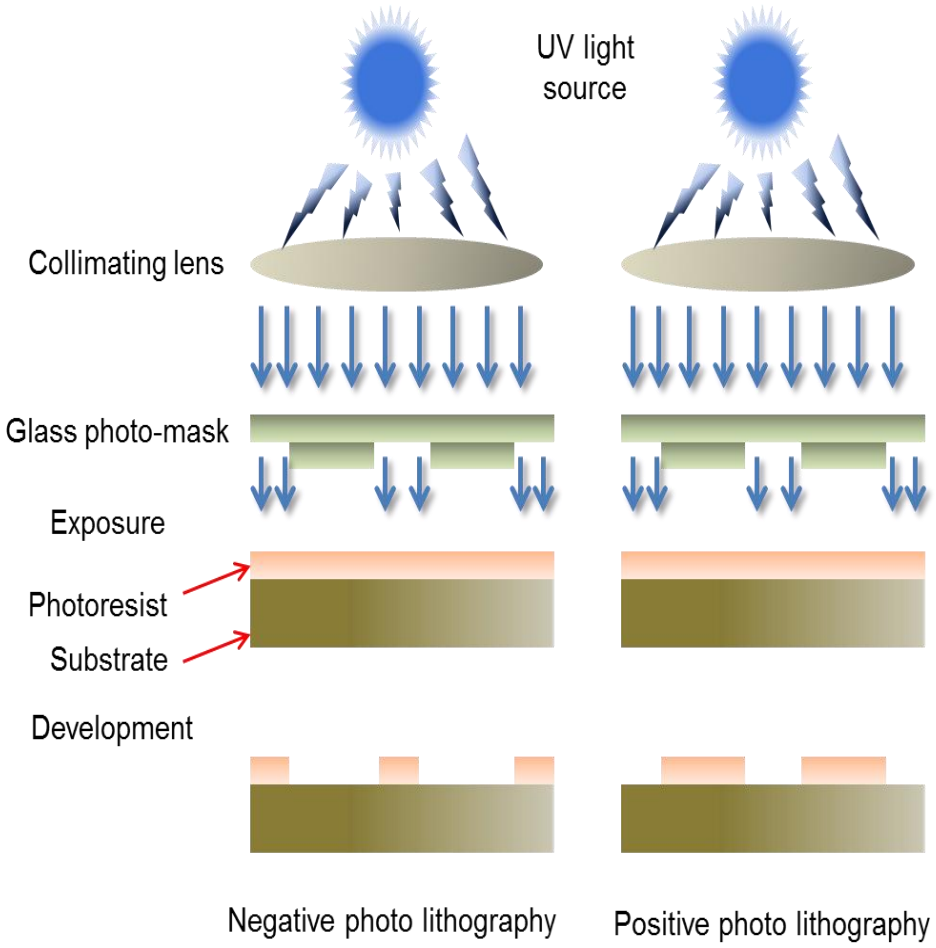

Figure 2.7: *Schematic of photolithographic process for negative and positive photoresist [37].*

The area which is unexposed exhibits no cross-linking of molecules so that it is washed away during development in a suitable solvent. When positive photoresist is exposed to the UV light the PAC reacts with the polymer and break down the polymer into the compound which can easily be dissolved in developer solution. A pattern is exposed into the photoresist by shining UV light through a glass plate that has the pattern on it (i.e. a photomask). The glass plate pattern is

transparent in some places and opaque in others. Where the areas are transparent the ultraviolet light shines through onto the wafer causing a chemical reaction in the photoresist. Where the mask areas are opaque the ultraviolet light is blocked and that area remain unreacted [37]. During the development process the pattern exposed on the wafer during the exposure step is developed and photoresist is either removed or remains to form the pattern depending upon the types of photoresist – negative or positive photoresist (Figure 2.7).

2.3.2. Spin coating

Spin coating is a process that forms uniform thin films on a flat substrate. In brief, the photoresist is placed on the substrate, which is attached to the vacuum holder and then spun at high speed and photoresist spreads via centrifugal force. A thin film of the coating material will remain on the substrate, which depends on a combination of the spinning speed and the viscosity of the resist.

Spin coating can be divided into different steps:

1. Deposition of the photoresist on substrate.
2. Spinning the substrate up to the required speed.
3. Substrate spinning at constant rate and viscous forces of the photoresist itself get into a thin layer.
4. Substrate spinning at constant rate and solvent of the photoresist gets evaporated until it achieves the thin coating.

The thickness of the photoresists depends on the time, rate of spinning and viscosity of the photoresist [38]. A basic schematic of the process is presented in Figure 2.8. The substrate is held by a vacuum and the resist is deposited in the center of the substrate. The sample stage is then spun at several thousand rpm, which will cause the resist flow outward and a smooth uniform layer is obtained.

The resist thickness can be calculated from the equation:

$$h = \frac{h_0}{\sqrt{1+\frac{16\pi^2 f^2}{3n}h_0^2 t}} \qquad (2.5)$$

where h_0 is the initial resist thickness (nm), f is the rotational speed (r/s), resist viscosity ($m^2\ s^{-1}$), and t is the spinning time (s) In order to improve the adhesion between the substrate and the resist, a primer layer is pre-spun coated. After spin coating, a soft bake is necessary to remove solvent of the resist, which improves the adhesion and internal stress. Spin coating is the first step for lithography some defects, such as particle; dust may destroy the imprinted structures [39].

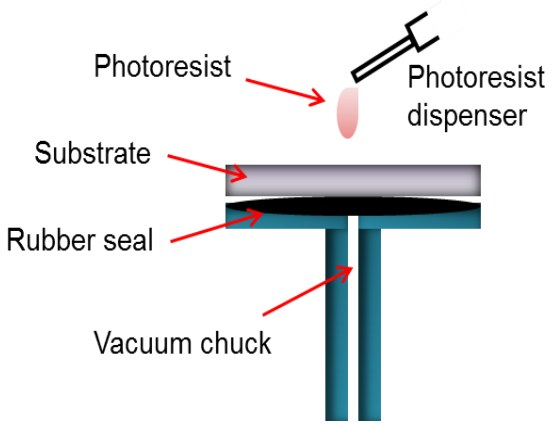

Figure: 2.8: *Schematic of spin coating of glass substrate.*

2.3.3. Wet chemical etching

Patterning underlying films through a photolithography and etching process is one reason that photoresist is used in the initial stage. Etching processes can be carried out using chemical (wet etching), physical (dry etching), or sometimes a combination of both methods. Wet chemical etching is usually characterized by low anisotropy and high selectivity (Figure 2.9). However, it is difficult to control the etch rate, which causes high defect levels. The dry etching is characterized by a high degree of anisotropy, but the etch rate is nearly

independent of the substrate material. The basic wet etching reactions in etching for Si as follows:

Solid + liquid etchant $\rightarrow$ soluble product

$Si\ (s) + 2OH^- + H_2O \rightarrow Si\ (OH)_2\ (O^-)_2\ (aq) + 2H_2\ (g)$

It is generally used for cleaning, polishing, shaping structures and to characterize structural features of substrate. The important parameters of wet chemical etching is etching rate, anisotropy of substrate, over-etching and size control.

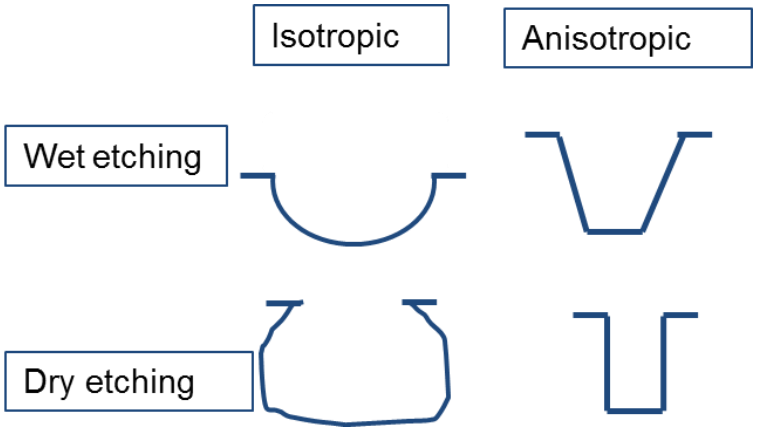

Figure 2.9: *Schematic illustration of cross-sectional trench profiles resulting from wet chemical etching.*

2.4. Plasma etching

Plasma etching is often used as a cleaning process for the material surfaces. It uses the ionized gases in a moderate vacuum chamber to generate plasma for the gas or air to do the surface etching. The chemical based wet etching is used only to remove thicker contaminants in the micron range such as flux residues; however plasma deals with contamination in the nanometer range on substrate surfaces. In previous research, plasma cleaning has been described as a very effective and cheap etching technology for various critical surfaces. The

oxygen plasma cleaning is used for removing oils and grease at the nano-scale. It also helps to reduce contaminants on the sample surface in comparison to the conventional wet etching. The conventional wet etching uses the different organic solvents which generally leave some residues on the surface after etching. Plasma cleaning is useful in making a surface clean for bonding or surface modification, and does not leave any residue as in wet etching. Most of the organic bonds which are present on the surface of the substrate are broken when it is exposed to UV light that is generated by the plasma [40]. In oxygen gas plasmas the cleaning of the sample substrate is achieved by the energetic oxygen species present. These species react with organic contaminants to form water and CO_2 which is pumped away in the vacuum chamber. Plasma cleaning is suitable for cleaning various surfaces including metal, plastics and ceramics.

2.5. References

1. Alexe-Ionescu, A.; Barbero, G.; Lelidis, I., Complex dielectric constant of a nematic liquid crystal containing two types of ions: limit of validity of the superposition principle. *The Journal of Physical Chemistry B* **2009,** 113, (44), 14747-14753.
2. Barbero, G.; Lelidis, I., Evidence of the ambipolar diffusion in the impedance spectroscopy of an electrolytic cell. *Physical Review E* **2007,** 76, (5), 051501.
3. Ganea, C., New approach of the AC electrode polarization during the measurements of impedance spectra. *Romanian journal of physics* **2012,** 57, (3-4), 664-675.
4. Bard, A. J., *Electrogenerated chemiluminescence*. CRC Press: 2004.
5. Zoski, C. G., Ultramicroelectrodes: design, fabrication, and characterization. *Electroanalysis* **2002,** 14, (15-16), 1041-1051.
6. Macdonald, J. R., Impedance spectroscopy. *Annals of biomedical engineering* **1992,** 20, (3), 289-305.

7. Garland, J.; Pettit, C.; Roy, D., Analysis of experimental constraints and variables for time resolved detection of Fourier transform electrochemical impedance spectra. *Electrochimica Acta* **2004,** 49, (16), 2623-2635.
8. Chang, B. Y.; Park, S. M., Electrochemical impedance spectroscopy. *Annual Review of Analytical Chemistry* **2010,** 3, 207-229.
9. Daniels, J. S.; Pourmand, N., Label-Free Impedance Biosensors: Opportunities and Challenges. *Electroanalysis* **2007,** 19, (12), 1239-1257.
10. Behrens, R. L. Electrochemical and Spectroscopic Interfacial Investigations of Small Organic Molecule Electrooxidation on Platinum Electrodes. University of Illinois, 2010.
11. Scholz, F.; Schrèoder, U.; Gulaboski, R., *Electrochemistry of immobilized particles and droplets*. Springer: 2005.
12. Orazem, M. E.; Agarwal, P.; Garcia-Rubio, L. H., Critical issues associated with interpretation of impedance spectra. *Journal of Electroanalytical Chemistry* **1994,** 378, (1), 51-62.
13. Pejcic, B.; De Marco, R., Impedance spectroscopy: Over 35 years of electrochemical sensor optimization. *Electrochimica Acta* **2006,** 51, (28), 6217-6229.
14. Macdonald, D. D., Reflections on the history of electrochemical impedance spectroscopy. *Electrochimica Acta* **2006,** 51, (8), 1376-1388.
15. Kerner, Z.; Pajkossy, T., Impedance of rough capacitive electrodes: the role of surface disorder. *Journal of Electroanalytical Chemistry* **1998,** 448, (1), 139-142.
16. Córdoba-Torres, P.; Mesquita, T.; Nogueira, R., Toward a better characterization of constant-phase element behavior on disk electrodes from direct impedance analysis: Methodological considerations and mass transport effects. *Electrochimica Acta* **2013,** 92, 323-334.
17. Ramón-Azcón, J.; Valera, E.; Rodríguez, Á.; Barranco, A.; Alfaro, B.; Sanchez-Baeza, F.; Marco, M., An impedimetric immunosensor based on interdigitated microelectrodes (IDμE) for the determination of atrazine residues in food samples. *Biosensors and Bioelectronics* **2008,** 23, (9), 1367-1373.
18. Mirsky, V. M.; Riepl, M.; Wolfbeis, O. S., Capacitive monitoring of protein immobilization and antigen–antibody reactions on monomolecular

alkylthiol films on gold electrodes. *Biosensors and Bioelectronics* **1997,** 12, (9), 977-989.

19. Ouerghi, O.; Touhami, A.; Jaffrezic-Renault, N.; Martelet, C.; Ouada, H. B.; Cosnier, S., Electrodeposited biotinylated polypyrrole as an immobilization method for impedimetric immunosensors. *Sensors Journal, IEEE* **2004,** 4, (5), 559-567.
20. Radi, A.-E., Electrochemical Aptamer-Based Biosensors: Recent Advances and Perspectives. *International Journal of Electrochemistry* **2011,** 2011.
21. Ahn, S.; Freedman, D. S.; Massari, P.; Cabodi, M.; Ünlü, M. S., A Mass-Tagging Approach for Enhanced Sensitivity of Dynamic Cytokine Detection Using a Label-Free Biosensor. *Langmuir* **2013,** 29, (17), 5369-5376.
22. Bazant, M. Z.; Thornton, K.; Ajdari, A., Diffuse-charge dynamics in electrochemical systems. *Physical Review E* **2004,** 70, (2), 021506.
23. Madou, M. J.; Cubicciotti, R., Scaling issues in chemical and biological sensors. *Proceedings of the IEEE* **2003,** 91, (6), 830-838.
24. Roy, P.; Patra, M. R.; Rahaman, H.; Dasgupta, P. In *A New design of a dual mode bioassay detection analyzer for digital microfluidic biochips*, Communications, Devices and Intelligent Systems (CODIS), 2012 International Conference on, 2012; IEEE: 2012; pp 310-313.
25. Roy, P.; Patra, M. R.; Rahaman, H.; Dasgupta, P. In *Automated parallel detection based analyzer for integrated bioassays in digital microfluidic biochip*, Electronics and Nanotechnology (ELNANO), XXXIII International Scientific Conference, IEEE **2013**; pp 310-315.
26. C.A.Volkert, A. M. M., Focused Ion Beam Microscopy and Micromachining. *MRS BULLETIN* **2007,** 32.
27. Gierak, J., Focused ion beam technology and ultimate applications. *Semicond. Sci. Technol.* **2009,** 24, 23.
28. Puers, S. R. a. R., A review of focused ion beam applications in microsystem technology,. *J. Micromech. Microeng.* **2001,** 11, 287 300.
29. Kwon, N.; Kim, K.; Heo, J.; Chung, I. *In Fabrication of ordered anodic aluminum oxide with matrix arrays of pores using nanoimprint*, AVS: **2009**; pp 803-807.

30. Shingubara, S.; Maruo, S.; Yamashita, T.; Nakao, M.; Shimizu, T., Reduction of pitch of nanohole array by self-organizing anodic oxidation after nanoimprinting. *Microelectronic Engineering* **2010,** 87, (5–8), 1451-1454.
31. Choi, J.; Wehrspohn, R. B.; Gösele, U., Mechanism of guided self-organization producing quasi-monodomain porous alumina. *Electrochimica Acta* **2005,** 50, (13), 2591-2595.
32. Liu, C. Y.; Datta, A.; Wang, Y. L., Ordered anodic alumina nanochannels on focused-ion-beam-prepatterned aluminum surfaces. *Applied Physics Letters* **2001,** 78, (1), 120-122.
33. Bo Chen, K. L., Zhipeng Tian, Understanding focused ion beam guided anodic alumina nanopore development. *Electrochimica Acta* **2011,** 56, 9802– 9807.
34. Chen, B.; Lu, K.; Tian, Z., Novel Patterns by Focused Ion Beam Guided Anodization. *Langmuir* **2010,** 27, (2), 800-808.
35. Lillo, M.; Losic, D., Ion-beam pore opening of porous anodic alumina: The formation of single nanopore and nanopore arrays. *Materials Letters* **2009,** 63, (3–4), 457-460.
36. Wang, Z.; Pan, J., Reflective optical systems for EUV lithography. In Google Patents: 2001.
37. Wu, B.; Kumar, A., Extreme ultraviolet lithography: A review. *Journal of Vacuum Science & Technology B: Microelectronics and Nanometer Structures* **2007,** 25, (6), 1743-1761.
38. Levinson, H. J. In *Principles of lithography*, 2005; SPIE Bellingham: 2005.
39. Wagner, C.; Harned, N., EUV lithography: Lithography gets extreme. *Nature Photonics* **2010,** 4, (1), 24-26.
40. Swart, K.; Keller, J.; Wightman, J.; Draughn, R.; Stanford, C.; Michaels, C., Short-term plasma-cleaning treatments enhance in vitro osteoblast attachment to titanium. *The Journal of oral implantology* **1992,** 18, (2), 130.

Chapter 3

INFLUENCE OF NANOPORE DIMENSIONS ON THEIR ELECTROCHEMICAL PROPERTIES STUDIED BY IMPEDANCE SPECTROSCOPY

K. Kant, C. Priest, J. G. Shapter, D. Losic, '*Influence of nanopore dimensions on electrochemical properties studied by impedance spectroscopy*' Sensors, 2014. (Under review)

3.1. Introduction

Nanopores with their unique properties and similarity with biological nanopore structures have attracted considerable research attention due to their several unique properties and applications [1, 2].The integration of biomolecules into nanopores and nanochannels has been recognized as a new approach for development of simple, inexpensive and highly sensitive biomolecule detection [3-5]. The sensitivity, low cost, simplicity, and easy miniaturization of electrochemical detection is particularly suited to the development of highly sensitive nanopores based biosensor [6]. To establish a nanochannel device we need to understand the electrical and electrochemical properties of the nanopores. The sensitivity of this nanopores based device is highly influenced by molecular transport of analyte molecules to reach binding receptors inside the nanopores where dimensions of nanopore structure (pore diameters and length) are critical parameters. Hence characterization of electrical and electrochemical properties of these structures is important to optimize performance of these devices based on nano-confined pore structures [7, 8]. Surprisingly there are only few electrochemical studies on nanopore arrays and membranes to address these questions [9].

Electrochemical impedance spectroscopy (EIS) commonly applies to describe a range of electrochemical properties of porous materials made up of either synthetic or biological membranes. It also offers evidence on the functional and structural characteristics of nanoporous membrane substrates. The EIS study on the ion-exchange system in membrane delivered a good way of considering the EIS behaviors of fouling phenomena (i.e., *deposition and accumulation of*

foulants on anion-exchange membranes) [10]. EIS is a potential method for analysing the compound electrical resistance of a system and possible changes of bulk properties, therefore it has been widely used for characterization of charge transport across nanopores in membranes and membrane/solution interfaces [11]. The applications of impedance sensors are not limited to gas sensors, humidity sensor etc., but also these impedance sensors are used in biological sensor which has very sophisticated interdigitated electrode structures [12, 13].

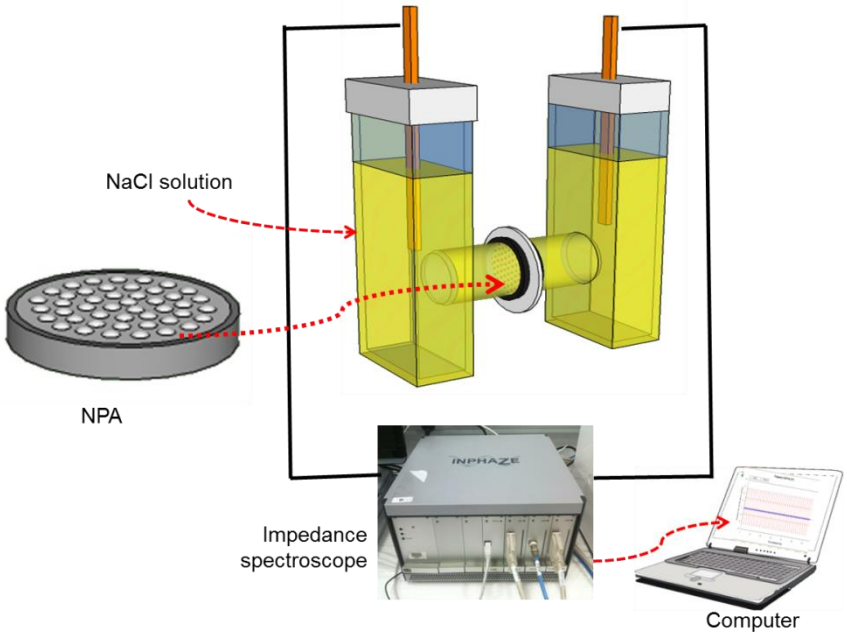

Figure 3.1: *A schematic of experimental setup, the fabricated nano porous alumina (NPA) is sandwiched between two cells filled with electrolyte for two electrode EIS measurements of NPA.*

Nanoporous alumina (NPA) prepared by electrochemical anodization process is very attractive for development of nanopore biosensing devices due their uniform pore size, high aspect ratio, high surface area, straight-forward and inexpensive fabrication. It has been demonstrated that the electron transfer resistance will decrease and the conductance increase as a result of an ion transfer inside the pores of NPA [14, 15]. Previous studies demonstrated that the transport

of ions or molecules passing through nanopore nanochannel is altered by steric and electrostatic effects [16-18]. The electrostatic effect is a long-range effect initiated by the interaction of surface charge and transporting ions [13, 19]. This transport is shown to be dependent on pore size and number of pores and can be changed by the surface charge or ionic strength of the bulk solution, which can also change their transport inside the nanopores [7, 20]. These studies clearly demonstrate the need for a detailed investigation on the influence of nanopore dimensions on their electrochemical properties and biosensing performance [21, 22].

In this work impedance spectroscopy is used to explore the effect of change in nanopore diameters and nanopore length on electrochemical properties of nanopores related to their sensing of molecular separation applications. NPA with different pore dimensions are used as a nanopore arrays platform and sodium chloride (NaCl) is used as electrolyte for the measurements. The scheme of proposed impedance devices and the experimental setup is shown in Figure 3.1. Where NPA is sandwiched in between two different chambers and impedance measurements is performed by Inphaze instrument.

3.2. Experimental Section

3.2.1. Materials and chemicals

Aluminum foil (0.1 mm, 99.997%) was supplied by Alfa Aesar (USA). Oxalic acid, phosphoric acid, Sodium chloride, ethanol (Chem Supply, Australia), chromium trioxide (Mallinckrodt, USA), De-ionized (DI) water (ELGA) grade (18.2 MΩ) water was used for preparation of all solutions.

3.2.2. Preparation of NPA

NPA was prepared by a two-step anodization process using 0.3 M oxalic acid as electrolyte at 0°C as described elsewhere [14]. The first anodized porous layer was prepared at a voltage of 60 to 80 V for 5 min, and then removed using an oxide removal solution (0.2 M chromium trioxide and 0.4 M phosphoric acid) for 1-2 hours at 60 ^{o}C. The second anodization was carried out in range of 30V to 70V to achieve different pore diameter. Mild anodization at 30V was used to get 25$\pm$5 nm and hard anodization at 70 V for large pore diameter of 65$\pm$5 nm was used. The length of NAP is controlled by the time duration of anodization. For mild anodization at 30 V it took 180 min to achieve pore length about 4-5 μm. However for hard anodization at 70 V it took only 20 min to grow 4-5 μm [23]. To prepare NPAs with different thicknesses or lengths (5-18 μm) of small diameter pores the anodization time was varied from 180 min to 720 min at 30 V. Once the anodization completed remaining aluminium was removed from the backside of the nanopore array to reveal a clear and clean barrier layer of the nanopore array by using $CuCl_2$/HCl. The removal of barrier layer from the pore structures was performed by using the 10 % phosphoric acid [24].

3.2.3. Photolithography on NPA

The fabricated NPA was patterned on the back side (barrier layer side) with photoresist using photolithography to prepare a 20x20 μm^2 area with the opened nanopore array. The photoresist (AZ1518) was spin-coated (1500 rpm) over the bottom side of NPA (barrier layer) and followed by baking of the sample at 100 ^{o}C for 50s. A photo-mask (chrome-on-glass mask, Bandwidth Foundry)

with a 20 μm^2 diameter transparent region was used to mask the sample with exposure of 330 mJ/m^2. The exposed photoresist was then removed by solvent. In this way an opening of a 20x20 μm^2 square on the NPA from bottom side was obtained.

3.2.4. Electrochemical measurements

The transport properties of membrane or array of nanopores are determined by the behaviour of a single pore. It was assumed that the solutions just inside and outside the pore are in equilibrium. Electrochemical measurements were carried out in using an EIS spectrometer, (Inphaze, Pty. Ltd. Sydney, Australia) with a two-electrode system which is specifically designed for EIS characterization of NPA [9]. Two gold electrodes formed the working and counter electrodes. The nanoporous array was sandwiched between two cell chambers filled with the electrolyte electrodes on each side. The working and counter electrodes were respectively placed at the end of two chambers (Figure 3.1). The Nyquist plot is one of the ways used to explain the existence of several elements and processes as it offers a direct view of the real component of the impedance (inverse of the conductance) varies with the imaginary component at each frequency points. An equivalent circuit is used to fit the experimental data with the theoretical model. This model assumes that there is no impedance contribution made from the limited diffusion of the ions. In practice, such contribution does exist but mainly influences the impedance characteristics within a very low frequency range [25, 26]. The resistance of the area of membrane, which is covered with photoresist, is so high that it does not appear in the equivalent circuit model. The pore resistance R_p can be calculated as:

$$R_p = \frac{4L}{\pi\sigma d^2} \quad (3.1)$$

Where R_p is pore resistance. L is length of the pore and d is the diameter of the pore. As we increase the diameter of the pore the value of pore resistance reduces but at the same time it increases if we vary the length of the nanopore array. The electrochemical impedances were acquired in the frequency range from 0.01 Hz to 1 MHz. In the system of nanopore conductance mostly depends on the pore diameter for high electrolyte concentration but also tends to have similar value for low concentrations as well. The conductance can be calculated as (Eq-3.2):

$$G_0 = K_b \left[\frac{4L}{\pi D^2} + \frac{1}{D}\right]^{-1} \quad (3.2)$$

Where K_b is the bulk conductivity, L length of nanopore and D is diameter of nanopore [27, 28]. Studies already been done on the overlap of electrical double layer (EDL) inside the nanopore [29]. The Debye length and the thickness of the EDL can be presented as:

$$\lambda_D = \left[\frac{\varepsilon k_B T}{2e^2 c_s}\right]^{1/2} \quad (3.3)$$

where c_s is the salt concentration, ε is the dielectric permittivity of water, k_B is the Boltzmann constant, T ~ 300 K is the absolute temperature and e is the elementary charge [30, 31]. The Dukhin length introduced $l_{Du} = K_S/K_b$ where K_s is the surface conductivity and K_b is the bulk conductivity. The Dukhin length compares directly with the diameter of the pore. In case of long length of nanopores both ends and inner surface of the nanopore can be defined by the (Eq-3.2). The ends of nanopore produce system resistance and this effect make that each nanopore can be considered as one resistance in series. Hille and Hall [27, 32] explained the pore electric conductance G_p is proportional to the bulk

conductivity

$$G_P = K_b \left[\frac{\pi D^2}{4L}\right] \quad (3.4)$$

If the surface conduction of nanopore (eq-4) combined with pore conductance the total pore conductance can be calculated by the expression:

$$G_P = \left[K_b \frac{\pi D^2}{4L} + K_s \frac{\pi D}{L}\right] \quad (3.5)$$

If the length L of the nanopore is large and the diameter is small the pore resistance (R_p) dominates the total conductance of nanopore [33]. The increase in the impedance across the pore is approximately equal to the applied potential which, provided information that the potential drops at the electrode/solution interfaces is small. The applied potential and generated resistance at interface may not be same on both sides of the membrane. R_p is small if the conductivity of the electrolyte is high and pore channel is very short.

3.3. Results and Discussion

3.3.1 SEM characterization of NPA arrays

SEM images of the top surface of the prepared NPA sensing platform with different pore diameter are presented in Figure 3.2(a-c). The images confirm the successful preparation of well-ordered nanopores with a diameter of 25±2 nm, 45±2 nm and 65±2 nm, depending on the anodization conditions. To achieve three different pore diameters at constant pore length the anodization potential was tuned between 30-70 V with the anodization time varied from 20-180 min. It is well known that pore diameter is determined by applied voltage during anodization and porosity (P) of the NPA can be estimated by assuming an ideal

hexagonal arrangement of the pores [34]. A typical cross-sectional structure of the prepared NPA is shown in Figure 3.2(d).

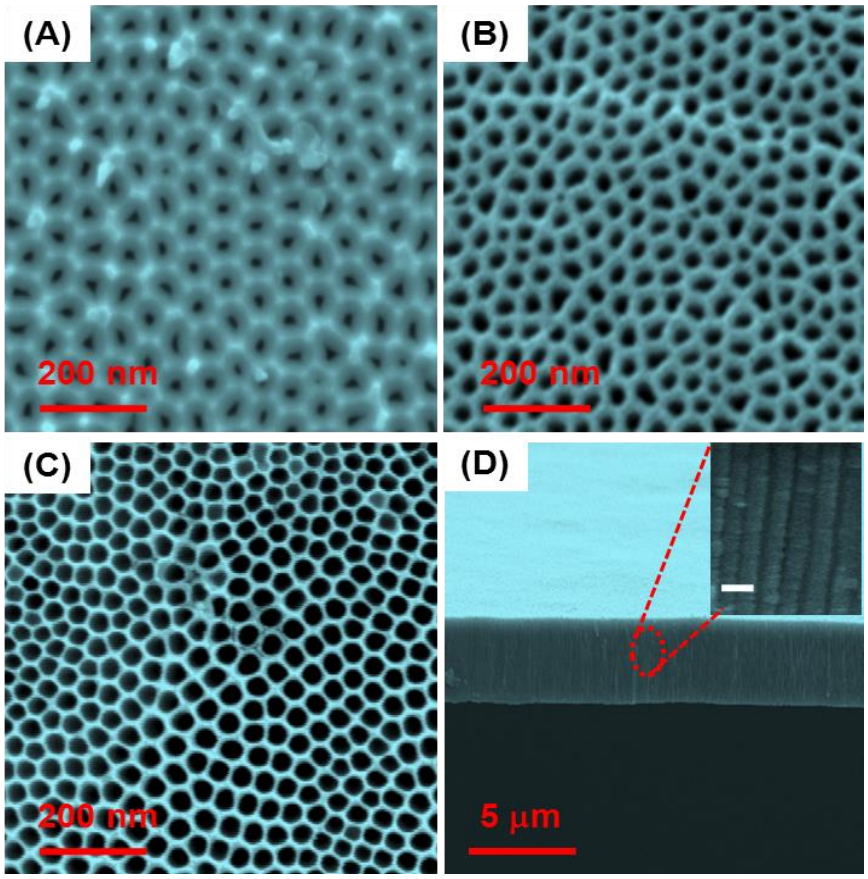

Figure 3.2: *SEM images of the top surface of NPA used as nanopore sensing platform with different pore diameters (a) small pore around 25±2 nm (b) medium size pore around 45±2 nm (c) large pore around 65±2 nm, prepared in 0.3M oxalic acid electrolyte using different anodization voltages 30 – 70 V and time 20 to 180 min to achieve the same pore length (d) Cross section SEM images of NPA with the inset Figure (scale bar 100nm) showing well-ordered and aligned pores through the full thickness of the membrane.*

3.3.2. EIS measurements on NPA arrays: influence of ion concentration

In order to characterize the performance of these NPA array and optimize the nanopore dimensions for sensing purposes, a series of electrochemical impedance spectroscopy experiments were carried out [35, 36]. In the first set of experiments, NPA was characterized using NaCl electrolyte with concentrations

from 1 μM to 100 μM. The collected impedance (Z) data for the constant pore diameters using various concentration of NaCl is shown in Nyquist plots (Figure 3.3).

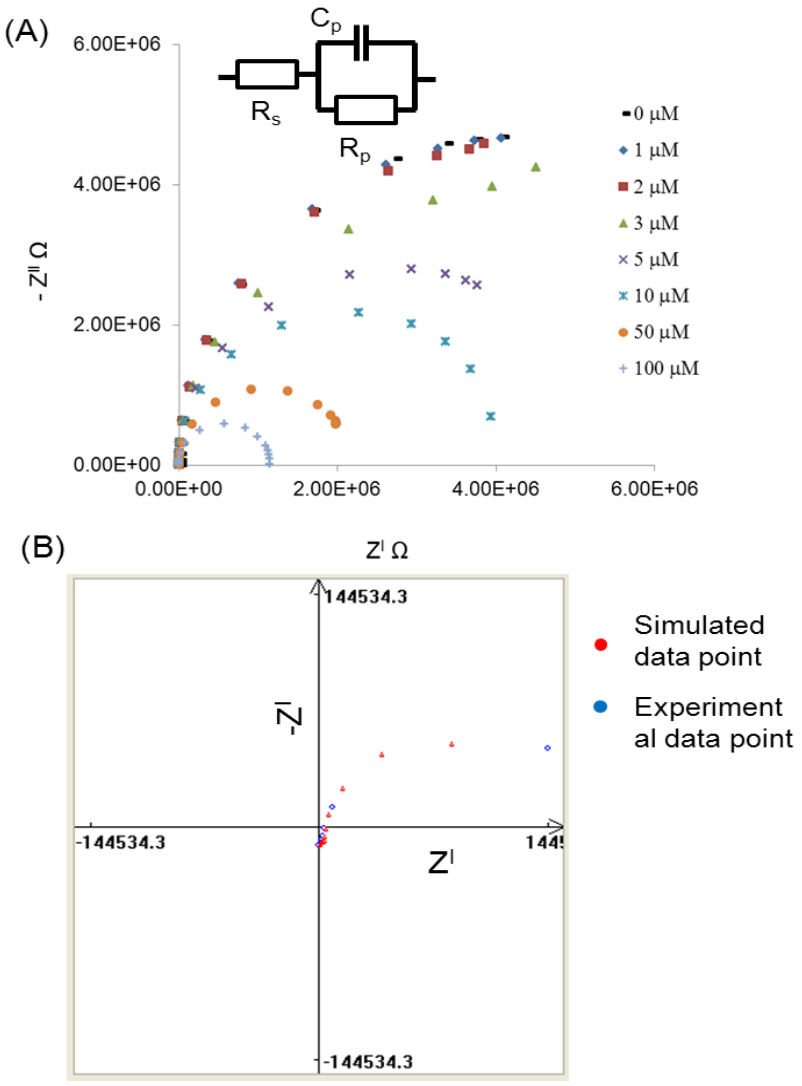

***Figure 3.3**: (a) Nyquist plot obtained for NPA at constant pore diameters of 45 nm with various different concentrations (1 μM to 100 μM) of NaCl (b) experimental data is showing the agreement against the simulated data with use of equivalent circuit.*

The Nyquist plot contains overlapping semicircles; each of them is related with a single time constant element. The top of the semicircle resembles to the distinctive frequency of elements in the system. The decrease in the radius of the

semicircle at high concentration is due to the diffusion of ions inside the nanopores and increase in the conductance of the nanopore array especially at the very high concentration. K_s changes due to high concentration of ions at the end of the nanopore and K_b has opposite impact on the system conductance and reduces the resistivity. Nyquist plot provides a more immediate indication of the ion diffusion due to the concentration gradation. It reveals the effect of concentration on the conductivity of the NPA. The graphs show that Z^1 (real) decreased with increasing electrolytic concentration inside pores of NPA. To estimate the impedance of NPA, we modeled the experimental system using EvolCRT software developed at department of Chemistry, Wuhan University Wuhan P.R. China [37]. The experimental data was simulated against the equivalent circuit and find out the exact value for the pore resistance (R_p). The R_p is a key parameter which reports changes that happened due to the diameter of nanopore. The wall thickness of NPA and available NaCl ions inside the nanopores generates EDL inside the nanopore surface resulted the high impedance inside the nanopores. Therefore, R_P is much larger than R_S. It is also found that both R_S and R_P decrease with increasing concentration indicating that the nanopore resistance is a function of the electrolyte concentration inside the nanopore. So the high concentration ratio induced by the trans-membrane potential increases the mobility of the charged ions inside the nanopore resulting in a relatively lower electrolyte resistance [38].

3.3.3. EIS measurements on NPA arrays: influence of nanopore diameters and length

NPA of three different pore diameters (25 nm, 45 nm, and 65 nm) were characterized using different concentration of NaCl. The collected impedance (Z)

data for the various pore diameters using constant concentration of 1 μM NaCl is shown in Nyquist plots (Figure 3.4e). The values for R_p obtained after simulation with equivalent circuit is plotted in Figure 3.3a, showing the influence of pore diameter on R_p. At the lowest concentration of electrolyte 1 μM, the pore resistance decreases from $5.61x10^6$ to $3.8x10^6$ Ω when the pore diameter is increased from 25 to 65 nm. For the large pore diameter, the impedance measurement is dominated by the bulk properties of the solution (Figure 3.4a, b) and small changes in impedance due to effects at the walls of the nanopores become insignificant. The conductance of nanopore (G_p) also been effected by the increase in the diameter of nanopore (Eq-3.3) as the diameter is increasing (25 nm, 45 nm, 65nm) conductance increases (0.12 nS, 0.38 nS, 0.77 nS) respectively (Figure 3.4f). The effect of electrical double layer is depending on the electrolyte concentration, it increases with decrease in electrolyte concentration. In case of large nanopores (65 nm) there is enough space for the ions to diffuse inside the nanopore so the double layer (~ 8 nm) is not affecting system resistance. However, in the case of the smaller pores (Figure 3.4d), the electrical double layer (at the same concentration of electrolyte) form on each side of the alumina wall is very close to each other and started effecting ion movement inside the nanopore and cause high resistance in the system. The relative surface effects are greater and the signal is affected significantly, as reported in previous studies [39, 40].

The conclusion from this experiment is that the NPA with smaller nanopore diameters (25 nm) are more sensitive (~ 120 Ω/μM) compared to the NPA with the larger pores (~ 45 Ω/μM) over the concentration range of 1 μM to 50 μM. Since we find that the smaller pore diameter provides greater sensitivity and performance, we used the 25 nm diameter pores to study the influence of pore

length on electrochemical signal. For that purpose we fabricated NPA biosensing platforms with different pore lengths (4.5 µm, 9 µm, 13.5 µm and 18 µm) and carried out a series of EIS measurements at different concentrations of NaCl.

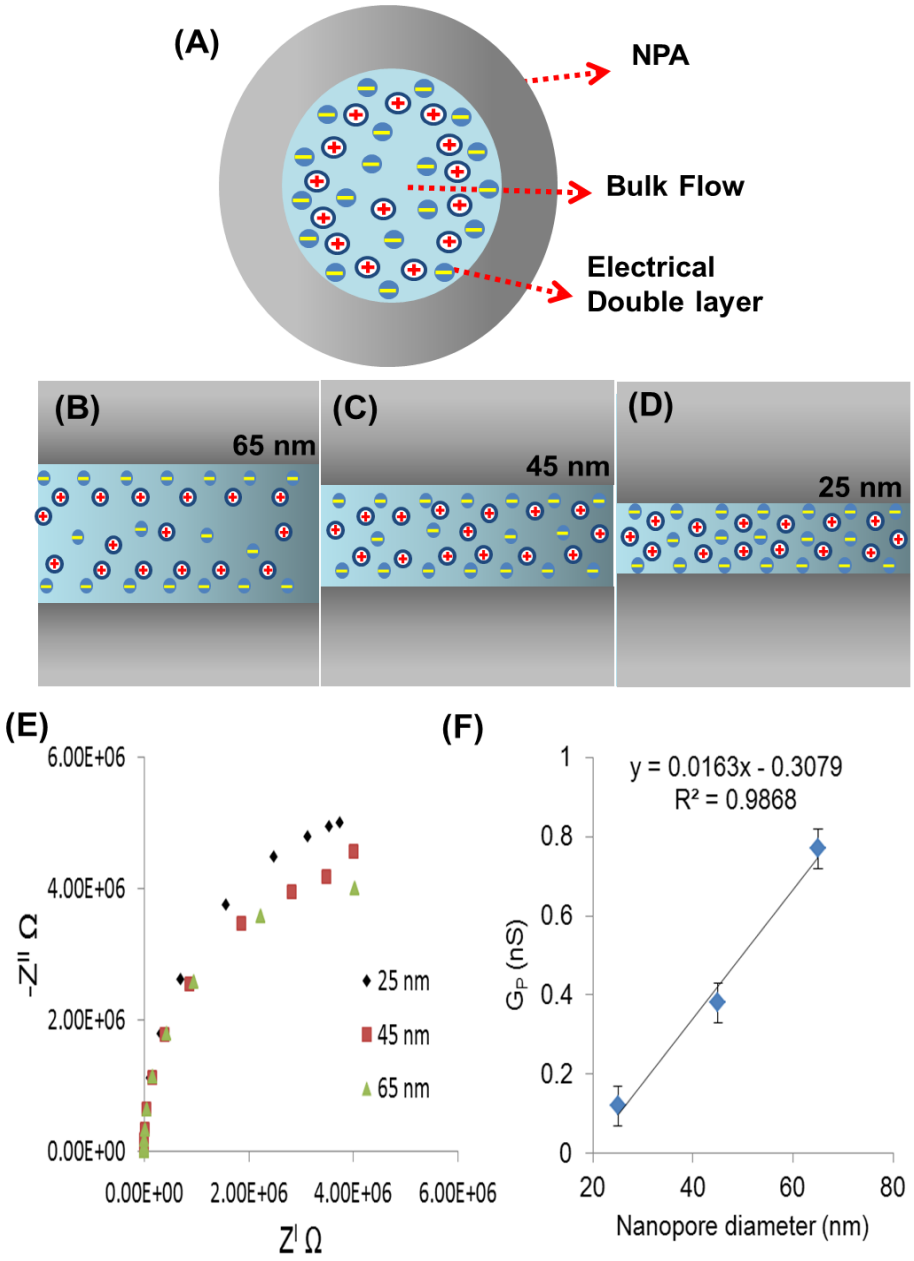

Figure 3.4: *Schematic presentation for formation of electrical double layer and bulk flow of electrolyte (a) inside the nanopore (b) large pore diameters (65 nm) has space for bulk flow of electrolyte but as pore diameter decreases (c) and (d) the density of ions increases inside nanopores (e) Nyquist plot between the three different pore diameters 25 nm, 45 nm and 65 nm of NPA at constant length 4.5 µm and concentration (1 µM) of electrolyte NaCl shows the decrease in pore resistance R_p with increased pore diameter.*

The calculated G_p is decreasing (0.126 nS, 0.062 nS, 0.041 nS and 0.031nS) with increase of length of nanopore (4.5 μm, 9 μm, 13.5 μm and 18 μm) respectively (Figure 3.5b). The Nyquist plot was generated from constant concentration of electrolyte (5 μM) as shown on Figure 3.5a.

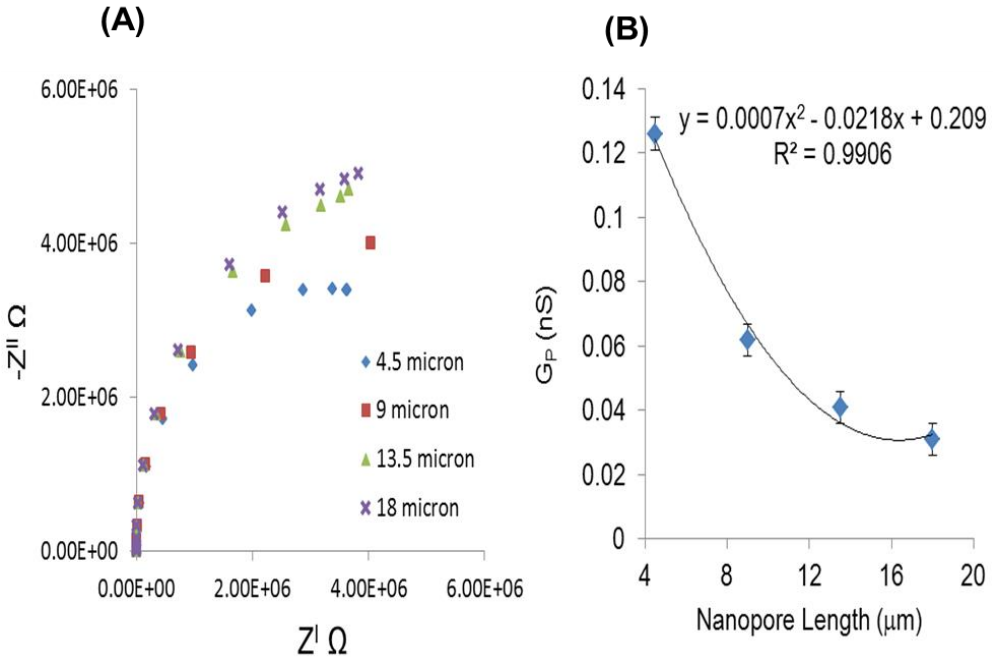

Figure 3.5*: At constant pore diameter (25 nm) and concentration (5 μM) four different pore lengths shows the increase in pore resistance R_p with increased pore length (a) Nyquist plot for various pore length and (b) conductance at different pore length.*

The graph shows the trend of increasing impedance over the range of frequencies with respect to increasing pore length. Further measurements were performed by simulating the experimental data with the proposed equivalent circuit to find value of R_p for various length of NPA. It was found that the R_p changes from 5.3×10^6 to 3.2×10^6 Ω as length of NPA increase from 4.5 μm to 18 μm. The graph clearly shows the increase in the pore resistance with increasing the pore length. The characteristic saturation in signal was observed at higher concentration of electrolyte [41]. It was found that increasing pore length beyond

10-15 μm will have higher system resistance, as ion path will be long inside nanopore and concentration of ion will not be in equilibrium at both end of the nanopore. Increasing nanopore length to more than 10 to 15 μm does not seem good for such type of biosensing detection where biomolecules need to diffuse through nanopore. As the longer pore lengths mean long for diffusion times of the ions and hence high resistance for the system. It was observed that pore resistance is a key factor to be considered in the optimization of NPA performance by EIS. In our case pore resistance with respect to lower concentration (1-10 μM) has a high sensitivity of small change in concentration of electrolyte. This behavior of NPA array is also limited with the morphology of nanopore array. A very small nanopore diameter (below 20 nm) is also been effected by the electrical double layer and has low conductance in the system [42]. The detection limit for electrolyte using this system was 1 μM. However we believe a detection limit can be improved by lowering nanopore diameters (<25 nm). Nanopores with a diameter below 20 nm were difficult to make using the anodization condition used in our experiments (oxalic acid anodization) and the use other electrolytes (sulphuric acid) is required. However, smaller nanopores may limit the diffusion of the molecules such as protein and enzymes and therefore considerable extend the response time. The best performance for the biosensing platform was observed with nanopore diameters of 20-40 nm with a length of 4-15 μm. Reduction in nanopore length below 4 μm could reduce robustness of NPA biosensor device because of fragility NPA substrate.

3.4. Conclusions

A new method was implemented to measure the impedance of the nanopore to achieve best pore size (20-40 nm) and length (5-15 μm) for device fabrication. Our results confirmed that pore dimensions including pore diameters and length have considerable influence on device performances including sensitivity, where pore resistance is used as measuring signal. However there is a limitation to size reduction as the size comparable to the size of analyte molecules will prevent diffusion of molecules inside the pore. In terms of pore length it was found that longer pores (>15 μm) are also not favorable for non-Faradaic EIS detection as results of higher impedance on the nanopores and long time for diffusion of analyte molecules inside nanopores. Hence it is critical to optimize pore dimensions to achieve optimal performances of nanopore based electrochemical biosensing devices which have considerable potential toward development simple and inexpensive sensing devices for broad biomedical applications.

3.5. References

1. Ronkainen, N. J.; Halsall, H. B.; Heineman, W. R., Electrochemical biosensors. *Chemical Society Reviews* **2010,** 39, (5), 1747-1763.
2. Komarova, E.; Reber, K.; Aldissi, M.; Bogomolova, A., New multispecific array as a tool for electrochemical impedance spectroscopy-based biosensing. *Biosensors and Bioelectronics* **2010,** 25, (6), 1389-1394.
3. Daniels, J. S.; Pourmand, N., Label-Free Impedance Biosensors: Opportunities and Challenges. *Electroanalysis* **2007,** 19, (12), 1239-1257.
4. Chang, B. Y.; Park, S. M., Electrochemical Impedance Spectroscopy. *Annual Review of Analytical Chemistry* **2010,** 3, (1), 207-229.

5. Pänke, O.; Balkenhohl, T.; Kafka, J.; Schäfer, D.; Lisdat, F., Impedance Spectroscopy and Biosensing. In *Biosensing for the 21st Century*, Renneberg, R.; Lisdat, F., Eds. Springer Berlin Heidelberg: 2008; Vol. 109, pp 195-237.
6. Kim, J.; Gonzalez-Martin, A., Nanopore membrane-based electrochemical immunoassay. *J Solid State Electrochem* **2009,** 13, (7), 1037-1042.
7. Eftekhari, F.; Escobedo, C.; Ferreira, J.; Duan, X.; Girotto, E. M.; Brolo, A. G.; Gordon, R.; Sinton, D., Nanoholes As Nanochannels: Flow-through Plasmonic Sensing. *Analytical Chemistry* **2009,** 81, (11), 4308-4311.
8. Yu, J.; Liu, Z.; Yang, M.; Mak, A., Nanoporous membrane-based cell chip for the study of anti-cancer drug effect of retinoic acid with impedance spectroscopy. *Talanta* **2009,** 80, (1), 189-194.
9. Chilcott, T. C.; Guo, C., Impedance and dielectric characterizations of ionic partitioning in interfaces that membranous, biomimetic and gold surfaces form with electrolytes. *Electrochimica Acta* **2013,** 98, (0), 274-287.
10. Park, J.-S.; Choi, J. H.; Woo, J. J.; Moon, S. H., An electrical impedance spectroscopic (EIS) study on transport characteristics of ion-exchange membrane systems. *Journal of Colloid and Interface Science* **2006,** 300, (2), 655-662.
11. Reimhult, E.; Kumar, K., Membrane biosensor platforms using nano- and microporous supports. *Trends in Biotechnology* **2008,** 26, (2), 82-89.
12. Zhang, J.; Zhu, J., A novel amperometric biosensor based on gold nanoparticles-mesoporous silica composite for biosensing glucose. *Sci. China Ser. B-Chem.* **2009,** 52, (6), 815-820.
13. Orazem, M. E.; Tribollet, B., An integrated approach to electrochemical impedance spectroscopy. *Electrochimica Acta* **2008,** 53, (25), 7360-7366.
14. Masuda, H.; Fukuda, K., Ordered Metal Nanohole Arrays Made by a Two-Step Replication of Honeycomb Structures of Anodic Alumina. *Science* **1995,** 268, (5216), 1466-1468.
15. Prakash, S.; Yeom, J.; Jin, N.; Adesida, I.; Shannon, M. A., Characterization of ionic transport at the nanoscale. *Proceedings of the Institution of Mechanical Engineers, Part N: Journal of Nanoengineering and Nanosystems* **2006,** 220, (2), 45-52.

16. Römer, W.; Steinem, C., Impedance Analysis and Single-Channel Recordings on Nano-Black Lipid Membranes Based on Porous Alumina. *Biophysical Journal* **2004,** 86, (2), 955-965.
17. Takhistov, P., Electrochemical synthesis and impedance characterization of nano-patterned biosensor substrate. *Biosensors and Bioelectronics* **2004,** 19, (11), 1445-1456.
18. Potucek, R. K.; Rateick, R. G.; Birss, V. I., Impedance Characterization of Anodic Barrier Al Oxide Film Beneath Porous Oxide Layer. *Journal of The Electrochemical Society* **2006,** 153, (8), B304-B310.
19. Herzog, G.; Arrigan, D. W. M., Electrochemical strategies for the label-free detection of amino acids, peptides and proteins. *Analyst* **2007,** 132, (7), 615-632.
20. Li, S. J.; Li, J.; Wang, K.; Wang, C.; Xu, J. J.; Chen, H. Y.; Xia, X. H.; Huo, Q., A Nanochannel Array-Based Electrochemical Device for Quantitative Label-free DNA Analysis. *ACS Nano* **2010,** 4, (11), 6417-6424.
21. Berdat, D.; Marin, A.; Herrera, F.; Gijs, M. A. M., DNA biosensor using fluorescence microscopy and impedance spectroscopy. *Sensors and Actuators B: Chemical* **2006,** 118, (1–2), 53-59.
22. Girginov, A.; Popova, A.; Kanazirski, I.; Zahariev, A., Characterization of complex anodic alumina films by electrochemical impedance spectroscopy. *Thin Solid Films* **2006,** 515, (4), 1548-1551.
23. Losic, D.; Velleman, L.; Kant, K.; Kumeria, T.; Gulati, K.; Shapter, J. G.; Beattie, D. A.; Simovic, S., Self-ordering Electrochemistry: A Simple Approach for Engineering Nanopore and Nanotube Arrays for Emerging Applications*. *Australian Journal of Chemistry* **2011,** 64, (3), 294-301.
24. Lillo, M.; Losic, D., Pore opening detection for controlled dissolution of barrier oxide layer and fabrication of nanoporous alumina with through-hole morphology. *Journal of Membrane Science* **2009,** 327, (1–2), 11-17.
25. Yu, X.; Lv, R.; Ma, Z.; Liu, Z.; Hao, Y.; Li, Q.; Xu, D., An impedance array biosensor for detection of multiple antibody-antigen interactions. *Analyst* **2006,** 131, (6), 745-750.

26. Lisdat, F.; Schäfer, D., The use of electrochemical impedance spectroscopy for biosensing. *Anal Bioanal Chem* **2008,** 391, (5), 1555-1567.
27. Hall, J. E., Access resistance of a small circular pore. *The Journal of general physiology* **1975,** 66, (4), 531-532.
28. Kowalczyk, S. W.; Grosberg, A. Y.; Rabin, Y.; Dekker, C., Modeling the conductance and DNA blockade of solid-state nanopores. *Nanotechnology* **2011,** 22, (31), 315101.
29. Ho, C.; Qiao, R.; Heng, J. B.; Chatterjee, A.; Timp, R. J.; Aluru, N. R.; Timp, G., Electrolytic transport through a synthetic nanometer-diameter pore. *Proceedings of the National Academy of Sciences of the United States of America* **2005,** 102, (30), 10445-10450.
30. Schoch, R. B.; Van Lintel, H.; Renaud, P., Effect of the surface charge on ion transport through nanoslits. *Physics of Fluids (1994-present)* **2005,** 17, (10), 100604.
31. Bocquet, L.; Charlaix, E., Nanofluidics, from bulk to interfaces. *Chemical Society Reviews* **2010,** 39, (3), 1073-1095.
32. Hille, B., Pharmacological Modifications of the Sodium Channels of Frog Nerve. *The Journal of general physiology* **1968,** 51, (2), 199-219.
33. Lee, C.; Joly, L.; Siria, A.; Biance, A.-L.; Fulcrand, R. m.; Bocquet, L. r., Large apparent electric size of solid-state nanopores due to spatially extended surface conduction. *Nano Letters* **2012,** 12, (8), 4037-4044.
34. Lee, W.; Ji, R.; Gösele, U.; Nielsch, K., Fast fabrication of long-range ordered porous alumina membranes by hard anodization. *Nature materials* **2006,** 5, (9), 741-747.
35. Sim, L. N.; Wang, Z. J.; Gu, J.; Coster, H. G. L.; Fane, A. G., Detection of reverse osmosis membrane fouling with silica, bovine serum albumin and their mixture using in-situ electrical impedance spectroscopy. *Journal of Membrane Science* **2013,** 443, (0), 45-53.
36. Rai, V.; Deng, J.; Toh, C.-S., Electrochemical nanoporous alumina membrane-based label-free DNA biosensor for the detection of Legionella sp. *Talanta* **2012,** 98, (0), 112-117.

37. Yu, J.; Cao, H.; He, Y., A new tree structure code for equivalent circuit and evolutionary estimation of parameters. *Chemometrics and intelligent laboratory systems* **2007,** 85, (1), 27-39.
38. Chien, M. C. W., Gou J.; Yu, Ming-Chang, Nanopore Size Estimation by Electrochemical Impedance Spectroscopy Analysis. *Japanese Journal of Applied Physics* **2008,** 47, (9), 7459.
39. K. Kant, M. K., J. Yu, J. G. Shapter, C. Priest, D. Losic, Impedance spectroscopy study of nanopore arrays for biosensing applications *Science of advance material* **2014,** 6, 1-7.
40. Tsai, Y. T.; Chang, K.; Wang, G. J., Measurement and control of the ion diffusion coefficient in a nanochannel. *Microsystem Technologies* **2013,** 19, (6), 937-944.
41. Cheng, I. F.; Yang, H. L.; Chung, C. C.; Chang, H. C., A Rapid Electrochemical Biosensor Based on an AC Electrokinetics Enhanced Immuno-reaction. *Analyst* **2013**.
42. Harrell, C. C.; Lee, S. B.; Martin, C. R., Synthetic Single-Nanopore and Nanotube Membranes. *Analytical Chemistry* **2003,** 75, (24), 6861-6867.

Chapter 4

IMPEDANCE NANOPORE BIOSENSOR: INFLUENCE OF PORE DIMENSIONS ON BIOSENSING PERFORMANCE

K. Kant, J. Yu, C. Priest, J. G. Shapter and D. Losic "*Impedance nanopore biosensor: influence of pore dimensions on biosensing performance*" Analyst, (RSC) 2014, 139 p. 1134-1140. Doi: 10.1039/c3an01933k

K. Kant, M. Kurkuri, J. Yu, J. G. Shapter, C. Priest, D. Losic, '*Impedance spectroscopy study of nanopore arrays for biosensing applications*'. Science of Advanced Materials, 6, (2014) 1375-1381.

4.1. Introduction

Integration of biomolecules into nanopores and nanochannels has attracted considerable attention due to the high surface area of the pores and similarity with nanopores in biological systems meaning there is the potential for new and advanced biosensing devices [1-3]. In these studies specific recognition molecules have been functionalized inside single or nanopore arrays for various applications including molecular or ionic gates, single molecule detection, and biosensing of enzymes DNA and antibodies [4, 5]. Development of nanochannel or nanopore array biosensing devices has proven to be an excellent approach toward the development of simple, inexpensive and highly sensitive biomolecule detection. In particular, their interactions and specific binding with the immobilized probe confined in a nanoscale volume are critical parameters which determine the performance of biosensing devices, e.g. sensitivity, response time and detection limit [6, 7]. Surprisingly there are only few electrochemical studies on nanopores that address these questions [8, 9]. Electrochemical impedance spectroscopy (EIS) is a powerful method for analysing the complex electrochemical properties of a system and possible changes of its bulk properties. Therefore, it has been widely used for characterization of charge transport across nanopores in membranes and membrane/solution interfaces [10, 11]. EIS is also very powerful and sensitive for the detection of antigen–antibody binding inside nanopores [12, 13]. Impedance biosensing can be performed using both Faradaic and non-Faradaic processes. In Faradaic processes charge is flowing across the interface of the sensing material; however in the case of non-Faradaic sensing, current flows without charge transfer through the interface material. The main disadvantage of the Faradaic process is that it requires a redox species to enhance the signal of the electron

transfer. On the other hand, there are no additional requirements of a redox species or signal enhancer for non-Faradaic EIS. Hence, in the field of nanopore biosensors the non-faradaic EIS is particularly well-suited for the detection of binding events inside nanopores and is recognized as the simpler method [2, 14].

Nanoporous alumina membranes (NPAs) prepared by electrochemical anodization process have been very attractive for development of nanopore biosensing devices, due their uniform pore size, high aspect ratio, high surface area and straight-forward and inexpensive fabrication [15]. It has been demonstrated that the electron transfer resistance will decrease and the conductance increase as a result of a binding reaction inside the pores of NPA [16, 17]. However, the binding reaction of the antigen at the antibody-immobilized surface is often insufficient to produce a large signal change for impedance measurements that are largely dependent of nanopore dimensions and the density of immobilized probes inside nanopores [18-20]. Previous studies demonstrated that the transport of ions or molecules passing through bio-functionalized nanopores is affected by steric and electrostatic effects [21-23]. The electrostatic effect is a long-range effect caused by the interaction between surface-immobilized charged molecules and the transporting ions [8, 16, 23]. This transport is shown to be dependent on pore size and number of pores and can be changed by the surface charge or ionic strength of the bulk solution, which can also change ion transport inside the nanopores [5, 24, 25]. These studies clearly demonstrate the need for a detailed investigation of the influence of nanopore dimensions on their electrochemical properties and biosensing performance. Herein the EIS electrochemical method was used to study the effect of nanopore diameters and length on the performance a label-free nanopore biosensor. The

NPA was used as sensing nanopore platform and biotin-streptavidin detection was used as a model of immune assay biosensor.

The aim was to demonstrate the application of a NPA array as simple, low cost and label-free electrochemical biosensing platform for detection of biomolecules based on affinity binding reactions. The scheme of the proposed biosensing device and the experimental setup is shown in Figure 4.1. The NPA sensing platforms with different diameters and length of the nanopores were prepared to characterize their electrochemical properties and biosensing performance using various concentrations of analytes [6, 26, 27].

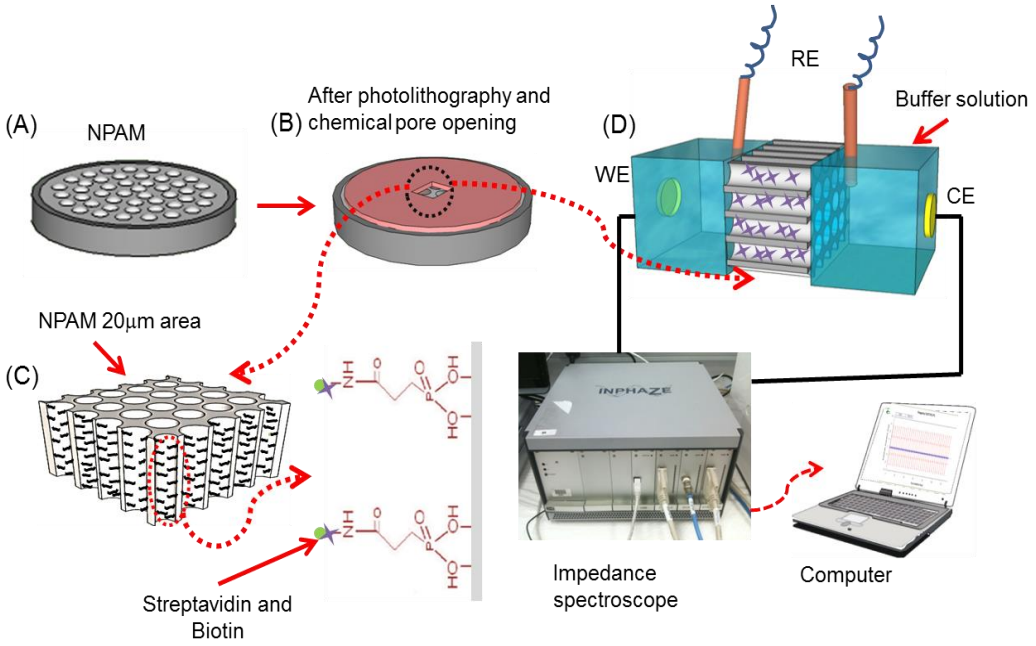

Figure 4.1: *A schematic of experimental setup (a) fabricated nano porous alumina membrane (NPA) (b) NPA after photolithography with a 20x20 μm^2 opening (c) NPA modified with streptavidin as sensing platform (d) NPA placed in EIS cell for impedance characterization*

The surface inside the pores was functionalized by phosphonic acid and NHS-EDC chemistry, followed by the covalent attachment of antibody molecules, which were used as a binding surface for the selective capture of antigen

molecules, i.e. biotin [28]. The NPA sensing platform with a reduced number of nanopores and working area of 20x20 μm^2 was prepared by photolithography in order to miniaturize the device. A four electrode cell was used to characterize the change in properties of the nanopore array using EIS technique for different pore diameter and length.

4.2. Materials and Methods

Aluminum foil (0.1 mm, 99.997%) was supplied by Alfa Aesar (USA). Oxalic acid, ethanol (Chem Supply, Australia), chromium trioxide (Mallinckrodt, USA), 2-Carboxyethyl phosphonic acid, N-Hydroxysuccinimide (NHS), ethyl (dimethyl aminopropyl) carbodiimide (EDC), streptavidin, biotin, albumin bovine-fluorescein isothiocyanate (BSA-FITC) were supplied by (Sigma–Aldrich, Australia) and used as received. High purity ultra-pure Milli Q grade (18.2 MΩ) water was used for preparation of all solutions.

4.2.1. Preparation of nanoporous alumina (NPA)

NPA were prepared by a two-step anodization process of Al foil using 0.3 M oxalic acid as the electrolyte at 0 °C as described elsewhere [9, 29]. The details about the fabrication of different nanopore diameter and length are given in Chapter 3 section 3.2.1.

4.2.2. Photolithography on NPA

The fabricated NPA substrates were patterned on the back side with photoresist using photolithography to prepare a 20 μm area with the opened nanopore array. Further details have been provided in Chapter 3 section 3.2.2.

4.2.3. Functionalization of NPA nanopores with streptavidin

Surface modification of the NPA nanopore array was performed by soaking it into an aqueous solution of 5 mM 2-carboxyethyl phosphonic acid for 72 hours at room temperature. The samples were rinsed with a sufficient amount of DI water to remove nonspecific bindings and then dried under a slow purge of nitrogen. The top and bottom surfaces of the nanopore array were exposed to air plasma etching for 30 seconds, using a plasma cleaner (Diener, Germany). After exposing the nanopore array to plasma etching, the samples were left in DI water for 24 hours at room temperature for pore wetting. After pore wetting the nanopore array was soaked in N-hydroxysuccinimide (NHS) 15 mg/mL in PBS and 1-ethyl-3- (3-dimethylaminopropyl) carbodimide (EDC) 20 mg/mL in PBS buffer solution for 30 min at room temperature, followed by rinsing with plenty of DI water. Subsequently the samples were soaked in streptavidin solution of 100 μg/mL concentration in PBS for 30 min at room temperature to functionalize the nanopores. The samples of prepared NPA biosensing platform were finally washed in copious amounts of DI water and mounted in the electrode cell for EIS measurements by addition different concentrations of biotin. The biotin stock solution of 50 μg/mL was prepared and used to make required concentrations (0.2 μM to 29 μM) by dilution. The prepared biotin solution were injected with the same volume on the streptavidin functionalized NPA sensor and left for the reaction time of 15 min to complete binding reaction followed by washing with DI water and EIS measurements.

4.2.4. Electrochemical measurements

Electrochemical measurements were carried out in using an EIS

spectrometer, (Inphaze, Pty. Ltd. Sydney, Australia) with a four-electrode system which is specifically designed for EIS characterization of NPA [30]. Two gold foils formed the working and counter electrodes with two Ag/AgCl as reference electrodes. The nanoporous array was sandwiched between two cell chambers filled with the buffer solution in contact with reference electrodes on each side. The working and counter electrodes were respectively placed at the end of two chambers (Figure 4.1). An equivalent circuit (Figure 4.5) is used to balance the resistance and capacitance for the entire system and monitor the behaviour of nanoporous arrays and changes on their surface. Since the streptavidin molecules can be negatively or positively charged depending on environment, an electric double layer is expected to be present at the streptavidin-solution interface. An impedance contribution from this interface is represented as a parallel RC element (R_{Fn} and C_{Fn}), and commonly introduced in series with the nanopore resistance [31, 32]. Here, R_{sol} is resistance of the electrolyte solution, R_p and C_p are the total contribution of resistance and capacitance of alumina membranes and free nanopores, R_{Fn} and C_{Fn} are the resistance and capacitance of the electric double layer formed at interface between the protein molecules and the solution. This simplified electrical model provides the best fit to our measurements. Particularly, a similar equivalent circuit is adopted to investigate glass nanopores in aqueous solutions [33]. This model assumes that there is no impedance contribution made from the limited diffusion of the ions. In practice, such contribution does exist but mainly influences the impedance characteristics within a very low frequency range [13, 34]. However, for our purposes the proposed model is sufficient, as we are able to extract the relevant model parameters, such as R_p, R_{Fn}, which are not affected by the limited diffusion. The resistance of the area of membrane, which is

covered with photoresist, is so high that it does not appear in the equivalent circuit model presented. Theoretically the pore resistance R_p can be calculated as eq 4.1:

$$R_p = \frac{4L}{\pi\sigma d^2} \quad (4.1)$$

Where R_p is pore resistance, L is length of the pore and d is the diameter of the pore [35]. As we increase the diameter of the pore the value of pore resistance reduces but at the same time it increase if we vary the length of the nanopore array. The biotin solutions of 0.2 μM – 29 μM concentrations in buffer 7.4 pH were tested in a series of experiments to explore their binding with functionalized streptavidin molecules inside the NPA arrays. The electrochemical impedances measurements were acquired for each biotin concentration separately in the frequency range from 1 Hz to 1MHz. A minimum of 3 spectra was taken for each concentration of the biotin and 3-4 samples were used.

4.3. Results and discussion

The morphological change in NPA leads to change in the sensing capability of biosensing device. To optimize these parameters a number of experiments with different morphologies were undertaken and are discussed in the following section.

4.3.1. SEM characterization of fabricated NPAs

SEM images of the top surface of the prepared NPA sensing platform with different pore diameter are presented in Figure 4.2(a-d). The images confirm the successful preparation of well-ordered nanopores with a diameter of 25±2 nm, 45±2 nm and 65±2 nm depending on the anodization conditions. To achieve three different pore diameters at constant pore length the anodization potential was tuned between 30-70 V with the anodization time varied from 20-180 min.

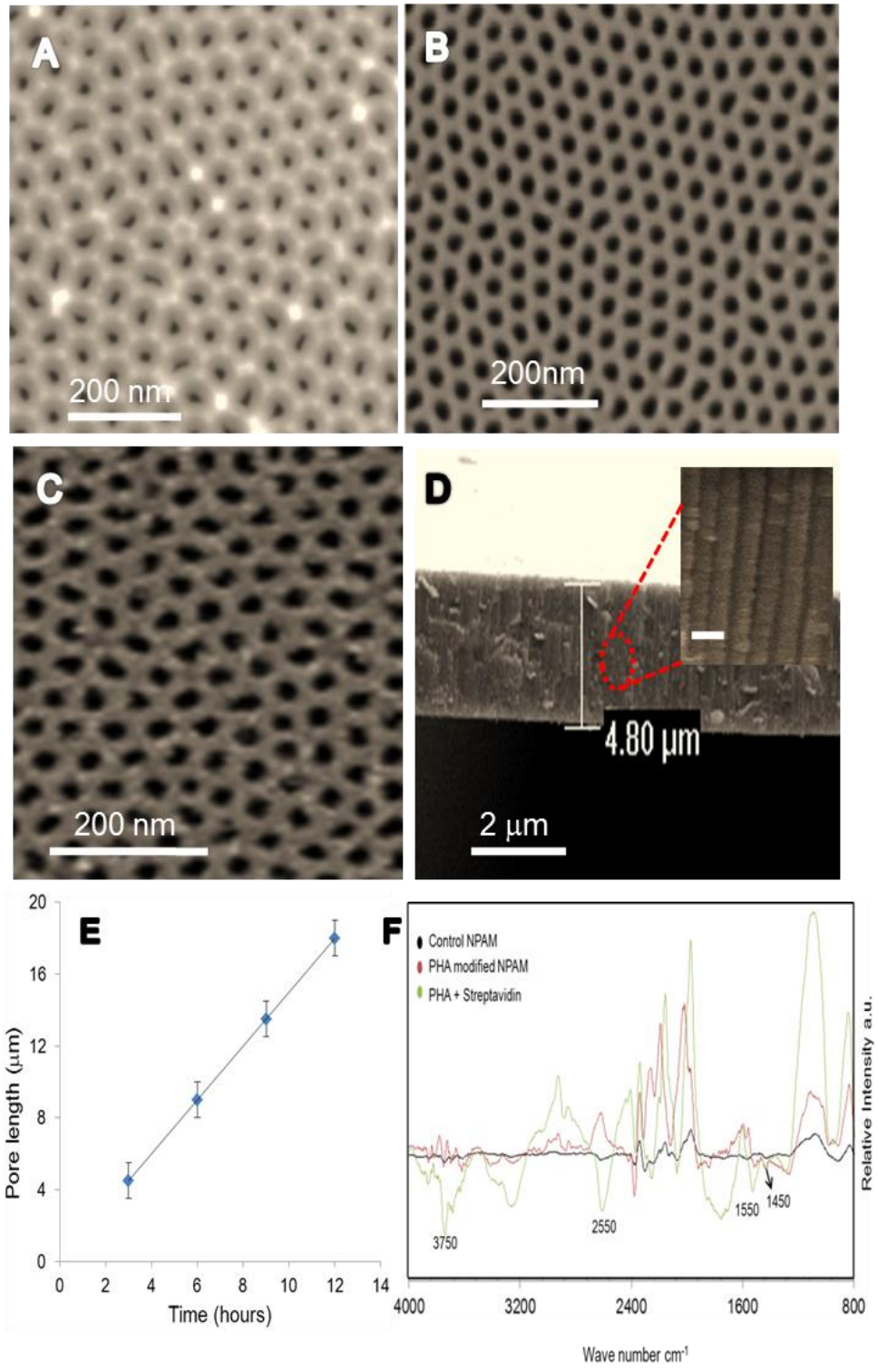

Figure 4.2: *SEM images of the top surface of NPA used as nanopore sensing with different pore diameters (a) small pore around 25±2 nm (b) medium size pore around 45±2 nm (c) large pore around 65+2 nm, prepared in 0.3 M oxalic acid electrolyte using different anodization voltages 30 – 70 V and time 20 to 180 min to achieve the same pore length (d) Cross section SEM images of NPA with magnified view of nanopores (100 nm scale) (e) calibration graph showing fabrication of NPA with the different pore length using anodization time from 3-12 hours (f) FTIR spectra of NPA before and after the first step of surface modification with phosphonic acid.*

It is well known that pore diameter is determined by applied voltage during anodization and that the porosity (P) of the NPA can be estimated assuming an ideal hexagonal arrangement of the pores;

$$P = \left(\frac{\pi}{2\sqrt{3}}\right)\left(\frac{D_p}{D_{int}}\right)^2 \qquad (4.2)$$

where D_p and D_{int} are pore diameter and the inter-pore distance respectively [36]. A typical cross-sectional structure of the prepared NPA is shown in Figure 4.2(d), with the inset Figure (scale bar 100 nm) showing well-ordered and aligned pores through the full thickness of the membrane. The pore length was calibrated against anodization time (2-10 h) for the 25 nm diameter pores, to allow the NPA pore length, which is equal to the thickness of the NPA, to be tuned. In Figure 4.2e, the calibration data is plotted for four different pore lengths from 5 μm to 20 μm at constant anodization potential 40 V [26, 37]. The linear fit to the calibration data is very good, providing excellent control over the pore length for this study.

4.3.2. Surface modification and characterization of NPAs

FTIR spectra of control NPA and modified NPA with phosphonic acid (PHA) are shown in Figure 4.2f. The results show evidence of surface modification of NPA by immobilization of biosensing molecules inside the nanopores. The peaks observed at 1450 cm^{-1} and 1485 to 1580 cm^{-1} are associated with available (COO^-) group which will lead to further bonding of protein molecules. The peaks at 2500 cm^{-1} to 2650 cm^{-1} show the presence of P-OH and P-H bonding and the peaks at 3650 to 3750 cm^{-1} represent the free OH groups are available at the surface of the NPA [38].

To achieve selective immobilization of the probe biomolecule

(streptavidin) inside the nanopores, it was developed as a surface functionalization procedure, which involves modification of NPA with phosphonic acid (PHA), activation of COOH with N-Hydroxysuccinimide/1-Ethyl-3-(3-dimethylaminopropyl) carbodiimide (NHS/EDC) and covalent binding of streptavidin/biotin. The most critical part of this process was to ensure that biologically active probes were exclusively inside the nanopores, i.e. that the top (outer) surface of the NPA was unmodified. Therefore, we used air plasma to clean the outer surface before and after NHS-EDC activation. This process is schematically represented in Figure 4.3a.

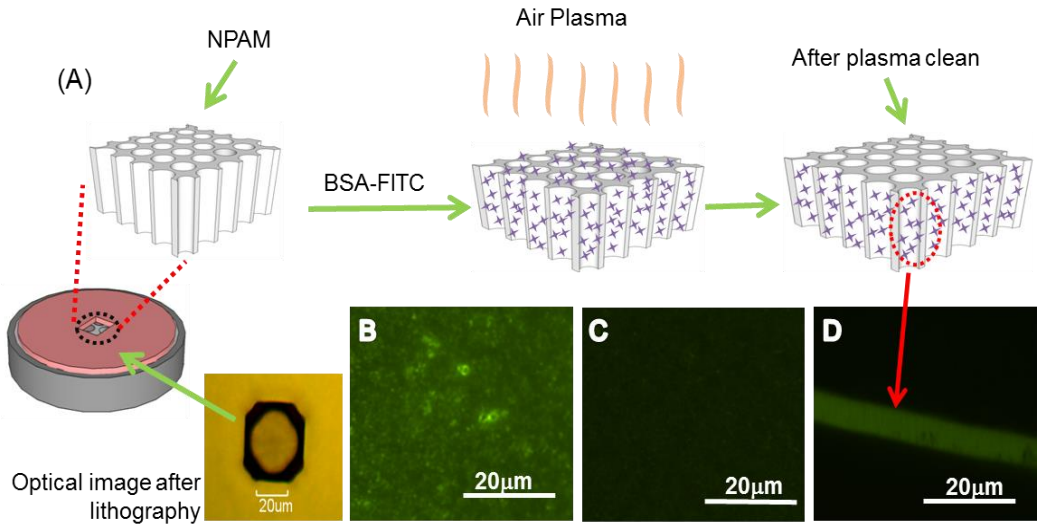

Figure 4.3: *Schematic of surface modification of NPA nanopores to demonstrate functionalization only internal pore structures and cleaned the top surface by plasma process. A fluorescent labelled albumin bovine serum) BSA-FITS are used as a model molecule. (a) NPA surface modification with phosphonic acid and covalently attached BSA-FITS followed by air plasma treatment. (b) fluorescent image of NPA before and (c) after plasma treatment (d) cross section image of NPA which proof that surface modification still remain inside the pores after air plasma treatment.*

To demonstrate that functional groups remain only inside the nanopores, fluorescence images of the top (outer) surface and the cross-section of the NPA were collected after treatment with BSA-FITC and plasma, see fluorescence

image from the top surface (Figure 4.3b) before plasma treatment clearly shows the bright fluorescence of the BSA-FITC image, confirming the presence of BSA on the top surface. The image in Figure 4.3c is the same top surface after plasma treatment and shows negligible fluorescence intensity, confirming that the removal of active biomolecules from the top surface of the NPA was successful. Furthermore, the cross-section image of the NPA (Figure 4.3d) clearly shows that the fluorescence signal remains inside nanopores, demonstrating that our method can achieve a highly selective surface modification inside the nanopores. The amino groups after NHS-EDC modification are active inside the nanopores for binding of streptavidin molecules and, therefore, the approach is suited to the preparation of a nanopore biosensing device.

4.3.3. EIS measurements of NPA biosensor

In order to characterize the label-free sensing performance of these NPA biosensors and optimization of the nanopore dimensions for sensing protein molecules, a series of electrochemical impedance measurements were carried out. In the first set of experiments, NPA biosensors with three different average pore diameters (25 nm, 45 nm and 65 nm) were characterized using biotin analytes with concentrations from 0.2 μM to 29 μM. The collected impedance (Z) data as a Nyquist plot for the different pore diameters using a fixed concentration of biotin (0.2 μM) are shown in Figure. 4.4 (a) reveal the impedance dependence on the pore diameter. The graphs show that Z decreased with increasing NPA pore size. To estimate the pore resistance, we modelled the experimental system using EvolCRT software [39] (developed by Department of Chemistry, Wuhan University, China) according to the equivalent circuit (Figure 4.5a inset).

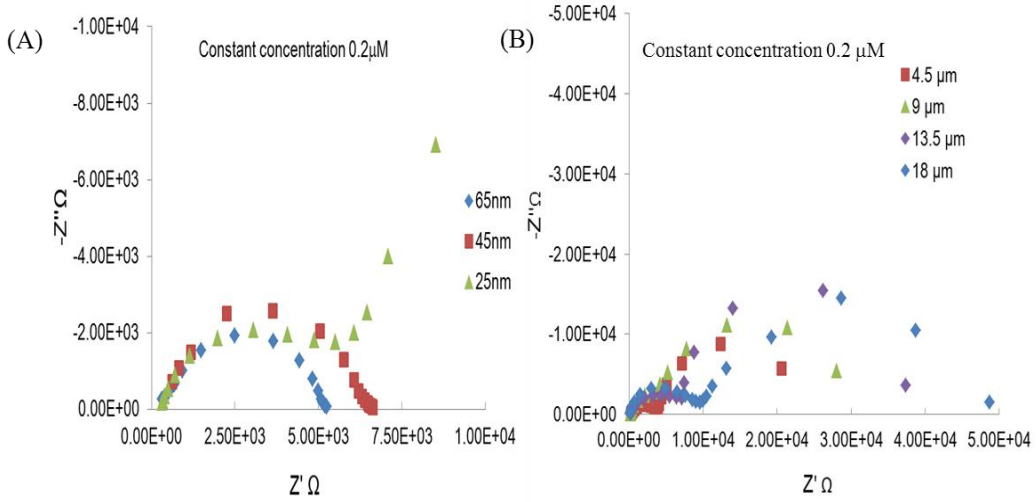

***Figure 4.4**: (a) Nyquist plot obtained for NPA biosensors with different pore diameters of NPA and (b) different pore length at constant pore diameter and their response using constant biotin concentration (0.2 μM).*

The simulation of the data was done using the following equation:

$$F = \frac{1}{N}\sum_{i=1}^{m}\left[\left(\tilde{Z}_i' - Z_i'\right)^2 + \left(\tilde{Z}_i'' - Z_i''\right)^2\right] \qquad (4.3)$$

where Z_i' and Z_i'' are the experimental values of the real part and the imaginary part of the electrochemical impedance at a given frequency f_i. Similarly $\tilde{Z}_i'$ and $\tilde{Z}_i''$ are the corresponding fitting values. Here *m* is the number of input frequencies, i.e. the number of data points. The extracted parameters of the proposed equivalent circuit are as follow in table 4.1:

Pore Diameter (nm)	R_{sol} (Ω)	R_p (Ω)	R_{Fn} (Ω)	C_p (F)	C_{Fn} (F)
65	5.87×10^{2}	3.07×10^{3}	1.81×10^{3}	1.54×10^{-9}	6.68×10^{-9}
45	6.35×10^{2}	5.35×10^{3}	5.43×10^{3}	3.29×10^{-9}	6.10×10^{-8}
25	6.02×10^{2}	6.16×10^{3}	1.8×10^{4}	3.68×10^{-9}	2.47×10^{-9}
Pore length (μm)					
4.5	6.46×10^{2}	6.41×10^{3}	1.79×10^{4}	4.50×10^{-9}	4.43×10^{-7}
9	6.39×10^{2}	7.54×10^{3}	2.26×10^{4}	1.58×10^{-8}	9.86×10^{-8}
13.5	6.79×10^{2}	8.25×10^{3}	2.98×10^{4}	3.53×10^{-9}	1.97×10^{-7}
18	6.94×10^{2}	1.61×10^{4}	3.34×10^{4}	4.47×10^{-9}	1.70×10^{-6}

***Table 4.1**: The extracted value for all the components of equivalent circuit for different NPA nanopore diameters and lengths are presented.*

The best fit for the pore resistance (R_p) was obtained from these simulations at several concentrations of biotin and three different pore diameters. The experimental data was simulated against the equivalent circuit to determine the exact value for the pore resistance. The R_p is a key parameter related to changes inside the nanopore because the active binding sites for the analyte are only available inside the nanopore. The values for R_p obtained after simulation with equivalent circuit are plotted in Figure. 4.5(a), showing the influence of pore diameter and biotin concentration on R_p. At the lowest concentration of biotin 0.2 μM, the pore resistance decreases from $6.1x10^3$ to $2.8x10^3$ Ω when the pore diameter is increased from 25 nm to 65 nm showing better sensitivity using NPA platform with smaller nanopores.

To explain the observed behaviour it is important to consider other parameters including not only pore diameters but also the size and charge of analyte molecules and charge of immobilized molecules inside nanopores (streptavidin). The molecular size of streptavidin tetramer is about 4-5 nm and it is immobilized as a monolayer inside pores, which increased in thickness by around 6-8 nm after the binding of biotin. This binding reaction causes a significant change of surface charge and conductivity of formed streptavidin-biotin complex and consequently pore resistance, which is used as parameter for impedance biosensing. These resistance/conductivity changes from binding reaction inside smaller nanopore (<25 nm) are more significant because charged analyte molecules are very close to each other and more sensitive to AC oscillation of ions inside the nanopore compared to large nanopores. In the case of large pore diameter (65 nm) the intermolecular interaction as result of binding of analyte molecules (biotin) is less influential and the impedance measurement is dominated

by the bulk properties of the solution. As there is enough space inside the pores and small changes in impedance due to effects at the walls of the nanopores become insignificant. So it can be concluded that the molecular size of biotin and streptavidin doesn't have significant effect for larger pore diameters. This type of nanopore biosensing concept based on changing conductivity without of the use of pore blocking mechanism was previously demonstrated for impedance biosensing of DNA hybridization [28, 40]. For this type of nanopore biosensors to have the smaller pores is beneficial because the influence of the surface effects is greater and the signal is affected significantly (lesser area available for bulk solution) as reported in previous studies [41-42]. However, there is limitation, if the pore diameters are reduced below 10 nm; we may observe high pore resistance due to the limited transport of biomolecules inside the nanopores, which could block nanopores at some point of concentration.

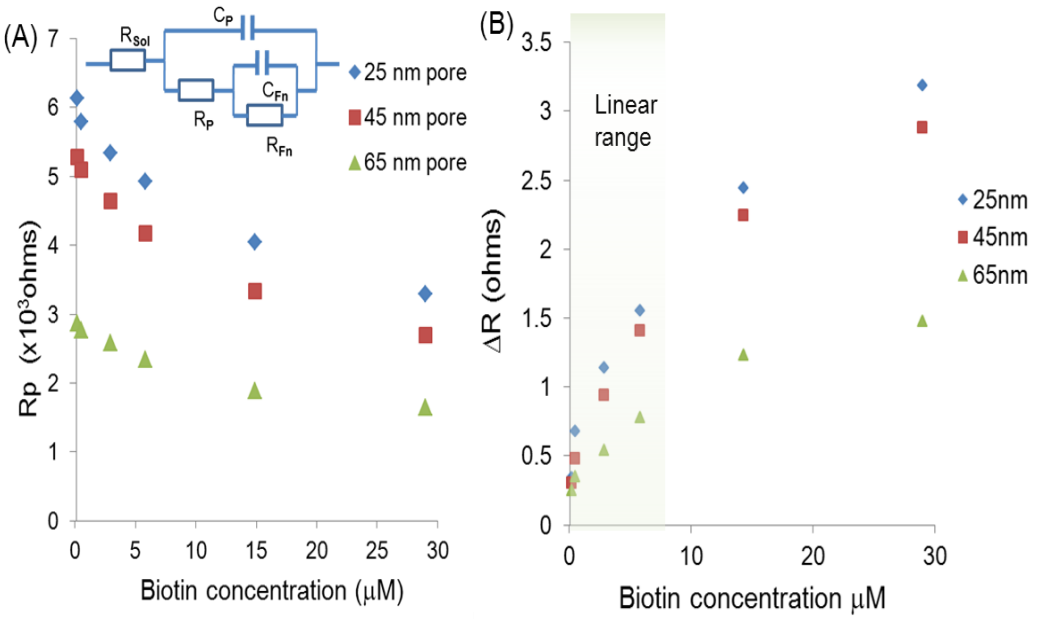

***Figure 4.5**: (a) A plot showing relation between the pore diameters and biotin concentrations and their influence on the nanopore resistance R_p. The proposed equivalent circuit (inset) used for the simulation of experimental data is presented in inset. (b) Calibration graph showing changes of pore resistance ΔR with biotin concentration using NPA biosensor with different pore diameters (25 nm to 65 nm).*

The resistivity change $\Delta R = R_0 - R_x$ is presented as a biosensing signal where R_0 is value taken with pore resistance at zero biotin concentration and Rx taken for pore resistance on each biotin concentration (Figure 4.5b). It was observed that the increase in ΔR value was linear at lower concentration range and after concentration over 10 μM the graph tends to reach saturation phase. Interestingly this behaviour is observed for both small and large nanopores and it is not influenced by the pore diameters. This result suggests that saturation signal is related to the surface reaction and binding all available streptavidin molecules (Figure 4.5b).

Since it was found that the smaller pore diameter provides greater sensitivity and performance, we used the NPA platform with 25 nm pore diameters to study the influence of pore length on electrochemical signal and biosensing performance. For that purpose we fabricated NPA biosensing platforms with different pore lengths (4.5 μm, 9 μm, 13.5 μm and 18 μm) and carried out a series of EIS measurements at different concentrations of biotin. The Nyquist plot was generated from constant concentration of biotin (0.2 μM) is shown in Figure 4.4b. The graph shows the trend of increasing impedance over the range of frequencies with respect to increasing pore length. Further measurements were performed by simulating the experimental data with the proposed equivalent circuit to find value of R_p for various length of NPA (Figure 4.6a). It was found that the R_p changed from $3x10^4$ to $10.5x10^4$ Ω as length of NPA increased from 4.5 μm to 18 μm. The graph clearly shows the increase in the pore resistance with increasing the pore length. The characteristic saturation in signal was observed at higher concentration of biotin (near 15 μM) showing the upper limit of detection for biotin.

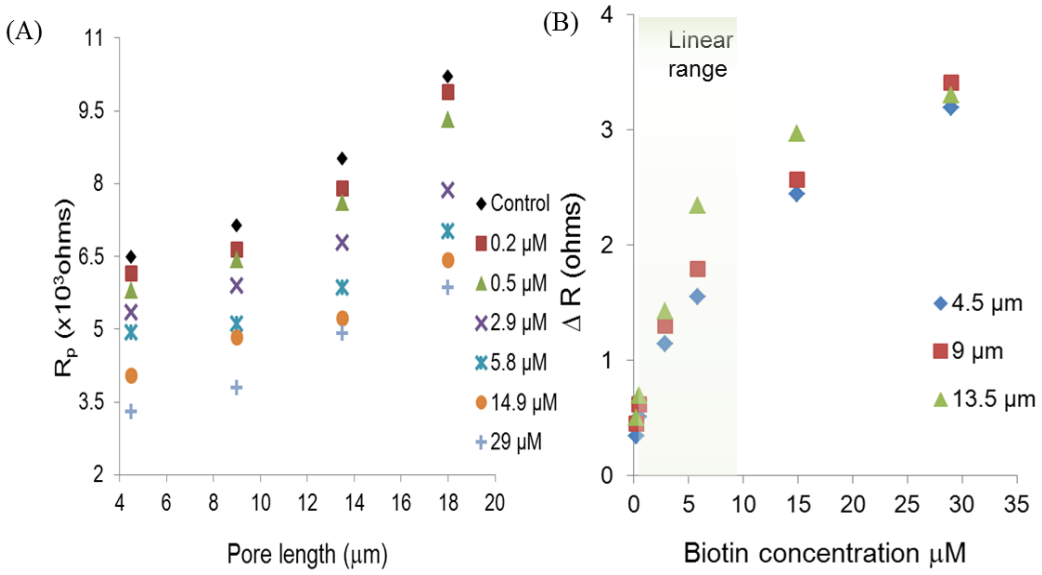

Figure 4.6: *(a) Graph showing changes of pore resistance ΔR of NPA biosensor with biotin concentration at different pore length (b) A calibration plot for different pore length of NPA biosensor at lower concentration (0.2 – 5.8 µM) of biotin show the significant linearity between actual pore resistance ΔR and biotin concentration.*

In the lower concentration range the sensor showed a linear response (R^2 = 0.96) from 0.2 to 10 µM (Figure. 4.6b). It was found that increasing pore length beyond 10-15 µm did not provide linear responses. Long nanopores presented very high resistances, hence small changes inside the nanopores were not detectable, and the pore impedance was dominated by NPA resistance. Increasing nanopore length to more than 10 µm to 15 µm does not seem too good for such type of biosensing detection as the longer pore lengths mean long for diffusion times of the analyte molecules and hence high resistance for the system.

It was observed that pore resistance is a key factor to be considered in the optimization of biosensing performance of EIS nanopore based devices. In our case the pore resistance with respect to lower concentration (0.2-10 µM) it has linear relationship (R^2 = 0.96). The detection limit for biotin concentration using this system was 0.2 µM. However we believe lower concentrations can be

detected by lowering nanopore diameters (< 25 nm). NPA with pore diameters below 20 nm are difficult to make using the anodization conditions used in our experiments (oxalic acid). The use of other electrolytes (sulphuric acid) and lower voltages (10-15V) is required to produce such pores. However, there is limitation that these smaller nanopores with a diameter between 5-10 nm may not perform well as non-Faradaic biosensing devices as the small pore size may limit the diffusion of the larger analyte molecules such as protein and enzymes. The best performance for the biosensing platform was observed with nanopore diameters of 20-40 nm with a length of 4-15 μm. Reduction in nanopore length below 4 μm could reduce robustness of NPA biosensor device.

4.4. Conclusion

The impact of pore dimensions and surface chemistry of nanopore arrays was explored and their application in a non-Faradaic impedance nanopore biosensor for the detection of biological entities such as protein molecules was demonstrated. A new method for specific functionalization exclusively inside nanopores was used to achieve the critical effect on electrochemical charge transfer by using nanopore array. The results show that measuring biotin concentrations from 0.2 μM to 29 μM in PBS buffer solution can be successfully achieved without using any labelled marker of signal enhancer redox probe. It was observed that pore resistance is a key factor to be considered in the optimization of biosensing performance of non-Faradaic EIS nanopore based devices. It was also observed that R_p with respect to concentration decreased with increasing concentration of analyte which is a consequence of the properties of binding biotin molecules inside the nanopores. This behaviour is more significant within

the low frequency range 1Hz - 20 KHz showing the magnitude of the impedance is affected considerably by the biotin concentration. However, linearity is limited with concentration showing typical saturation at higher concentration of 30 μM and linear range from 0.2 -10 μM. Our results confirmed that pore dimensions including pore diameters and length have considerable influence on biosensing performance. It was found that lowering pore diameters (<30 nm) provides better response and sensitivity. However there is a limitation to the size reduction as sizes comparable to the size of analyte molecules will prevent diffusion molecules inside the pore. Regarding pore length it was found that longer pores (>10 μm) are also not favourable for non-Faradaic EIS detection due to the higher resistance and long time for diffusion of analyte molecules inside nanopores. Hence it is critical to optimize pore dimensions to achieve optimal performances of nanopore based electrochemical biosensing devices. These devices have considerable potential toward development simple and inexpensive sensing devices for broad biomedical applications.

4.5. References

1. Feng, J.; Liu, J.; Wu, B.; Wang, G., Impedance Characteristics of Amine Modified Single Glass Nanopores. *Analytical Chemistry* **2010,** 82, (11), 4520-4528.
2. Daniels, J. S.; Pourmand, N., Label-Free Impedance Biosensors: Opportunities and Challenges. *Electroanalysis* **2007,** 19, (12), 1239-1257.
3. Pänke, O.; Balkenhohl, T.; Kafka, J.; Schäfer, D.; Lisdat, F., Impedance Spectroscopy and Biosensing. In *Biosensing for the 21st Century*, Renneberg, R.; Lisdat, F., Eds. Springer Berlin Heidelberg: 2008; Vol. 109, pp 195-237.
4. Yameen, B.; Ali, M.; Neumann, R.; Ensinger, W.; Knoll, W.; Azzaroni, O., Synthetic Proton-Gated Ion Channels via Single Solid-State Nanochannels

Modified with Responsive Polymer Brushes. *Nano Letters* **2009,** 9, (7), 2788-2793.

5. Li, S. J.; Li, J.; Wang, K.; Wang, C.; Xu, J. J.; Chen, H. Y.; Xia, X. H.; Huo, Q., A Nanochannel Array-Based Electrochemical Device for Quantitative Label-free DNA Analysis. *ACS Nano* **2010,** 4, (11), 6417-6424.
6. Darder, M.; Aranda, P.; Hernández-Vélez, M.; Manova, E.; Ruiz-Hitzky, E., Encapsulation of enzymes in alumina membranes of controlled pore size. *Thin Solid Films* **2006,** 495, (1–2), 321-326.
7. Reimhult, E.; Kumar, K., Membrane biosensor platforms using nano- and microporous supports. *Trends in Biotechnology* **2008,** 26, (2), 82-89.
8. Nguyen, B. T. T.; Koh, G.; Lim, H. S.; Chua, A. J. S.; Ng, M. M. L.; Toh, C. S., Membrane-Based Electrochemical Nanobiosensor for the Detection of Virus. *Analytical Chemistry* **2009,** 81, (17), 7226-7234.
9. Lillo, M.; Losic, D., Pore opening detection for controlled dissolution of barrier oxide layer and fabrication of nanoporous alumina with through-hole morphology. *Journal of Membrane Science* **2009,** 327, (1–2), 11-17.
10. Cheng, I. F.; Yang, H. L.; Chung, C. C.; Chang, H. C., A Rapid Electrochemical Biosensor Based on an AC Electrokinetics Enhanced Immuno-reaction. *Analyst* **2013**.
11. Ronkainen, N. J.; Halsall, H. B.; Heineman, W. R., Electrochemical biosensors. *Chemical Society Reviews* **2010,** 39, (5), 1747-1763.
12. Pei, R.; Cheng, Z.; Wang, E.; Yang, X., Amplification of antigen–antibody interactions based on biotin labeled protein–streptavidin network complex using impedance spectroscopy. *Biosensors and Bioelectronics* **2001,** 16, (6), 355-361.
13. Yu, X.; Lv, R.; Ma, Z.; Liu, Z.; Hao, Y.; Li, Q.; Xu, D., An impedance array biosensor for detection of multiple antibody-antigen interactions. *Analyst* **2006,** 131, (6), 745-750.
14. González, J. A.; López, V.; Bautista, A.; Otero, E.; Nóvoa, X. R., Characterization of porous aluminium oxide films from a.c. impedance measurements. *Journal of Applied Electrochemistry* **1999,** 29, (2), 229-238.
15. de la Escosura-Muñiz, A.; Merkoçi, A., Label-free voltammetric immunosensor using a nanoporous membrane based platform. *Electrochemistry Communications* **2010,** 12, (6), 859-863.

16. Herzog, G.; Arrigan, D. W. M., Electrochemical strategies for the label-free detection of amino acids, peptides and proteins. *Analyst* **2007,** 132, (7), 615-632.
17. Xiao, Y.; Li, C. M.; Liu, Y., Electrochemical impedance characterization of antibody–antigen interaction with signal amplification based on polypyrrole–streptavidin. *Biosensors and Bioelectronics* **2007,** 22, (12), 3161-3166.
18. Ouerghi, O.; Touhami, A.; Jaffrezic-Renault, N.; Martelet, C.; Ouada, H. B.; Cosnier, S., Impedimetric immunosensor using avidin–biotin for antibody immobilization. *Bioelectrochemistry* **2002,** 56, (1–2), 131-133.
19. Dickey, E.; Varghese, O.; Ong, K.; Gong, D.; Paulose, M.; Grimes, C., Room Temperature Ammonia and Humidity Sensing Using Highly Ordered Nanoporous Alumina Films. *Sensors* **2002,** 2, (3), 91-110.
20. Takhistov, P., Electrochemical synthesis and impedance characterization of nano-patterned biosensor substrate. *Biosensors and Bioelectronics* **2004,** 19, (11), 1445-1456.
21. Potucek, R. K.; Rateick, R. G.; Birss, V. I., Impedance Characterization of Anodic Barrier Al Oxide Film Beneath Porous Oxide Layer. *Journal of The Electrochemical Society* **2006,** 153, (8), B304-B310.
22. Nguyen, B. T. T.; Peh, A. E. K.; Chee, C. Y. L.; Fink, K.; Chow, V. T. K.; Ng, M. M. L.; Toh, C.-S., Electrochemical impedance spectroscopy characterization of nanoporous alumina dengue virus biosensor. *Bioelectrochemistry* **2012,** 88, (0), 15-21.
23. Orazem, M. E.; Tribollet, B., An integrated approach to electrochemical impedance spectroscopy. *Electrochimica Acta* **2008,** 53, (25), 7360-7366.
24. Eftekhari, F.; Escobedo, C.; Ferreira, J.; Duan, X.; Girotto, E. M.; Brolo, A. G.; Gordon, R.; Sinton, D., Nanoholes As Nanochannels: Flow-through Plasmonic Sensing. *Analytical Chemistry* **2009,** 81, (11), 4308-4311.
25. Zhang, J.; Zhu, J., A novel amperometric biosensor based on gold nanoparticles-mesoporous silica composite for biosensing glucose. *Sci. China Ser. B-Chem.* **2009,** 52, (6), 815-820.
26. Masuda, H.; Fukuda, K., Ordered Metal Nanohole Arrays Made by a Two-Step Replication of Honeycomb Structures of Anodic Alumina. *Science* **1995,** 268, (5216), 1466-1468.

27. Berdat, D.; Marin, A.; Herrera, F.; Gijs, M. A. M., DNA biosensor using fluorescence microscopy and impedance spectroscopy. *Sensors and Actuators B: Chemical* **2006,** 118, (1–2), 53-59.
28. Vlassiouk, I.; Takmakov, P.; Smirnov, S., Sensing DNA Hybridization via Ionic Conductance through a Nanoporous Electrode. *Langmuir* **2005,** 21, (11), 4776-4778.
29. Losic, D.; Velleman, L.; Kant, K.; Kumeria, T.; Gulati, K.; Shapter, J. G.; Beattie, D. A.; Simovic, S., Self-ordering Electrochemistry: A Simple Approach for Engineering Nanopore and Nanotube Arrays for Emerging Applications. *Australian Journal of Chemistry* **2011,** 64, (3), 294-301.
30. Chilcott, T. C.; Guo, C., Impedance and dielectric characterizations of ionic partitioning in interfaces that membranous, biomimetic and gold surfaces form with electrolytes. *Electrochimica Acta* **2013,** 98, (0), 274-287.
31. Nandigana, V. V. R.; Aluru, N. R., Characterization of electrochemical properties of a micro–nanochannel integrated system using computational impedance spectroscopy (CIS). *Electrochimica Acta* **2013,** 105, (0), 514-523.
32. Zhu, Z.W.; Wang, Y.; Zhang, X.; Sun, C.F.; Li, M.G.; Yan, J.W.; Mao, B.W., Electrochemical Impedance Spectroscopy and Atomic Force Microscopic Studies of Electrical and Mechanical Properties of Nano-Black Lipid Membranes and Size Dependence. *Langmuir* **2012,** 28, (41), 14739-14746.
33. Feng, J.; Liu, J.; Wu, B.; Wang, G., Impedance Characteristics of Amine Modified Single Glass Nanopores. *Analytical Chemistry* **2010,** 82, (11), 4520-4528.
34. Lisdat, F.; Schäfer, D., The use of electrochemical impedance spectroscopy for biosensing. *Anal Bioanal Chem* **2008,** 391, (5), 1555-1567.
35. Siwy, Z.; Fuliński, A., A nanodevice for rectification and pumping ions. *American Journal of Physics* **2004,** 72, (5), 567-574.
36. Lee, W.; Ji, R.; Gösele, U.; Nielsch, K., Fast fabrication of long-range ordered porous alumina membranes by hard anodization. *Nature materials* **2006,** 5, (9), 741-747.

37. Md Jani, A. M.; Losic, D.; Voelcker, N. H., Nanoporous anodic aluminium oxide: Advances in surface engineering and emerging applications. *Progress in Materials Science* **2013,** 58, (5), 636-704.
38. Zenobi, M. C.; Luengo, C. V.; Avena, M. J.; Rueda, E. H., An ATR-FTIR study of different phosphonic acids in aqueous solution. *Spectrochimica Acta Part A: Molecular and Biomolecular Spectroscopy* **2008,** 70, (2), 270-276.
39. Yu, J.; Cao, H.; He, Y., A new tree structure code for equivalent circuit and evolutionary estimation of parameters. *Chemometrics and intelligent laboratory systems* **2007,** 85, (1), 27-39.
40. Takmakov, P.; Vlassiouk, I.; Smirnov, S., Hydrothermally shrunk alumina nanopores and their application to DNA sensing. *Analyst* **2006,** 131, (11), 1248-1253.
41. Girginov, A.; Popova, A.; Kanazirski, I.; Zahariev, A., Characterization of complex anodic alumina films by electrochemical impedance spectroscopy. *Thin Solid Films* **2006,** 515, (4), 1548-1551.
42. Singh, R.; Sharma, P. P.; Baltus, R. E.; Suni, I. I., Nanopore immunosensor for peanut protein Ara h1. *Sensors and Actuators B: Chemical* **2010,** 145, (1), 98-103.

Chapter 5

CHARACTERIZATION OF IMPEDANCE BIOSENSING PERFORMANCE OF SINGLE AND NANOPORE ARRAYS OF ANODIC POROUS ALUMINA FABRICATED BY FOCUSED ION BEAM (FIB) MILLING

K. Kant, C. Priest, J. G. Shapter, D. Losic, "*Characterization of impedance biosensing performance of single and nanopore arrays of anodic porous alumina fabricated by focused ion beam (FIB) milling*" Electrochemica Acta 139 (2014) 225–231.

K. Kant, J. G. Shapter, C. Priest, D. Losic, '*Impedance spectroscopy study on focused ion beam (FIB) milled nanopore arrays of alumina membrane*' Nanotoday, 8-12 Dec. **2013** Singapore.

5.1. Introduction

The characterization of electrochemical properties of materials with micro and nano dimensions is one of the critical issues for application of these materials based on these properties. In particular the characterization of nanoscale structures fabricated with various nano-tubular morphologies is difficult. The FIB provides fabrication of nanostructures by the removal of material form the solid surface (milling) or their deposition or surface modifications, but also at the same time has the capability to provide topographical analysis [1, 2]. Nanostructures fabricated by FIB are very well defined and can be characterize by use of electrochemical techniques.

In recent years, nanoporous anodic alumina fabricated by self-ordered electrochemical anodization process with vertically aligned nanopores has created great curiosity due to their unique properties and broad applications such as molecular separations, biosensing, energy storage and drug delivery [3, 4]. The NPA possess uniform and high density pore structures with perfectly ordered hexagonal pattern and controllable pore dimensions which are important features for membrane biosensing [5-7]. The NPA structures are fabricated from an aluminium foil by electrochemical anodization in a certain acid electrolyte involving several steps with a thin barrier layer at the end of nanopore [6]. This formed barrier layer closes one end of the nanopores and requires removal of oxide layer to make open pores. This process is performed by dissolution in phosphoric acid and has a limitation in cases where single or controllable number of opened nanopores is required [7, 8]. To address this problem, previous studies demonstrated that FIB milling can be productively used for controlled removal of the oxide barrier film and pore opening of a NPA to form a single or array of

nanopores [9, 10]. The milling and patterning of this small area to open nanopores because it requires very fine tunings of position of ion beam. The use of 30 keV Ga^+ focused beam at 1.5 pA beam current for a short duration of time is required to open single nanopore of a NPA [11]. In another approach FIB is used to create arrays of close-packed patterns with flexible depths on polished Al surfaces [12-14]. It was found that FIB milled concaves of few nanometres can effectively guide the growth of the NPA during anodization process.

The fabrication of NPA pores with different pores sizes, inter-pore distance, shapes and patterns is demonstrated and combination FIB and anodization method open exciting opportunity to design more sophisticated sensing devices based on nanopore structure [11]. However electrochemical properties and application of NPA arrays with smaller number of nanopores for biosensing is not well explored. High electrochemical sensitivity with ability for single molecular detection is observed on single pore devices prepared by FIB on Si but this fabrication is very complex as it needs several steps of lithography and FIB milling [15]. The preparation of NPA based pore array devices is simpler and inexpensive and will provide a better understanding of the electrochemical properties important for their application for nanopore biosensing [16, 17]. Electrochemical impedance spectroscopy (EIS) is recognized as a promising technique to perform these characterizations. EIS could provide useful information about electrochemical properties of nanopores; influence of ion concentration, dimensions and morphology of nanopores which are important for optimization their biosensing performances. Herein to address some of these questions we are reporting the fabrication of these NPA arrays with different number of nanopores combined with FIB and study their properties

The aim of this work is to explore electrochemical properties of NPA arrays and their applications for impedance biosensing [18, 19]. The specific objectives are to determine the performance of nanopore biosensor depending of number of nanopores. To demonstrate this biosensing concept a FIB patterned nanopore array based label free electrochemical biosensor for biotin detection is used. The scheme of FIB fabrication process and proposed biosensing device is presented in Figure 5.1.

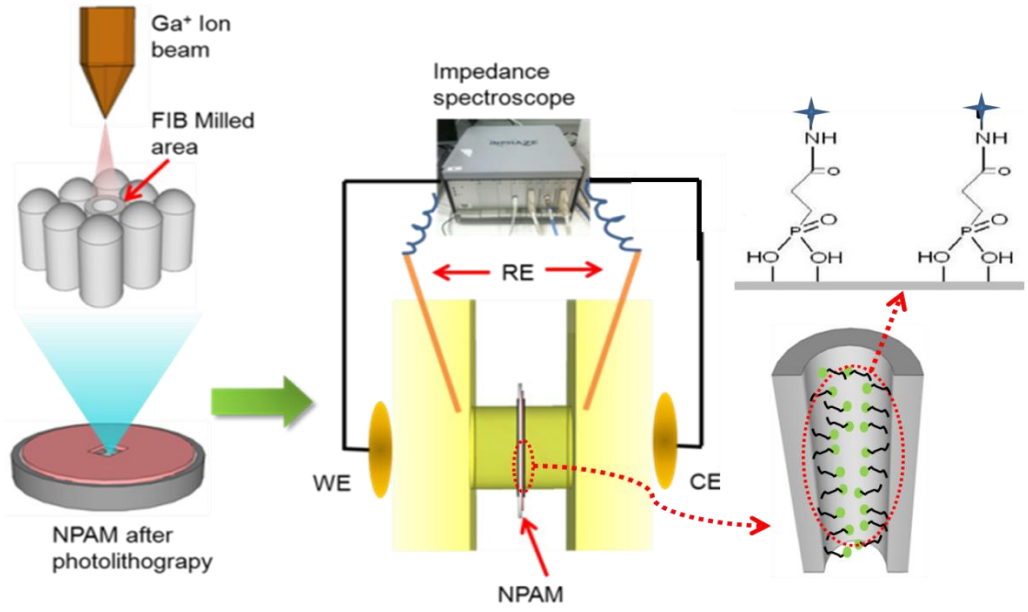

Figure 5.1: *A schematic of experimental setup for fabricated nano porous alumina (NPA) modified with streptavidin as sensing platform. The FIB milled open nanopore of NPA placed in EIS cell for impedance characterization.*

The fabrication of the NPA sensing platform is carried out using anodization of aluminum foil, followed by photolithography to mask bottom surface (a barrier layer) with photoresist followed by FIB milling on the bottom to remove barrier layer of selected number of nanopores. The surface inside the opened pores was functionalized by phosphonic acid (PHA) and (N-hydroxysuccinimide, 1-ethyl-3-(3-dimethylaminopropyl) carbodimide) NHS-EDC

chemistry, followed by the covalent attachment of antibody molecules (streptavidin), which is used as a binding surface for the selective capture of antigen molecules i.e. biotin. A four electrode cell electrochemical cell was used to characterize the electrochemical properties of NPA devices with different number of nanopores and their biosensing performance after addition of different concentration of analyte (biotin). The EIS is applied here for detection of binding analyte molecules inside nanopores because as, it is a very sensitive, simple and low cost method, suitable for development of portable biosensing devices.

5.2. Materials and Methods

The details have been provided in Chapter 4 section 4.2.

5.2.1. Preparation of NPA and photolithographic patterning

NPA was prepared by a two-step anodization process as details are provided in Chapter 3 section 3.2.1 [20]. The fabricated NPA is patterned with photoresist using photolithography to expose the nanoporous array in a selected area of the membrane. Further details have been provided in Chapter 3 section 3.2.2. In this way an opening of 20 μm circular pin-hole in the photoresist was obtained for further FIB pore opening. Fabricated NPAs were characterized using SEM before FIB milling process.

5.2.2. Pore opening of NPA by FIB milling

The FIB Helios Nano-lab 600 from FEI, consisting of a focused ion-beam for sample milling and patterning, and a high resolution scanning electron microscope (SEM) for imaging of the surface of the sample after milling was used. The oxide wall thickness between two neighbouring nanopores and the

barrier layer thickness is determined by the anodization voltage. If the anodization is done at high voltage (hard anodization) the barrier layer is thicker than the low voltage (mild anodization) anodization. Instrument software generated pre-designed square patterns with 100 nm^2, 2x100 nm^2, 3x100 nm^2, 1 μm^2 and 20 μm^2 areas were mapped onto the NPA samples and then milled by using a 30 keV Ga^+ focused beam, with a beam current of between 1.5 and 48 pA. Milling times varied from 2 second to 10 min depending on the area and depth of the pattern. The milling rate varies with the ion beam current and a small beam current is always preferred for milling process of structures with nanoscale dimensions. The SEM beam line was used to characterize NPA samples before and after FIB patterning.

5.2.3. Surface modification inside NPA array

Surface modification of NPA was performed by soaking the membrane in aqueous solution of 5 mM 2-carboxyethyl phosphonic acid for 72 hours [21]. Further details have been provided in Chapter 4 section 4.3.2.

5.2.4. EIS measurements of FIB milled NPA

Electrochemical measurements were carried out using an EIS spectrometer (Inphaze, Pty. Ltd. Sydney, Australia) with a four-electrode system which is specifically designed for EIS characterization of NPA. Two gold foils formed the working and counter electrodes and two Ag/AgCl electrodes used as reference electrodes [22]. The FIB patterned nanoporous membrane was sandwiched between two chambers filled with the buffer solution and in contact with reference electrodes on each side. The working and counter electrodes were respectively placed at the end of two chambers (Figure 5.1). An equivalent circuit is used to

balance the resistance and capacitance for entire system and monitor the changes inside the nanopores of nanoporous array. Biotin solutions of 0.2 μM – 29 μM concentrations were tested in a series of experiments to explore binding with functionalized streptavidin molecules inside the NPA arrays. The electrochemical impedances were acquired in the frequency range from 0.01 Hz to 1MHz.

5.3. Results and discussion

5.3.1. Structural characterization of NPA arrays

SEM images of prepared NPAs from single opening to multi pore arrays opening are summarised in Figure 5.2 showing their typical morphology with the FIB milled bottom surface of NPA. The SEM image of the corresponding bottom surface shows typical hexagonal cell structures, which form the barrier film surface [6, 23]. These were examined before and after patterning the square pattern on NPA by FIB. The NPA nanopores prepared by 100 nm^2, 2x100 nm^2, 3x100 nm^2, 1 μm^2 FIB milling NPA and 20 μm^2 with chemically opened pores are presented in Figure 5.2. The NPA array before FIB milling in Figure 5.2a shows the bottom view of nanopore array with high resolution image, Figure 5.2b shows the 100 nm square pattern by FIB milling where we observe to have average of 2-3 nanopores. Our goal was to make single nanopore by milling 20-40 nm area, but it is important to note that it was extremely difficult to mill the central part on NPA bottom cell because low energy ion beam was not very stable at very small area. Therefore we choose to mill higher area 100 nm^2 (square) which we found as the minimum size of the FIB beam which gives stable and reproducible milling of NPA. Even this surface area correspond to actual size of single NPA cell we were not able to perfectly mill central part of the cell to get single opened pore.

This was reason why the most of our 100 nm^2 milled NPA have opened 2-3 pores as a results milling of area between several cells (Figure. 5.2b).

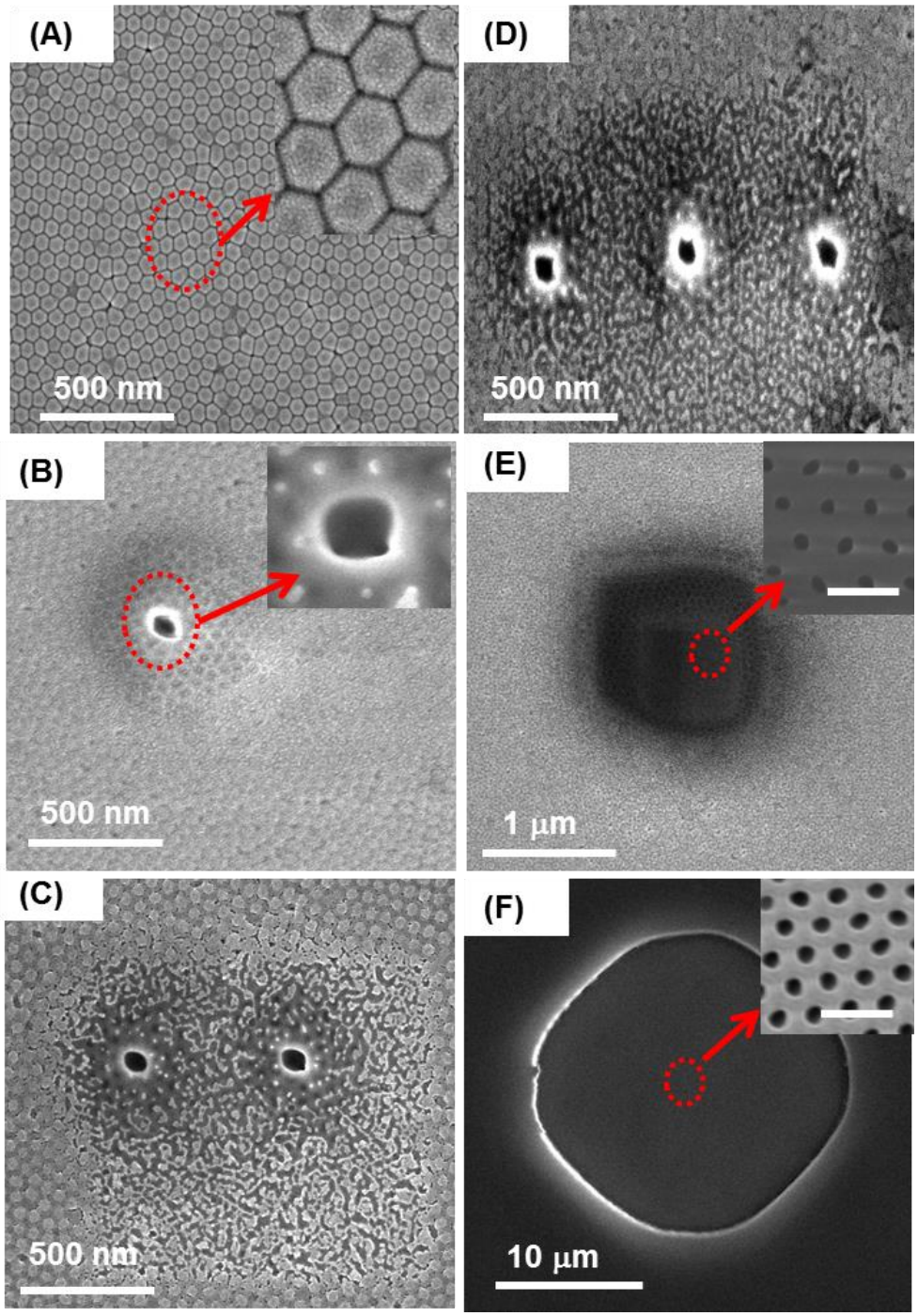

Figure 5.2: *SEM images of the bottom surface of NPA used for FIB patterning and nanopore sensing platform (a) bottom view of nanopore array with high resolution image. Pore opening with FIB milling of (b) 100 nm square area (c) 2x100 nm area (d) 3x100 nm area (e) 1 μm^2 area Chemically opened nanopores with 20 μm^2 of pore area is presented in (f). High resolution images of opened pores are shown in insets (100 nm scale).*

The Figure 5.2c, 5.2d, 5.2e presents patterns of 2x100 nm^2, 3x100 nm^2 respectively with corresponding number of pores. Figure 5.2e presents NPA with 1 μm^2 milled area showing that nanopores were opened. It also indicates that the FIB milling just removes the barrier layer from the bottom side of NPA. Figure 5.2f is 20 μm^2 square with high resolution image showing open nanopore array which is removed chemically etching by 10% phosphoric acid for 30min. The number of nanopore in this sample is determined by SEM characterization considering that each 100 nm square pattern contains 2-3 nanopores, so we can also define the nanopore surface area in terms of number of nanopores available in the pattern. So for pattern of 100 nm^2, 2x100 nm^2, 3x100 nm^2, 1 μm^2 and 20 μm^2 the number of pores increases respectively.

5.3.2. Characterization for surface modification inside nanopore array

FTIR spectra of NPAs before after modification with phosphonic acid (PHA) were taken to provide evidence of surface modification of NPA, which is required for immobilization of biosensing molecules inside nanopores [24, 25]. To achieve selective immobilization of probing biomolecule (streptavidin) specifically inside nanopores of prepared NPAs a special surface functionalization process has been developed which includes: modification of NPA with PHA, activation of COOH with NHS/EDC and covalent binding of streptavidin/biotin [25]. Details are presented in Chapter 4 section 4.3.2.

5.3.3. Impedance spectroscopy characterization of nanopore array

In order to characterize the label free sensing performance of FIB fabricated nanopore array with protein molecules, a series of electrochemical

impedance spectroscopy measurements has been carried out [26]. To have the best fit from obtained impedance measurements a simplified electrical model has been established and presented in Figure 5.4. The equivalent circuit contributes to simulate practical impedance value circuit consists one series resistance with two parallel resistances and capacitance [27-29]. The total impedance could be expressed with the following equivalent circuit where R_{sol} is the resistance for the buffer of the cell; R_p is resistance for array of nanopore [30]. As we increase the diameter of the pore the value of pore resistance reduces but at the same time it also increases if we vary the length of the nanopore array [25]. The detailed information about the equivalent circuit and the pore resistance is been given in Chapter 4 section 4.2.4.

The collected impedance value for different number of pores/ working area shows the change in impedance with range of frequency. All NPA nanopore arrays of 100 nm^2, 2x100 nm^2, 3x100 nm^2, 1 μm^2 and 20 μm^2 were used to explore the change of impedance of NPA depending of number of opened nanopores. The impedance graphs form these samples were obtained for broad frequency range from 0.01Hz to 1MHz. The changes at low frequency range (0.01 Hz to 1 KHz) show significant influence of frequency on impedance signal. These impedance changes are minor for the NPA sample scanned at high range of frequency (100 KHz – 1 MHz). These results indicate that biosensing measurement using nanopores should be performed at frequency range (0.01 Hz to 20 KHz). The impedance biosensing measurements were performed from these NPA nanopore platforms with streptavidin modified after addition of series of biotin concentrations from 0.2 μM to 29 μM to explore the influence of number of nanopores on biosensor sensitivity. The resulting impedance showed the

characteristic frequency dependence of the sensing performance as shown in Figure 5.3.

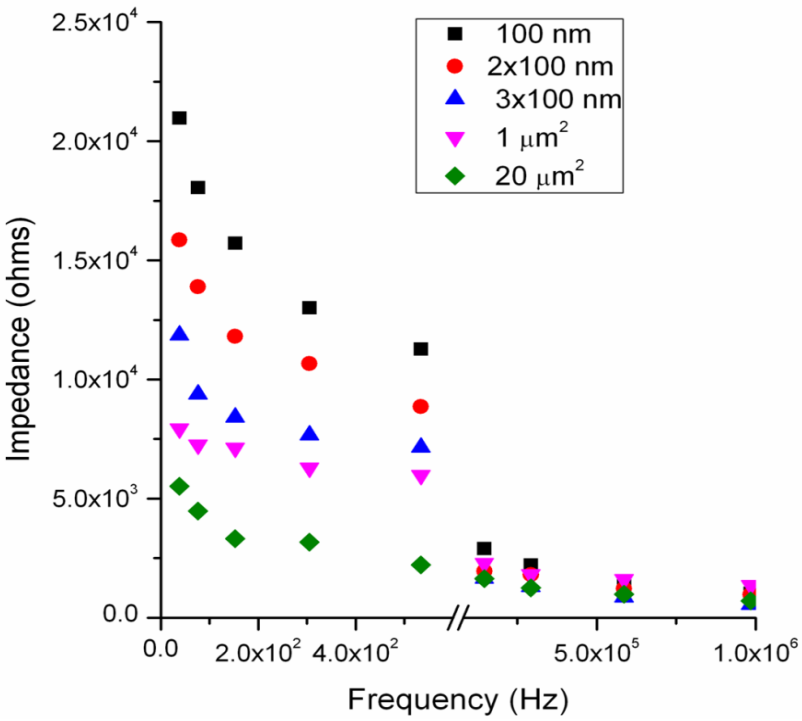

***Figure 5.3**: Impedance vs frequency plot obtained for NPA sensing platform in buffer with different number of opened pores prepared by FIB milling bottom part of NPA (100 nm to 1 μm^2) and chemical etched (20 μm^2). The graph shows the differences in impedance value at lower range of frequencies (inset).*

To provide better understanding of influence number of nanopores on biosensing performance The Nyquist plot (Z real Vs -Z imaginary) at constant concentration (0.2 μM) of biotin is created and presented in Figure 5.4. The Nyquist plot shows an increase in impedance with decreasing number of pores or working area as presented in other previous studies [12]. The experimental value was simulated by software [31] as detailed in Chapter 4 section 4.3.3. using the suggested equivalent circuit (Figure 5.4) to obtain the best-fit pore resistance (R_p) for the nanopore at particular concentration. The R_p value of a nanopore is observed to increase in resistance with decreasing the number of pores or working area.

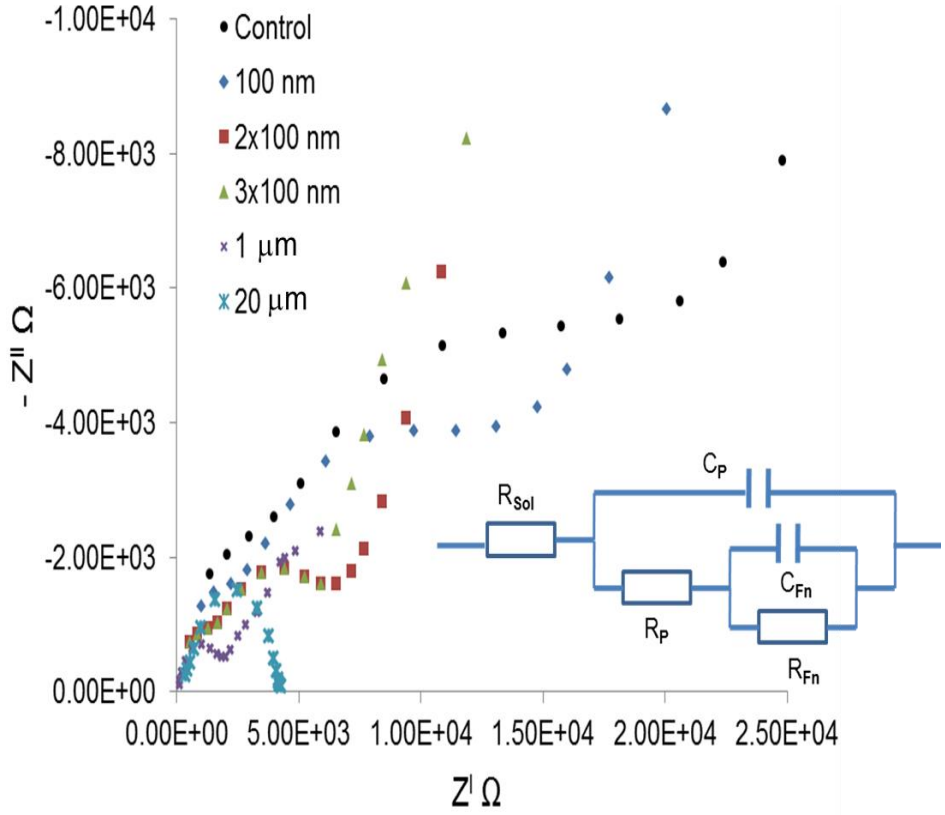

***Figure 5.4**: Nyquist plot obtained for NPA with different number of pores of NPA at constant concentration of biotin (0.2 µM) and proposed equivalent circuit is used to simulate the impedance data.*

The experimental data was simulated against the equivalent circuit and find out the exact value for the pore resistance. The R_p value of a nanopore was obtained as below table:

Working Area (nm)	R_{sol} (Ω)	R_p (Ω)	R_{Fn} (Ω)	C_p (F)	C_{Fn} (F)
Control	$5.35x10^{2}$	$11.02x10^{3}$	$9.43x10^{3}$	$5.29x10^{-9}$	$6.10x10^{-8}$
100	$5.20x10^{2}$	$9.81x10^{3}$	$8.81x10^{3}$	$6.5x10^{-10}$	$1.55x10^{-8}$
2x100	$5.28x10^{2}$	$8.09x10^{3}$	$7.22x10^{3}$	$1x10^{-9}$	$4.78x10^{-8}$
3x100	$5.18x10^{2}$	$7.48x10^{3}$	$6.54x10^{3}$	$1.11x10^{-8}$	$7.81x10^{-7}$
1000	$5.02x10^{2}$	$6.02x10^{3}$	$5.72x10^{3}$	$2x10^{-9}$	$2.68x10^{-7}$
20000	$5.11x10^{2}$	$3.12x10^{3}$	$4.22x10^{3}$	$4.38x10^{8}$	$5.24x10^{-6}$

***Table 5.1**: The extracted value for all the components of equivalent circuit for different working area.*

The impedance data shows one small semicircle at higher frequencies and the remaining points are tending to make another big semicircle at low frequencies. Due to the increase in signal to noise ratio and electrical double layer we were unable to take spectra at very lower frequencies below 0.1Hz. It is observed that the other remaining points are not the part of the tail but it is an incomplete semicircle.

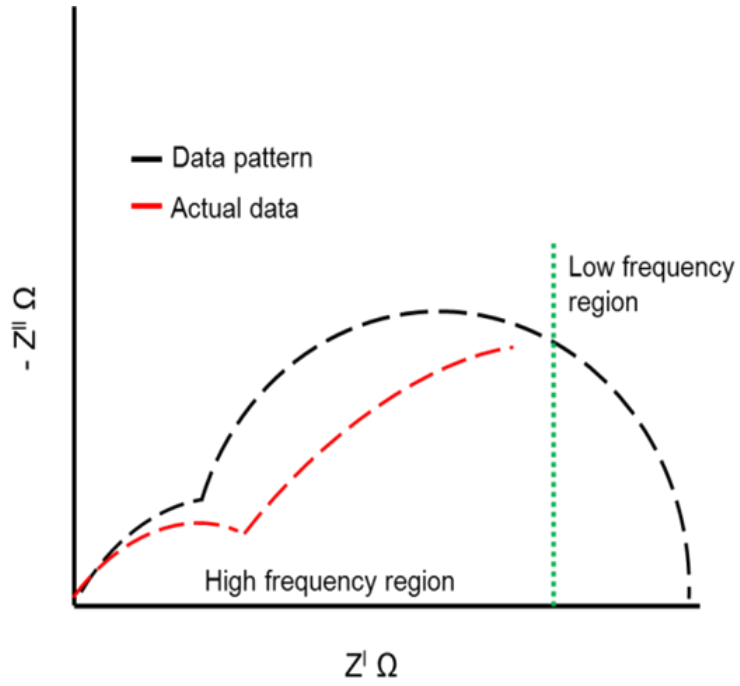

***Figure 5.5**: A Schematic of Nyquist plot obtained from NPA EIS measurement.*

In Figure 5.5 it is shown schematically how the remaining semicircle will be completed with the data points. In these two semicircles the first semicircle shows the impedance of the bulk of the membrane, the second semicircle represents the membrane-solution interface. In our system reducing the number of pores or active surface area in the system enhances the sensitivity and provides clear difference in impedance within the lower range of concentration. While a larger working area or higher number of pores provides increased bulk properties of the nanopore array and it is hard to distinguish the minor changes that happen

inside the nanopores. In case of 1 μm^2 and 20 μm^2 nanopore array areas we find a rapid decrease in the resistance of the system, which represents the bulk properties of the nanopore array. We calculated ΔR by subtracting value of pore resistance $\Delta R = R_0 - R_x$ where R_0 is without biotin and R_x is at particular biotin concentration. A linear relation between ΔR and concentration is observed in the lower range of biotin concentration with the signal becoming saturated at higher concentrations of biotin (Figure 5.6).

It also important to state that further reduction in working area below 100 nm (2-3 nanopores) reduces the rate of diffusion of ions across the nanopore array [32, 33]. These results are very small and undistinguishable impedance signals from nanopore due to the high resistance values for surrounding alumina material with non-opened pores. This signal is similar to the control NPA sample without of pore opening. Increasing the number of pores shows the reduction in the system resistance with lower impedance value and thus has high diffusion of ions across the membrane. However a large number of nanopores from nanopore arrays also do not provide a distinct difference in biosensing. The exposed nanopore array of 1 μm^2 or 20 μm^2 in area have around 250 to 50000 of closely located nanopores in it and provides the combined effect of all the pores together [34, 35]. The changes observed in EIS for different working areas of the nanopore array were very significant even at the lower concentrations of biotin. However, the detection limit (0.2 μM) can be achievable by using minimum of 100 nm^2 (2-3 nanopores) area of nanopore array. The large nanopore arrays have early saturation concentrations (above 5 μM) but small working area array can have high saturation concentration (above 25 μM).

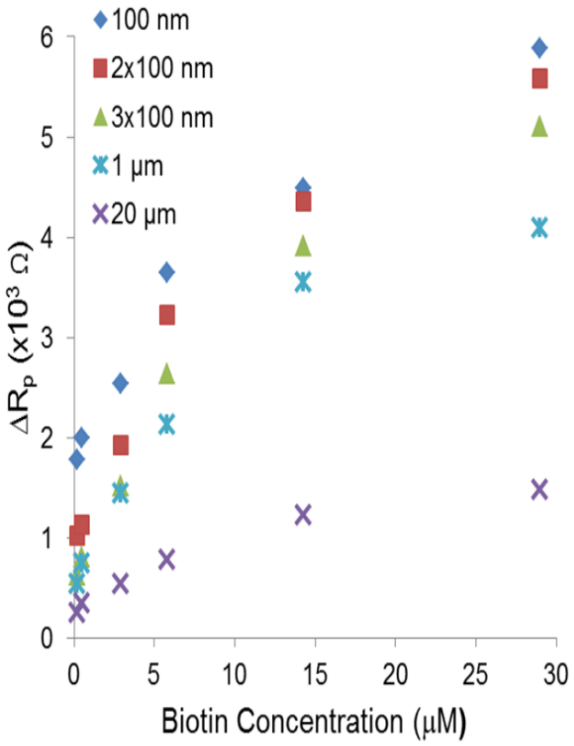

***Figure 5.6**: Graph showing response (pore resistance ΔR) of prepared NPA nanopore biosensors with different number of nanopores for various concentration of biotin.*

The impedance measurement for frequencies between 1 Hz – 20 KHz can achieve a significant change between two different nanopore arrays with only 3-10 nanopores in it. We believe that further reducing the number of pores for biosensing will require a signal probe to achieve reliable measurement. This label free impedance sensing method doesn't require any labelled markers for signal enhancement, and it is very simple, fast and reproducible.

5.4. Conclusion

The impact of the number of nanopores on the label free biosensing performance of a nanopore impedance biosensor for the detection of biological entities such as protein molecules is evaluated. The sensing device was based on a four-electrode electrochemical impedance system integrated with a nanopore

array-sensing platform functionalized with streptavidin, which specifically binds to biotin. The sensing principle was to measure changes in resistance as results of binding reaction without of use redox probe. The results show that measuring biotin concentrations from 0.2 μM in PBS buffer solution using a small sample volume (100 μL) can be successfully achieved without using any labelled marker of signal enhancer redox probe. The lower concentration below 0.2 μM was not distinguishable because of the limitation of the detection in this system. In this study it was found that small number of nanopores prepared by FIB milling area of 100 nm^2 to 3x100 nm^2 compared with large area of nanopore arrays are more sensitive for resistance based impedance label-free biosensing. The signal to noise ratio and electrical double layers are the limiting factor in such type of impedance biosensing and can be further improved by improving the FIB milling process and the design of device.

5.5. References

1. Liu, N. W.; Liu, C. Y.; Wang, H. H.; Hsu, C. F.; Lai, M. Y.; Chuang, T. H.; Wang, Y. L., Focused-Ion-Beam-Based Selective Closing and Opening of Anodic Alumina Nanochannels for the Growth of Nanowire Arrays Comprising Multiple Elements. *Advanced Materials* **2008,** 20, (13), 2547-2551.
2. Choi, J.; Wehrspohn, R. B.; Gösele, U., Mechanism of guided self-organization producing quasi-monodomain porous alumina. *Electrochimica Acta* **2005,** 50, (13), 2591-2595.
3. Chen, W.; Wu, J. S.; Xia, X. H., Porous Anodic Alumina with Continuously Manipulated Pore/Cell Size. *ACS Nano* **2008,** 2, (5), 959-965.
4. Hall, A. R.; van Dorp, S.; Lemay, S. G.; Dekker, C., Electrophoretic Force on a Protein-Coated DNA Molecule in a Solid-State Nanopore. *Nano Letters* **2009,** 9, (12), 4441-4445.

5. Masuda, H.; Fukuda, K., Ordered Metal Nanohole Arrays Made by a Two-Step Replication of Honeycomb Structures of Anodic Alumina. *Science* **1995,** 268, (5216), 1466-1468.
6. Losic, D.; Velleman, L.; Kant, K.; Kumeria, T.; Gulati, K.; Shapter, J. G.; Beattie, D. A.; Simovic, S., Self-ordering Electrochemistry: A Simple Approach for Engineering Nanopore and Nanotube Arrays for Emerging Applications*. *Australian Journal of Chemistry* **2011,** 64, (3), 294-301.
7. Harrell, C. C.; Lee, S. B.; Martin, C. R., Synthetic Single-Nanopore and Nanotube Membranes. *Analytical Chemistry* **2003,** 75, (24), 6861-6867.
8. Kim, J.; Gonzalez-Martin, A., Nanopore membrane-based electrochemical immunoassay. *J Solid State Electrochem* **2009,** 13, (7), 1037-1042.
9. Ayub, M.; Ivanov, A.; Hong, J.; Kuhn, P.; Instuli, E.; Edel, J. B.; Albrecht, T., Precise electrochemical fabrication of sub-20 nm solid-state nanopores for single-molecule biosensing. *Journal of Physics Condensed Matter* **2010,** 22, (45).
10. Lanyon, Y. H.; De Marzi, G.; Watson, Y. E.; Quinn, A. J.; Gleeson, J. P.; Redmond, G.; Arrigan, D. W. M., Fabrication of Nanopore Array Electrodes by Focused Ion Beam Milling. *Analytical Chemistry* **2007,** 79, (8), 3048-3055.
11. Lillo, M.; Losic, D., Ion-beam pore opening of porous anodic alumina: The formation of single nanopore and nanopore arrays. *Materials Letters* **2009,** 63, (3–4), 457-460.
12. Singh, R.; Sharma, P. P.; Baltus, R. E.; Suni, I. I., Nanopore immunosensor for peanut protein Ara h1. *Sensors and Actuators B: Chemical* **2010,** 145, (1), 98-103.
13. Feng, J.; Liu, J.; Wu, B.; Wang, G., Impedance Characteristics of Amine Modified Single Glass Nanopores. *Analytical Chemistry* **2010,** 82, (11), 4520-4528.
14. de la Escosura-Muñiz, A.; Merkoçi, A., Nanochannels Preparation and Application in Biosensing. *ACS Nano* **2012,** 6, (9), 7556-7583.
15. Vlassiouk, I.; Kozel, T. R.; Siwy, Z. S., Biosensing with Nanofluidic Diodes. *Journal of the American Chemical Society* **2009,** 131, (23), 8211-8220.

16. Liu, Q.; Yu, J.; Xiao, L.; Tang, J. C. O.; Zhang, Y.; Wang, P.; Yang, M., Impedance studies of bio-behavior and chemosensitivity of cancer cells by micro-electrode arrays. *Biosensors and Bioelectronics* **2009,** 24, (5), 1305-1310.
17. Römer, W.; Steinem, C., Impedance Analysis and Single-Channel Recordings on Nano-Black Lipid Membranes Based on Porous Alumina. *Biophysical Journal* **2004,** 86, (2), 955-965.
18. Han, A.; Schurmann, G.; Mondin, G.; Bitterli, R. A.; Hegelbach, N. G.; de Rooij, N. F.; Staufer, U., Sensing protein molecules using nanofabricated pores. *Applied Physics Letters* **2006,** 88, (9), 093901-3.
19. Rai, V.; Deng, J.; Toh, C.-S., Electrochemical nanoporous alumina membrane-based label-free DNA biosensor for the detection of Legionella sp. *Talanta* **2012,** 98, (0), 112-117.
20. Zhang, J.; Li, C. M., Nanoporous metals: fabrication strategies and advanced electrochemical applications in catalysis, sensing and energy systems. *Chemical Society Reviews* **2012,** 41, (21), 7016-7031.
21. Zhang, B.; Kong, T.; Xu, W.; Su, R.; Gao, Y.; Cheng, G., Surface Functionalization of Zinc Oxide by Carboxyalkylphosphonic Acid Self-Assembled Monolayers. *Langmuir* **2010,** 26, (6), 4514-4522.
22. Chilcott, T. C.; Guo, C., Impedance and dielectric characterizations of ionic partitioning in interfaces that membranous, biomimetic and gold surfaces form with electrolytes. *Electrochimica Acta* **2013,** 98, (0), 274-287.
23. Nguyen, B. T. T.; Koh, G.; Lim, H. S.; Chua, A. J. S.; Ng, M. M. L.; Toh, C. S., Membrane-Based Electrochemical Nanobiosensor for the Detection of Virus. *Analytical Chemistry* **2009,** 81, (17), 7226-7234.
24. Zenobi, M. C.; Luengo, C. V.; Avena, M. J.; Rueda, E. H., An ATR-FTIR study of different phosphonic acids in aqueous solution. *Spectrochimica Acta Part A: Molecular and Biomolecular Spectroscopy* **2008,** 70, (2), 270-276.
25. Kant, K.; Yu, J.; Priest, C.; Shapter, J. G.; Losic, D., Impedance nanopore biosensor: influence of pore dimensions on biosensing performance. *Analyst* **2014,** 139, 1134-1140.

26. Md Jani, A. M.; Losic, D.; Voelcker, N. H., Nanoporous anodic aluminium oxide: Advances in surface engineering and emerging applications. *Progress in Materials Science* **2013,** 58, (5), 636-704.
27. Yu, X.; Lv, R.; Ma, Z.; Liu, Z.; Hao, Y.; Li, Q.; Xu, D., An impedance array biosensor for detection of multiple antibody-antigen interactions. *Analyst* **2006,** 131, (6), 745-750.
28. Vlassiouk, I.; Takmakov, P.; Smirnov, S., Sensing DNA Hybridization via Ionic Conductance through a Nanoporous Electrode. *Langmuir* **2005,** 21, (11), 4776-4778.
29. Lisdat, F.; Schäfer, D., The use of electrochemical impedance spectroscopy for biosensing. *Anal Bioanal Chem* **2008,** 391, (5), 1555-1567.
30. Siwy, Z.; Fuliński, A., A nanodevice for rectification and pumping ions. *American Journal of Physics* **2004,** 72, (5), 567-574.
31. Yu, J.; Cao, H.; He, Y., A new tree structure code for equivalent circuit and evolutionary estimation of parameters. *Chemometrics and intelligent laboratory systems* **2007,** 85, (1), 27-39.
32. Girginov, A.; Popova, A.; Kanazirski, I.; Zahariev, A., Characterization of complex anodic alumina films by electrochemical impedance spectroscopy. *Thin Solid Films* **2006,** 515, (4), 1548-1551.
33. Lemay, S. G., Nanopore-Based Biosensors: The Interface between Ionics and Electronics. *ACS Nano* **2009,** 3, (4), 775-779.
34. Prakash, S.; Yeom, J.; Jin, N.; Adesida, I.; Shannon, M. A., Characterization of ionic transport at the nanoscale. *Proceedings of the Institution of Mechanical Engineers, Part N: Journal of Nanoengineering and Nanosystems* **2006,** 220, (2), 45-52.
35. Yu, J.; Liu, Z.; Yang, M.; Mak, A., Nanoporous membrane-based cell chip for the study of anti-cancer drug effect of retinoic acid with impedance spectroscopy. *Talanta* **2009,** 80, (1), 189-194.

Chapter 6

DESIGNING AN IMPEDANCE BIOSENSING DEVICE

6.1. Introduction

This chapter describes designing a new two-electrode impedance sensing system based on bio-functionalized nanopores arrays. In our previous experiments, we used a commercial four-electrode system (Inphaze Pty. Ltd.). Obtaining impedance measurements using special electrochemical cells has limitation for miniaturization and sensor development. Therefore, a two electrode system is highly desirable. The two-electrode device can be realized by coordinating impedance programs that apply the excitation signal, captures the output signals, and extracts amplitude and phase (impedance) information. The requirement of scaling down the electrode size and device volume was discussed in Chapter 1. Impedance sensing measurements have been made with 4 and 2 electrode configurations, with each configuration providing unique information about the cell-electrode-electrolyte system. In two-electrode measurements, current is passed between the same pair of electrodes as is used for the voltage measurement. Two-electrode measurements are very sensitive to changes at the electrode interface, but the formation of electrical double layer and other parasitic capacitances means that low frequency measurements are difficult to obtain with this setup [1-3]. In a four-electrode system an oscillating signal is applied between the two reference electrodes and the impedance is measured across the two working and counter electrodes[4, 5]. Physical separation of the current and sensing electrodes in the four-electrode configuration results in reduced parasitic double layer impedance, especially at lower frequencies. Most impedance based biosensors in the literature use the two-electrode configuration and only a few four-electrode based systems have been reported [6, 7]. The main advantage of the four-electrode setup is that the double layer capacitance at the current electrodes

does not play a part since the current and sense electrodes are physically separated and therefore it can be ignored [8, 9]. In the two-electrode system the current and voltage electrodes are the same and therefore double layer capacitance cannot be ignored, especially at the low signal frequencies.

To address these limitations reported in previous studies few designs have implemented multiple independent electrode measurements [10]. The design of a developed system with three electrodes each having diameter of 4 mm has been reported [11, 12]. The large sensing electrode results in an averaging effect, if electrodes are in micro size. Giaever and Keese have developed the electric cell substrate impedance sensing (ECIS) technique into a commercial system (available through Applied Biophysics) that allows real-time impedance measurements inside a humid incubator [13, 14]. A variety of electrode designs have been developed, including single electrode devices and a device with two independent working electrodes [15-18]. This chapter details the fabrication of a simple two-electrode system which requires very small system volumes as well as the small quantity of sample. It also has a comparison of the electrochemical performance with available complex four-electrode systems. All these previous designs are considered and the new device is designed such that it is suitable for miniaturization and combination with simple microfluidic set-ups. The commercial devices are complex and need expertise to do measurements. So a simple cost effective and small size device is required for improving the capability of sensing of the biological molecules as well as characterization of NPA.

6.2. Device fabrication

The two-electrode device was made from Plexiglass material at the workshop of School of Chemical Engineering, Adelaide University. This

fabricated device contains 2 small chambers with a volume of (400 μL) each which is schematically presented in Figure 6.1a and photos 6.1b. The size of the electrode is also reduced by four times when compared to the commercial four-electrode cell. One part of the device contains one inlet and outlet for the injection of the electrolyte solution. These inlets and outlets are sealed by plastic micro tubes fittings. At the center part of the cell a large O-ring is present to hold the nanoporous alumina membrane (NPA) sample and seal the chamber while measurement. The NPA is sandwiched between the two cell chambers by these O-rings. The entire device is held together by four steel nut and bolts. Each of these is at a corner of the device as shown in Figure 6.1 and provides support to hold the sample in between the two chambers of the device.

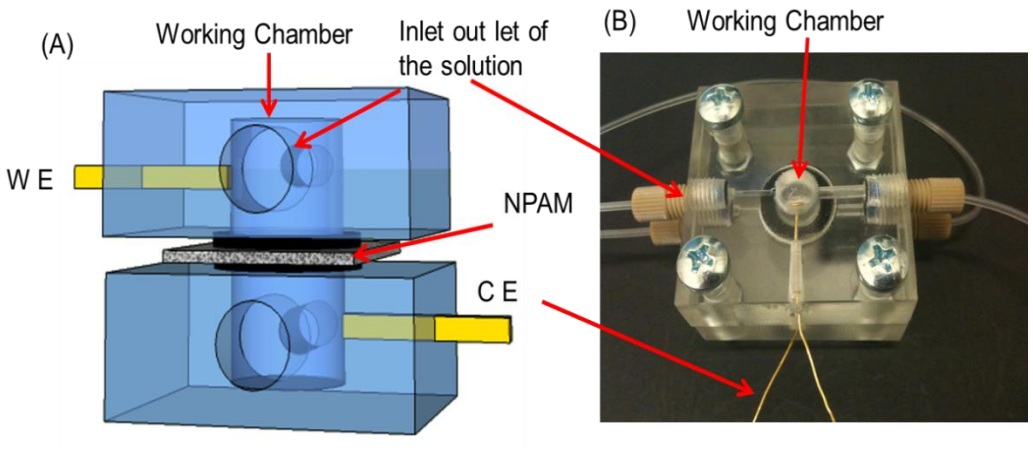

Figure 6.1: *(a) Schematic of the two-electrode device shows the basic sketch of the device and arrangement of electrodes and sample (b) an optical image of the original device showing various parts of the device.*

6.3. Experimental characterizations

The experimental characterization of NPA array and its EIS characterization after surface modification with biological molecules are described in this section.

6.3.1. Materials and methods

As detailed in Chapter 4, Section 4.2.

6.3.2. Fabrication and photolithographic patterning on NPA

NPAs were prepared by a two-step anodization process using 0.3 M oxalic acid as electrolyte at 0°C as described in Chapter 3 (section 3.2.1). The fabricated NPA was patterned on the back side with photoresist using photolithography to prepare a 20 μm area with the opened nanopore array as described in details at Chapter 3 (section 3.2.2).

6.3.3. Surface modification inside nanopore array and preparation of biosensing platform

Surface modification of NPA nanopore array was performed by series of steps of using phosphonic acid and plasma cleaner as detailed in the Chapter 4 (section 4.3.2). The nanopore wetting of the NPA and modification with N-hydroxysuccinimide (NHS), 1-ethyl-3- (3-dimethylaminopropyl) carbodimide (EDC) also been detailed in Chapter 4 (section 4.2.3).

6.3.4. Two electrode biosensing measurements by impedance spectroscopy

Electrochemical measurements were carried out using an EIS spectrometer, (Inphaze, Pty. Ltd. Sydney, Australia) with a two-electrode system which is specifically designed for EIS characterization of NPA in this chapter. The gold foil formed the working and counter electrodes in each side of the cell, reference electrodes was also paired with working and counter electrode. The distance between the counter and working electrodes from the sample was 4 mm which was very small in comparison to the commercial device which has a separation of

3 cm. The nanoporous array was sandwiched between two cell chambers filled with the PBS buffer solution (400 μL each). The working and counter electrodes were respectively placed at the end of two chambers (Figure 6.1). An equivalent circuit is used to balance the resistance and capacitance for the entire system and monitor the changes on nanoporous arrays surface as detailed in Chapter 4 (section 4.3.3). The bare NPA sample was used as the control sample to check the difference in the measurement in between the 2 electrode system and 4 electrode systems. All the EIS measurements were repeated three times to check the reproducibility of the data in the newly developed device in comparison with 4 electrode system. Most of the experimental conditions were kept identical with the previous studies (chapter 4 section 4.2.3). In Figure 6.2 the impedance measurement for control sample for NPA was presented using both the electrode system showing impedance and Nyquist graphs. Impedance graphs shows that the values are different at the low and high frequency ranges.

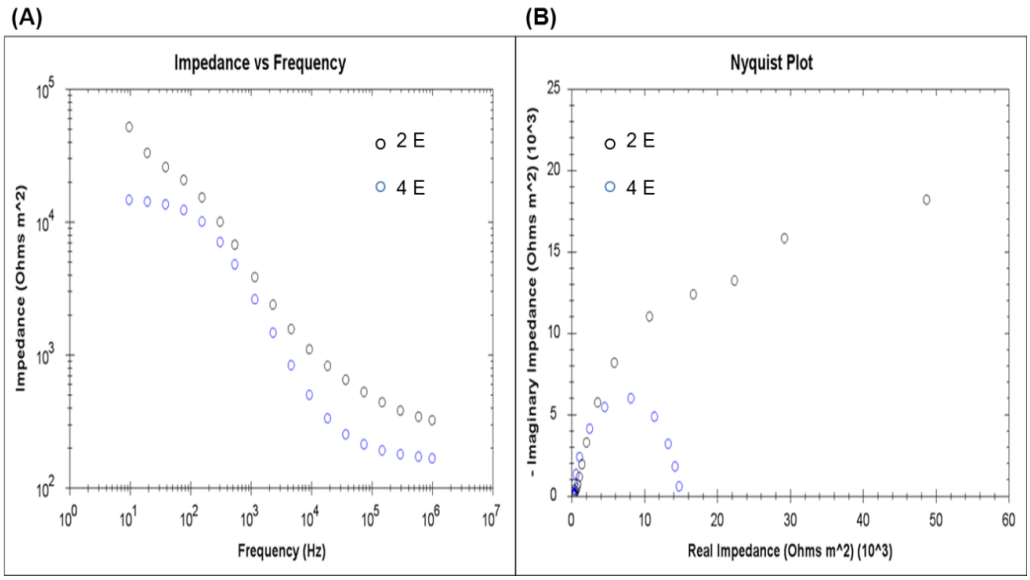

***Figure 6.2**: Inphaze software generated original plots taken on control NPA sample in buffer (a) Impedance vs frequency plot for two (2E) and four-electrode (4E) system measurement (b) Nyquist plot for two and four-electrode system*

6.4. Results and discussion

The sensing performance of the newly designed two-electrode impedance biosensing device (Figure 6.1) is evaluated by measuring biotin molecule concentration as a model substrate molecule. To optimize the device, a series of experiments with different concentrations of the analytes were undertaken. The electrodes effect on the impedance sensing on the biotin molecule by two and four-electrode system over the range of frequencies 0.1 Hz to 10 MHz was examined. The electrode admittance effect arises from highly resistive/capacitive surface of the sample [19]. The parameter (bulk resistance and parasitic capacitance) for the bulk properties can be derived from the equivalent circuit but may not be meaningful in this measurement [20].

The inter electrode distance between electrodes in the two-electrode system is less than 1 cm and this distance is very high for the four-electrode system. In spite of difference in the electrode spacing, the bulk resistance of the system scaled with length. There is noticeable difference found in the spectrum of the two systems, as the multi electrode system is nearly a semicircle but two-electrode system not have enough data point at low frequency range to complete semicircle (Figure 6.3). One possible explanation for differences between the two-electrode verses four-electrode measurement is that at low frequencies two-electrode systems generate a very high capacitance and electrical double layer effect. However the multi-electrode system is unable to provide reliable data of the bulk properties of the system and generated high frequency data is not very reproducible [21]. It is proposed that this non reproducible property arises due to the asymmetry in the sensing electrode resistance/capacitance or their placement in the system. It was observed that there is shifting of data points in the negative

imaginary to negative real quadrant. Because these types of distortions occur in the MHz frequency range, it may also be due to their inter-electrode interference if electrodes are placed very close to each other. The electrochemical impedance measurements were carried out using the two-electrode system.

The streptavidin functionalized NPA nanopore platform was used with different concentrations (0.2 μM to 29 μM) of biotin for measurement of change in impedance magnitudes (Z) at different frequencies in both the system (2E and 4E) to find clear changes in the sensitivity of the system. After reaction between streptavidin and biotin, the recorded impedance magnitude graphs showed characteristic concentration and frequency dependence.

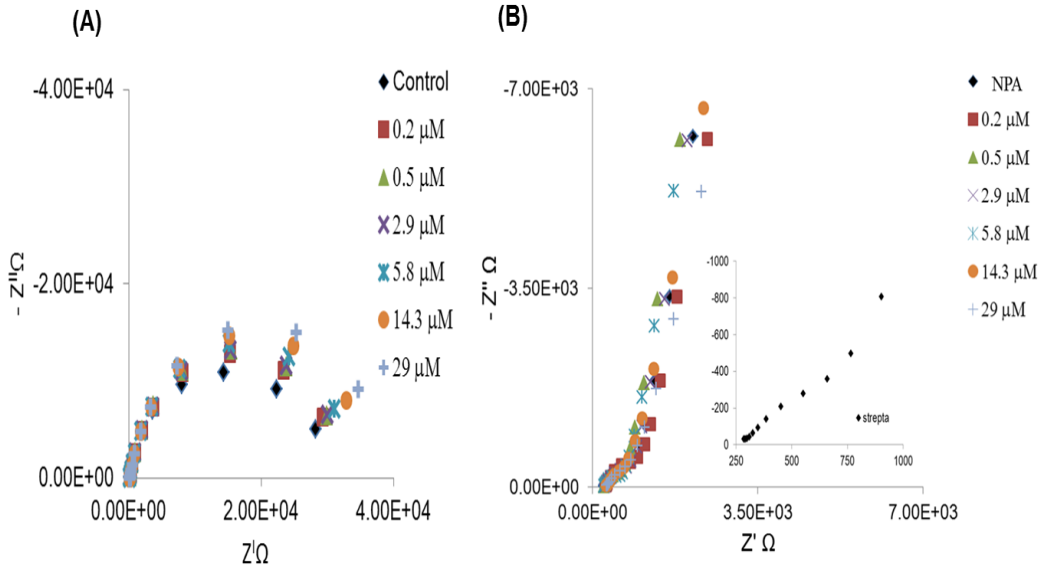

***Figure 6.3**: (a) Nyquist plot for four-electrode system measurement having the almost semicircle structure at various concentrations of biomolecules (b) Nyquist plot for two-electrode system for various concentrations of analyte molecules (biotin), lacking the data points at low range of frequencies, Nyquist plot of control sample bare NPA (inset).*

In the four electrode system it was observed that at high frequency range above 1 kHz to 10 MHz the impedance signal does not have any distortion or noise in the signal. However, within the high frequency range all the points

overlap and no significant differences are observed due to the overlapping of the bulk properties of the system. The Nyquist plot in Figure 6.3a obtained from the four electrode measurements shows a clear change in the concentration at lower range of frequencies. The two-electrode system shows lower signal to noise at low frequencies (0.1 Hz to 1 kHz) but has one small semicircle for high frequency range above 1 kHz to 10 MHz and the other uncompleted big semicircle defined the different concentrations (Figure 6.3b). In both cases, the Nyquist plot shows an increase in the diameter of semicircles with a decrease in the concentration of biotin molecules. To understand the difference between Nyquist plots for two-electrode systems and four-electrode systems, a schematic diagram is proposed in Figure 6.4. If the collected data from the four-electrode system is compared to the schematic plot (Figure 6.4b red line) it was observed that the available data points have very tiny semicircle at high frequency zone which represent the negligible effect of the generated electrical double layer resistance and capacitance.

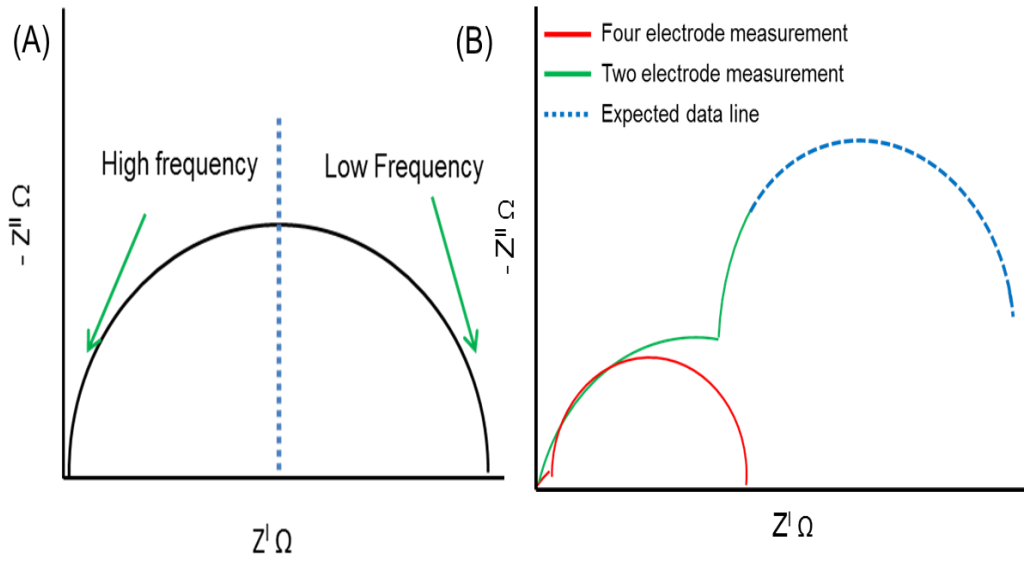

Figure 6.4: *A Schematic diagram of Nyquist plots (A) the zone for high frequency (1 kHz to 1 GHz) and low frequency (0.01 Hz – 1 kHz) (B) difference between the measurement of two-electrodes and four-electrode systems.*

Most of the data fits a perfect semicircle. In this case the bulk properties of the material are very tiny and the measurement for the sample can be done at small range of frequencies. On the other hand with two-electrode measurement (Figure 6.4b green line) the effect of electrical double layer resistance and capacitance is very high and produce a bigger semicircle as compared to four-electrode system and the data points are lacking at very low range of frequencies. The data points from these measurements tend to have a big semicircle which is incomplete in this case. The trend for the semicircle is indicated by the blue dotted line in Figure 6.4b.

The difference in the sensitivity and the sensing properties of these two different systems can be illustrated by the impedance vs. concentration plot (Figure 6.5) at constant medium frequency (to have optimal sensing) of 1 kHz. The concentration range used is plotted on the x axis and the collected impedance (Z) in Ω on Y axis.

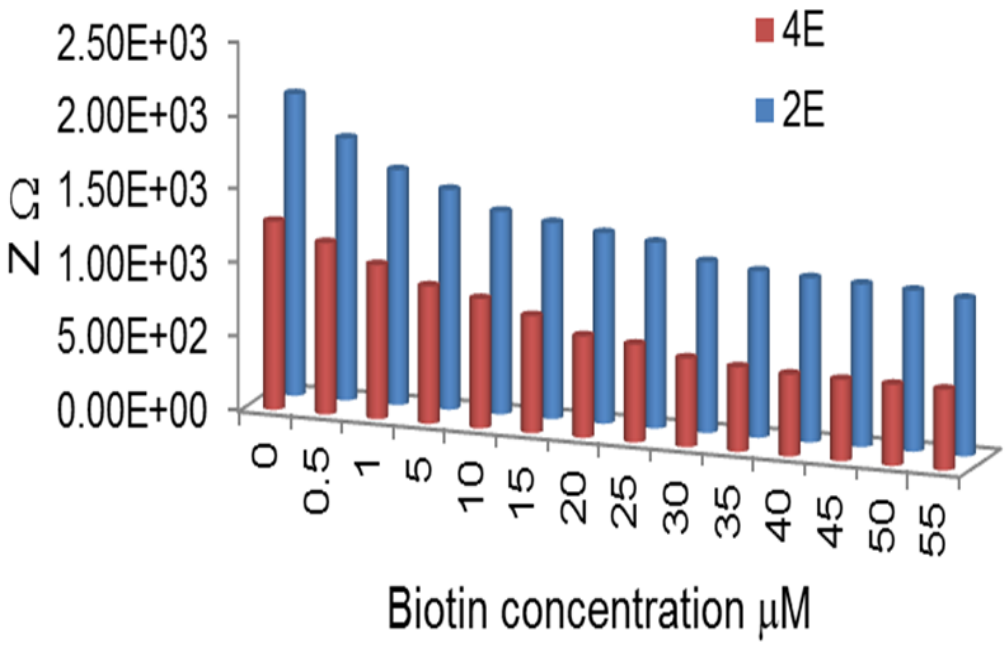

Figure 6.5: *At constant frequency of 1 KHz, **c**oncentration vs. impedance plot for two (2E) and four electrode (4E) systems.*

It was observed that both systems exhibit noticeable changes at small (0.2 μM to 5 μM) concentrations and the value of impedance decrease with increasing concentration. Once the concentration was increased above 10 μM the signal started to show saturation in the impedance value in both systems, but four-electrode systems saturated more quickly than the two-electrode systems. There was decrease in the impedance value with concentration and after 40 μM the signal started to be stable and no further changes took place at high concentration. This point is observed as the saturation point for the nanopores in this sensing arrangement. To use the NPA as biosensing platform we need to find out the value of pore resistance for the system. R_p is a key parameter related to changes inside the nanopore because the active binding sites for the analyte are only available inside the nanopore. The values for R_p obtained after simulation with equivalent circuit. The detailed information about Rp and equivalent circuit is discussed in Chapter 4 (Section 4.3.3).

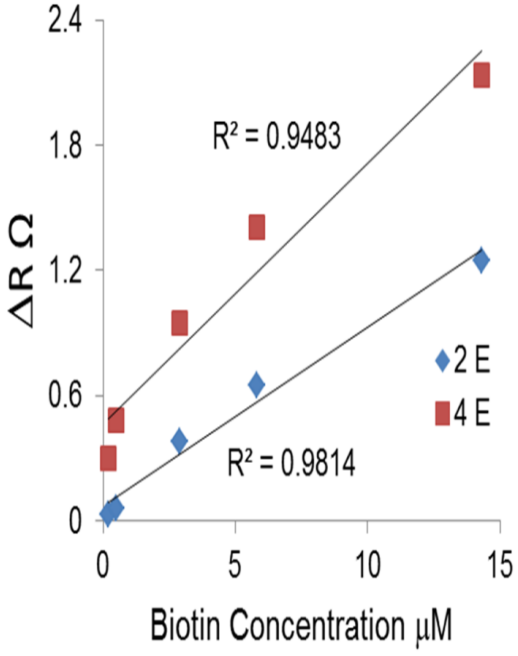

Figure 6.6: *Graph showing changes of pore resistance ΔR of NPA biosensor with biotin concentration with 2E and 4E system for NPA biosensing at lower concentration (0.2 – 15 μM) of biotin show the significant linearity between actual pore resistance ΔR and biotin concentration.*

To compare the sensing capability for both systems, we calculated ΔR by subtracting the value of pore resistance $\Delta R = R_0 - R_x$ where R_0 is without biotin and R_x is at a particular biotin concentration. A linear relationship between ΔR and concentration is observed in the lower range of biotin concentration with the signal becoming saturated at higher concentrations of biotin. As it is known from Figure 6.5; the four-electrode system saturates earlier than the two-electrode system (in terms of sensing) so is the results are not very linear when the concentration of analyte is high. At the same place two-electrode system has better linearity (R^2= 0.98) in long range of concentration (0.2 μM to 15 μM) as shown in graph (Figure 6.6).

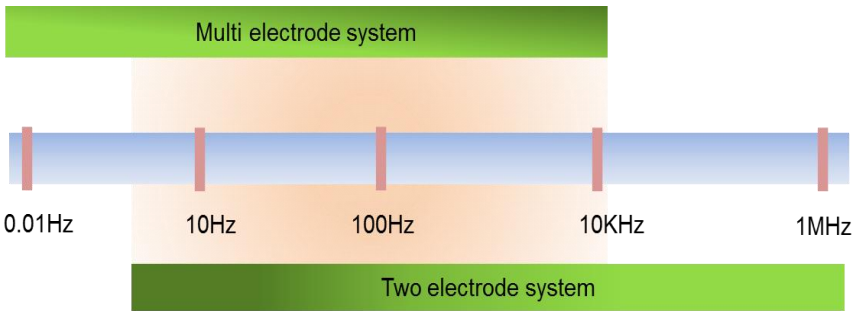

Figure 6.7: *Schematic for the optimal frequency range for the 2 E and multi electrode (4E) system.*

The advantage of the two-electrode system is its ease of use; small device and system volume. It lacks data at the low frequency zone because of the generated electrical double layer effects at the sample surface and parasitic capacitance, but can be used for high frequency measurements. The four-electrode system has the advantage of having data analysis at low frequency and very negligible electrical double layer and parasitic capacitance effect. The four-electrode system is good in the low frequency zone but measurements of the bulk properties of the sample which generally took place in high frequency zone (10

kHz to 1 GHz) are not possible. The optimal range for both systems is in between 1 Hz to 10 KHz (Figure 6.7).

6.5. Conclusion

The newly developed two-electrode device with the specific functionalized biosensing molecules inside the nanopores was characterized for impedance biosensing application. The obtained EIS biosensing measurements were compared with a four-electrode electrochemical impedance system. It was observed that there is some agreement in the results with two- and four-electrode systems on their overall sensing. Both electrode systems have their advantages and disadvantages but can be used for the sample measurement at optimum frequency range. The type of sample and their morphology also determines which system is more suitable. The two-electrode measurement is much more susceptible to large amounts of surface capacitance and double layer effects but for multi-electrode systems there is a negligible amount of offset resistance generated at high frequency range and the bulk properties of the sample is suppressed at the real impedance axis in the Nyquist plot. The multi-electrode measurement establishment of the true dielectric constant for the sample and extreme care is required to take data with multi-electrode system. The presented device provides direct, fast and label-free detection of biomolecules, using small system volume, without complex analysis and processing. The measured impedance is in close agreement with the theoretical concept, and offers a sensitive and reliable detection method. Further optimization is required which can be done by designing a system with micro electrodes to improve these disadvantages.

6.6. References

1. Schwan, H., Electrode polarization impedance and measurements in biological materials. *Annals of the New York Academy of Sciences* **1968,** 148, (1), 191-209.
2. Schwan, H., Linear and nonlinear electrode polarization and biological materials. *Annals of biomedical engineering* **1992,** 20, (3), 269-288.
3. York, T., Status of electrical tomography in industrial applications. *Journal of Electronic Imaging* **2001,** 10, (3), 608-619.
4. Brown, B., Electrical impedance tomography (EIT): a review. *Journal of medical engineering & technology* **2003,** 27, (3), 97-108.
5. Yufera, A.; Rueda, A. In *A method for bioimpedance measure with four- and two-electrode sensor systems*, Engineering in Medicine and Biology Society, EMBS, 30th Annual International Conference of the IEEE, **2008**; pp 2318-2321.
6. Sanchez, B.; Bragos, R. In *Fast Electrical Impedance Spectroscopy for Moving Tissue Characterization Using Bilateral QuasiLogarithmic Multisine Bursts Signals*, 4th European Conference of the International Federation for Medical and Biological Engineering, 2009; Springer: 2009; pp 1084-1087.
7. Huh, D.; Gu, W.; Kamotani, Y.; Grotberg, J. B.; Takayama, S., Microfluidics for flow cytometric analysis of cells and particles. *Physiological measurement* **2005,** 26, (3), R73.
8. Nasir, M.; Ateya, D. A.; Burk, D.; Golden, J. P.; Ligler, F. S., Hydrodynamic focusing of conducting fluids for conductivity-based biosensors. *Biosensors and Bioelectronics* **2010,** 25, (6), 1363-1369.
9. Wang, Y.; Song, H.; Bhatt, K.; Pant, K.; Roman, M. C.; Webster, E.; Diffey, W.; Ashley, P. *Electrokinetics Models for Micro and Nano Fluidic Impedance Sensors*; DTIC Document: 2010.
10. Inzelt, G., *Conducting polymers: a new era in electrochemistry*. Springer: **2012**.
11. Wegener, J.; Sieber, M.; Galla, H.-J., Impedance analysis of epithelial and endothelial cell monolayers cultured on gold surfaces. *Journal of biochemical and biophysical methods* **1996,** 32, (3), 151-170.

12. Arndt, S.; Seebach, J.; Psathaki, K.; Galla, H. J.; Wegener, J., Bioelectrical impedance assay to monitor changes in cell shape during apoptosis. *Biosensors and Bioelectronics* **2004,** 19, (6), 583-594.
13. Wegener, J.; Keese, C. R.; Giaever, I., Electric cell–substrate impedance sensing (ECIS) as a noninvasive means to monitor the kinetics of cell spreading to artificial surfaces. *Experimental cell research* **2000,** 259, (1), 158-166.
14. Keese, C. R.; Wegener, J.; Walker, S. R.; Giaever, I., Electrical wound-healing assay for cells in vitro. *Proceedings of the National Academy of Sciences of the United States of America* **2004,** 101, (6), 1554-1559.
15. Kirstein, S. L.; Atienza, J. M.; Xi, B.; Zhu, J.; Yu, N.; Wang, X.; Xu, X.; Abassi, Y. A., Live cell quality control and utility of real-time cell electronic sensing for assay development. *Assay and drug development technologies* **2006,** 4, (5), 545-553.
16. Arias, L. R.; Perry, C. A.; Yang, L., Real-time electrical impedance detection of cellular activities of oral cancer cells. *Biosensors and Bioelectronics* **2010,** 25, (10), 2225-2231.
17. Chen, Y.; Zhang, J.; Wang, Y.; Zhang, L.; Julien, R.; Tang, K.; Balasubramanian, N., Real-time monitoring approach: assessment of effects of antibodies on the adhesion of NCI-H460 cancer cells to the extracellular matrix. *Biosensors and Bioelectronics* **2008,** 23, (9), 1390-1396.
18. Xiao, C.; Luong, J. H., A simple mathematical model for electric cell-substrate impedance sensing with extended applications. *Biosensors and Bioelectronics* **2010,** 25, (7), 1774-1780.
19. Ford, S.; Mason, T.; Christensen, B.; Coverdale, R.; Jennings, H.; Garboczi, E., Electrode configurations and impedance spectra of cement pastes. *Journal of Materials Science* **1995,** 30, (5), 1217-1224.
20. Beltrán, N. H.; Finger, R. A.; Santiago-Aviles, J.; Espinoza-Vallejos, P., Effect of parasitic capacitances on impedance measurements in microsensors structures: a numerical study. *Sensors and Actuators B: Chemical* **2003,** 96, (1), 139-143.
21. Chiao, M.; Chiao, J. C.; Chiao, J. C., *Biomaterials for MEMS*. Pan Stanford Publishing: **2011**.

Chapter 7

MICROBIAL CELL LYSIS AND NUCLEIC ACID EXTRACTION THROUGH FOCUSED ION BEAM MILLED NANOFLUIDIC CHANNEL

K. Kant, S. Amos, M. Erkelens, C. Priest, J. G. Shapter and D. Losic, *'Microbial cell lysis and nucleic acid extraction through focused ion beam milled nanofluidic channel'* Lab on Chip, 2014 (Under review)

K. Kant, S. Amos, M. Erkelens, C. Priest, J. G. Shapter and D. Losic, *'Microchip nanofludic channel for microbial cell lysis and nucleic acids extraction'* RACI National Congress 7-12 Dec. 2014, Adelaide, South Australia. (Accepted)

7.1. Introduction

Nanofluidic techniques enable extreme miniaturization of devices and enhanced analytical performance. These devices offer high sensitivity and reproducibility, low consumption of expensive, rare, or hazardous chemicals, and less energy on a single integrated device [1, 2]. Coupled with advanced analytical techniques, they offer potential in applications from point of care to single cell analysis, and other examples where resources are limited [3, 4]. The incorporation of biological membranes and synthetic nanochannels (alumina nanopores) in a device will create new opportunities for advanced analytical applications [5, 6] due to the increased surface area and reduced use of chemical reagents [7, 8]. Nanofluidic devices may also manipulate cell entities such as proteins, nucleic acids and cell organelles, and previous research has shown that high-resolution analysis is possible using ion source and electrochemical detection [9]. Single-cell analysis can be achieved by integration of several biochemical steps into a micro total analysis system (μTAS) on a single chip [10, 11]. However, it is difficult to handle and manipulate single cells in microsystems, since very small volumes are involved in the analysis [12]. The genome of any simple organism may contain thousands of base pairs and it is even more complex in higher species [13, 14]. Consequently, an integrated nanofluidic chip is a useful approach to handling these tiny volumes of complex cell material without damage or loss. Ideally, all steps from cell lysis to analysis of the molecular cell contents, including DNA analysis, are needed on a single integrated chip [15-17]. Furthermore, integration of several devices for parallel analysis for different molecules is an attractive prospect.

A number of sophisticated fabrication tools have been used to fabricate

nanochannels in recent years [18]. E-beam lithography followed by etching has been used to prepare nanochannels (and nanostructures within nanochannels) with certain limitations of length and depth (depends on reactive ion etching (RIE) techniques) [19]. Nanoimprint lithography is capable of producing nanofluidic channels with dimensions of 10 nm in width [11, 13, 20, 21].

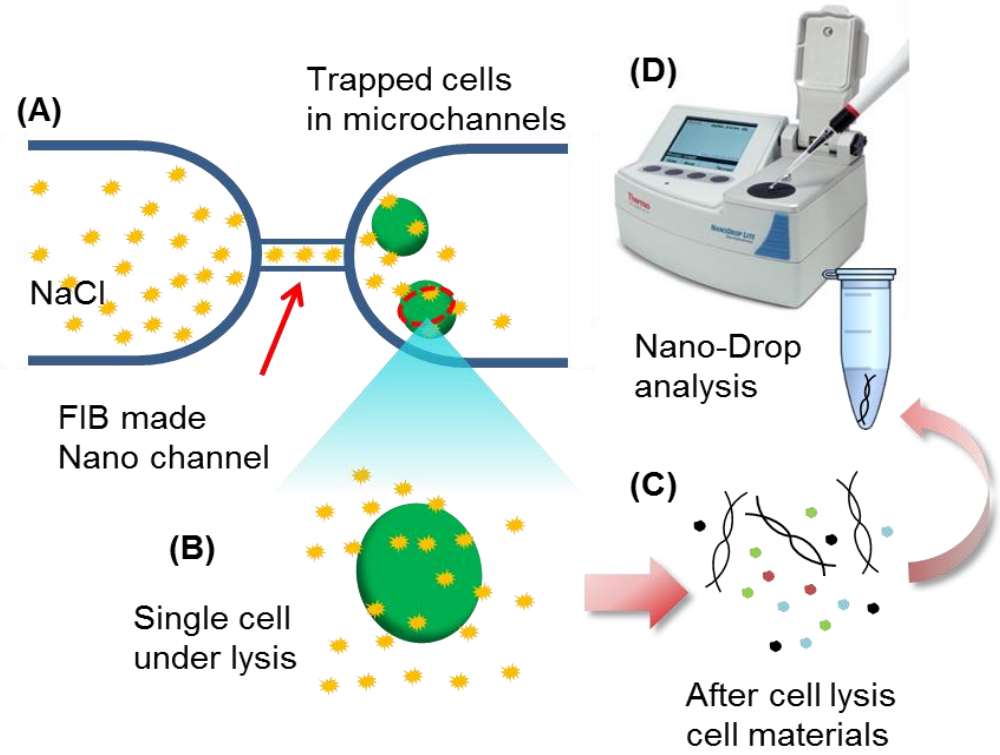

Figure 7.1: *(a) Schematic representation of microfluidic chip integrated with FIB made nanochannel. (b)The cells are trapped in micro-channel for cell lysis (c) collected DNA and protein sample was analysed by (d) Nano-Drop instrument.*

In this chapter, a suitable technique for the fabrication of nanochannels using focused ion beam (FIB) milling is been described. The prepared devices offer an integrated micro- and nanofluidic system, with features that enable several functions performed during chemical analysis (sample preparation, fluid handling and injection, separation, and detection) and new potential for the next generation of analytical chips [22, 23]. In this paper, we demonstrate a chip that is capable of flowing, capturing, and lysing microbial alga cells, before separating

the genetic material via flow through a nanochannel. The schematic of the micro/nano-system (Figure 7.1) shows the flow of sodium chloride and alga cells into the micro-channels and diffusion of NaCl through the nanochannel for cell lysis. The collected raw material is analysed using a bench top Nano-Drop spectrophotometer and UV/VIS spectrophotometer.

7.2. Experimental methodology

7.2.1. Fabrication of micro-channel by photolithography

Microfluidic chips were prepared in Quartz (Viosil, from Shin Etsu, Japan) slide coated with chromium and gold. It was first spin-coated with AZ 1518 photoresist (Delta 80, from SUSS MicroTec) and then baked for 1 min at 105 ^{0}C, the UV exposure is carried out at 340 nm by (EVG 620) Mask Aligner at 120 mJ cm^2. The exposed chip was developed using MIF 726 (Micro-chemicals). The wet chemical etching of the pattern is then achieved using hydrofluoric acid (HF) for 12 min to achieve 15 – 18 μm depth of the micro-channel. After HF etching, the gold layer was removed using a mixture of 4:1 of KI and I_2, and Cr was removed using ceric ammonium nitrate. The access ports were drilled using abrasive powder blasting in the cover slide and the slides were then bonded at 1100 ^{0}C in a vacuum furnace.

7.2.2. Nanochannel fabrication by FIB milling

The nanochannels were patterned by FIB milling using a Helios NanoLab 600 Dual Beam instrument (FEI Company). After photolithography the chip was again sputter coated with 40 nm thick Cr layer to have good control over the ion beam milling and imaging of channel [20]. 100 nm width and 250 nm depth

nanochannel was milled into a quartz substrate through a 40 nm thick Cr film using an ion beam probe with a beam current of 20 kV and 0.17 nA on milling pattern of 100 nm width and 500 nm depth. Before milling the nanochannel to connect the two microchannels an extension (Figure 7.2d) of 5 -10 μm was milled to control the distance between the two big microchannels and provide a flat and smooth surface for final milling of nanochannel. The milled nanochannel has triangular shape in the cross sections. Operating in this mode, the width of the nanochannels depends on the input pattern of the milling. The obtained milled area depends on Cr film thickness and ion beam current. It is controlled by the user-defined width of the scan area.

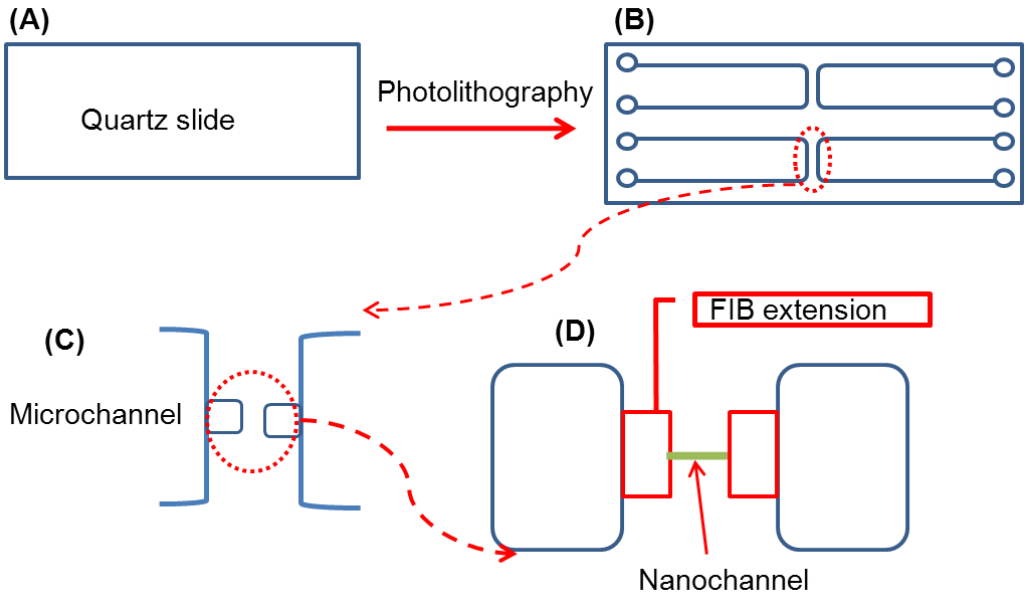

Figure 7.2: *Schematic representation of fabrication of microfluidic chip by photolithography (a,b) and followed by FIB milling to extended micro-channels and join them by making a nanochannel in between them (c,d).*

7.2.3 Cell injection and lysis into microfluidic channel

A low concentration ($1x10^5$ cells/ml) of alga cells having size of 4-8 μm were injected into the microfluidic channel by use of syringe pump (Chemyx,

Fusion-200) with flow of (2-5 µl/min). The fluorescence microscopy (Olympus BH 2-UMA microscope, integrated with a Moticam 2000 digital camera using Motic Images plus 2.0 software) was used to monitor the flow of the alga cells inside the microchannel.

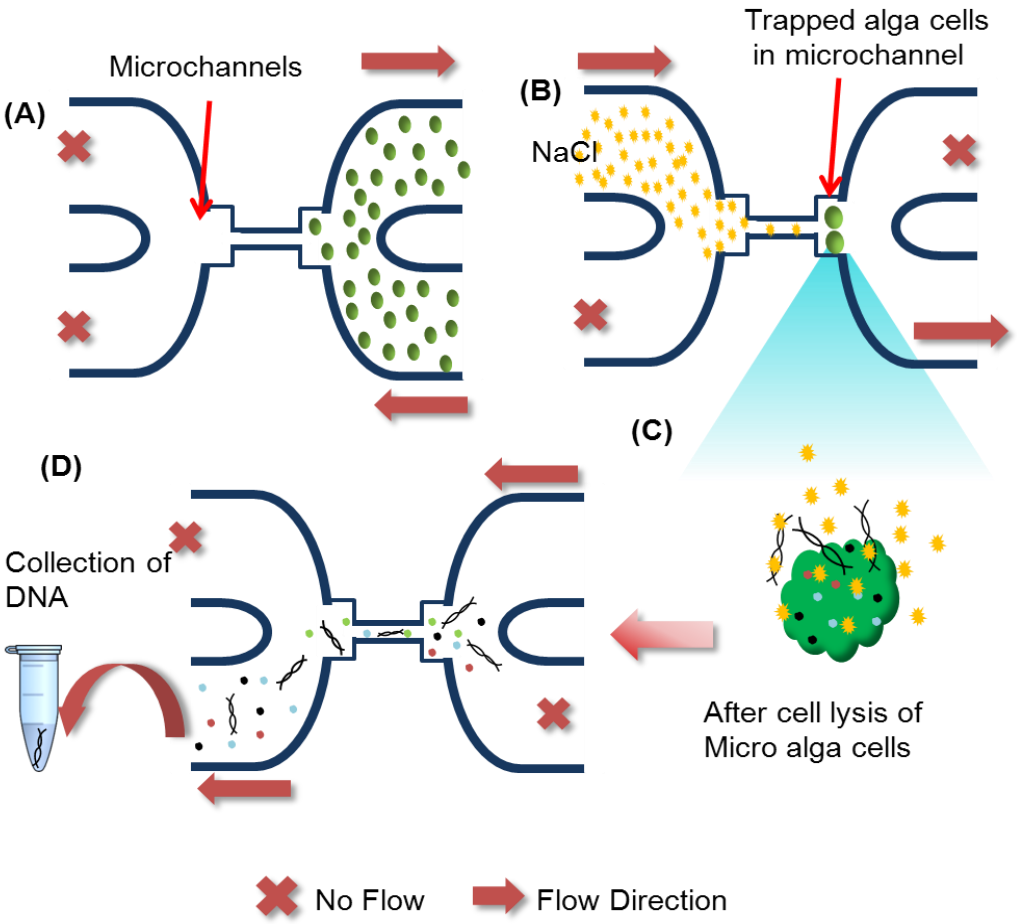

Figure 7.3: *Schematic representation of microfluidic chip integrated with nanochannel. (a) Cells and NaCl are transported in micro-channel and (b) cells were trapped in to the small area of the microchannel (c) cell lysis (d) after cell lysis DNA flows across the nanochannel and collected in to collection vial.*

Once the alga cells were flowing inside the microfluidic channel, 100 mM NaCl was injected with flow of 5 µl/min into other side of the microchannel. By changing the direction of the flow of NaCl and alga cells, NaCl was flowed through the nanochannel and reaches to the other side of the microchannel where the alga cells were trapped. As soon as the NaCl reach to the other microchannel

through the nanochannel it started the lysis of alga cells. The decrease in fluorescence intensity of the cell after lysis was clearly visualised under the fluorescence microscope. The cell movement and lysis was observed using a CCD camera (Moticam 2000 digital camera) at frame rate of 25 frames per second. After the cell lysis is completed, the direction of flow was changed and cell material along with cell's genetic material (DNA, RNA) tend to flow through nano channel towards the other side of microchannel. Due to the narrow size of nano channel cell material was separated on basis of their size along with other cell material. Finally cell material flowed along the microchannel and was collected in vials for further analysis.

7.2.4. Detection of DNA

To determine the quantity and quality of the DNA extracted by the chip a Nanodrop Lite (Thermo scientific, Wilmington, DE, USA) and UV/VIS spectrophotometer were used as a validation method. The quantity of DNA was displayed, while the protein to DNA ratio was determined from the ratio of absorbance at 260 and 280 nm, which also gives the quality of the DNA extraction.

7.3. Results and discussion

The functionality of the nanofluidic device was tested using dye solution. Once flow was demonstrated, indicating that the nanocahnnel fabrication was successful, cell separation, lysis, and extraction of genetic material were carried out, as described in the following sections.

7.3.1 Characterization of fabricated nanochannel

The SEM images of the fabricated microfluidic channel were taken before and after the FIB milling. In figure 4a two microchannels are shown before FIB milling. The distance between the two microchannels was around 15- 20 μm depending on the chosen duration of the HF etching. In this way, the length of the separation between the micro-channels can be controlled. In our case, we used FIB to extend the microchannel segments to adjust the length of the nanochannel and prepare a flat surface for FIB milling of the nanochannel (Figure 7.4b). Once we have the extended microchannel using FIB, the distance between the microchannels is much smaller and we can easily mill a nanochannel with low energy (0.17 nA) ion beam in a very short time (2-3 min depending on the Cr layer thickness). The magnified view of the microchannel (Figure 7.4c) shows the milled extension of the microchannel and a triangle shaped nanochannel (inset) with dimensions of 100 nm width and 290 nm depth and has length of 1 μm. The length of nanochannel can be varied form few hundred nanometer to 20 μm. The width and depth of the fabricated nano channel is dependent on the input parameters of the pattern and ion beam energy. A small variation in parameter can vary the dimension of the nanochannel; however it is also difficult to control the ion beam form shifting due to the charging effect from the sample surface. However use of low energy beam and recoating on the surface reduces this effect. After making the nanochannel on the chip it was cleaned by use of Cr etchant (ceric ammonium nitrate) and bonded under vacuum at 1100 ^{0}C. This quartz nanochannel chip was then used in the specially designed plastic holder with the inlet and outlet micro bore tubing (Figure 7.4d).

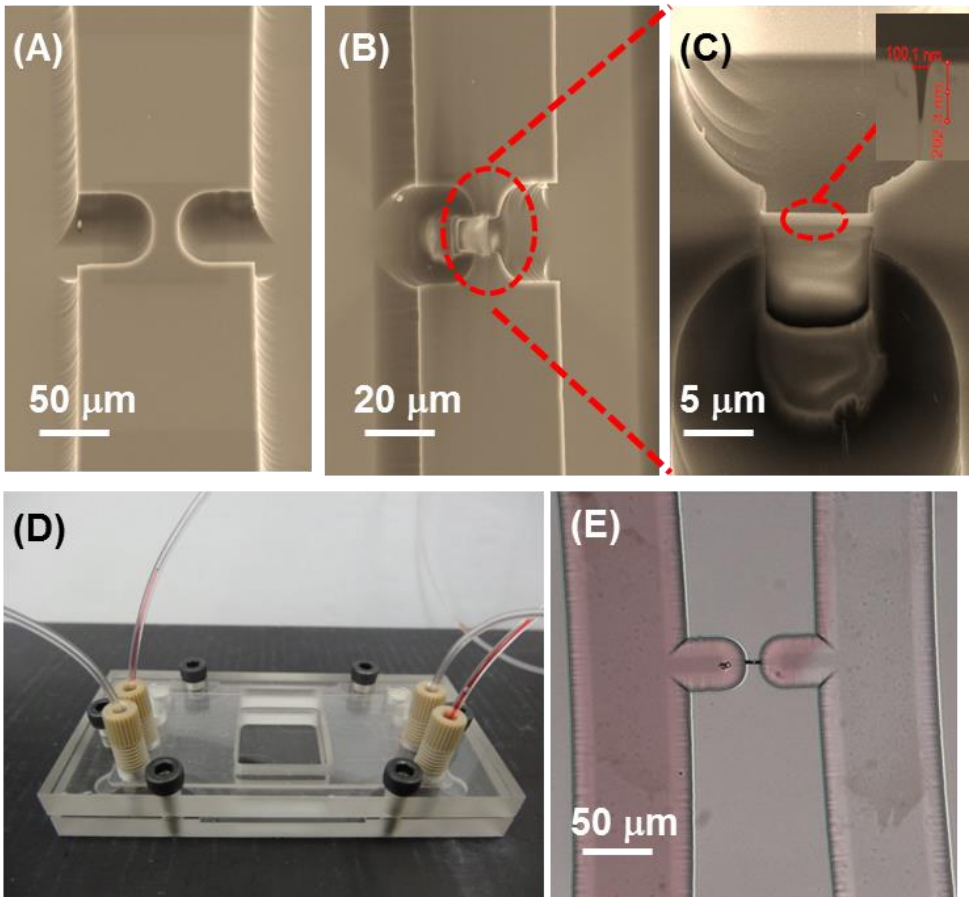

Figure 7.4: *SEM images of the fabricated micro and nano channels. (a) microchannels after lithography (b) extension of microchannel by FIB milling to achieve required length of nano channel (c) magnified image of the microchannel and nanochannel (inset) (d) optical image of actual working device (e) red dye testing to confirm flow through nanochannel. This device is prepared with support of Australian nanofabrication facility South Australia node. University of South Australia, FIB expert Len Green at Adelaide microscopy, and mechanical workshop at School of Chemical Engineering at University of Adelaide.*

To confirm that nanochannel is working well and chip is bonded perfectly we perform a small test with the flow of dye (red fruit dye) in the nano channel. In one microchannel red dye was flowed rate of 10 μl/min using a syringe pump and the other channel was filled with deionised (DI) water at same rate of flow. Once completely filled with the aqueous dye solution and DI water, the dye solution was pumped through the nanochannels and, after some time, the dye was observed in the second microchannel, Figure. 7.4e. This demonstrated that the nanochannel was unblocked and able to transport liquid between the channels.

7.3.2. Cell flow and lysis

The algal cells were injected into the microchannels (no.1) with controlled flow of less than 5 μl/min. Once the microchannel is filled with cell and maintain the flow of alga cells, NaCl was flowed in the other microchannel (no.2) at a flow rate of 10 μl/min. once both microchannels were filled and flow was maintained continuously, we trapped a few alga cells in the small extended 'beak' of the microchannel by changing the direction of the flow by the syringe pump. Alga cells contain chlorophyll, which is fluorescent under the green fluorescent light at 735 nm, so the alga cells can be observed using fluorescence microscopy Figure 7.5a. The trapped alga cells in the microchannel beak are shown in Figure 7.5b (fluorescence) and 7.5c (optical). Once we have the alga cells trapped in the microchannel, injection of extra alga cells was stopped and the unwanted cells were removed from the microchannel by washing them with water. The cross flow of NaCl solution was started through nanochannel (as schematically shown in Figure 7.3b). The flow rate was maintained very low to keep the trapped cells in their place. An alga cell is large in size (more than 20 μm) and the low flow of NaCl solution does not move the cell. The osmotic pressure created by the high concentration of NaCl caused the alga cell walls to rupture. Lysis of the alga cell was thus triggered and the cell material was released (Figure 7.5d). After lysis of the cell, the flow of NaCl was stopped in microchannel (no.2) and cross flow of water was started from microchannel no.1 to no.2. The cell organelles started moving towards microchannel (no.2) but due to small dimension of the nanochannel only small size molecules can pass through. In this way we separated the small molecules like DNA, RNA and protein along with some cell debris from the rest of the cell material. The separated molecules are collected and used for

further quantification of the material. However we know this collected material is not very pure and has some damaged cell material in it. Therefore, we tested the material before and after filtration through a 0.2 μm filter, as discussed in the following section.

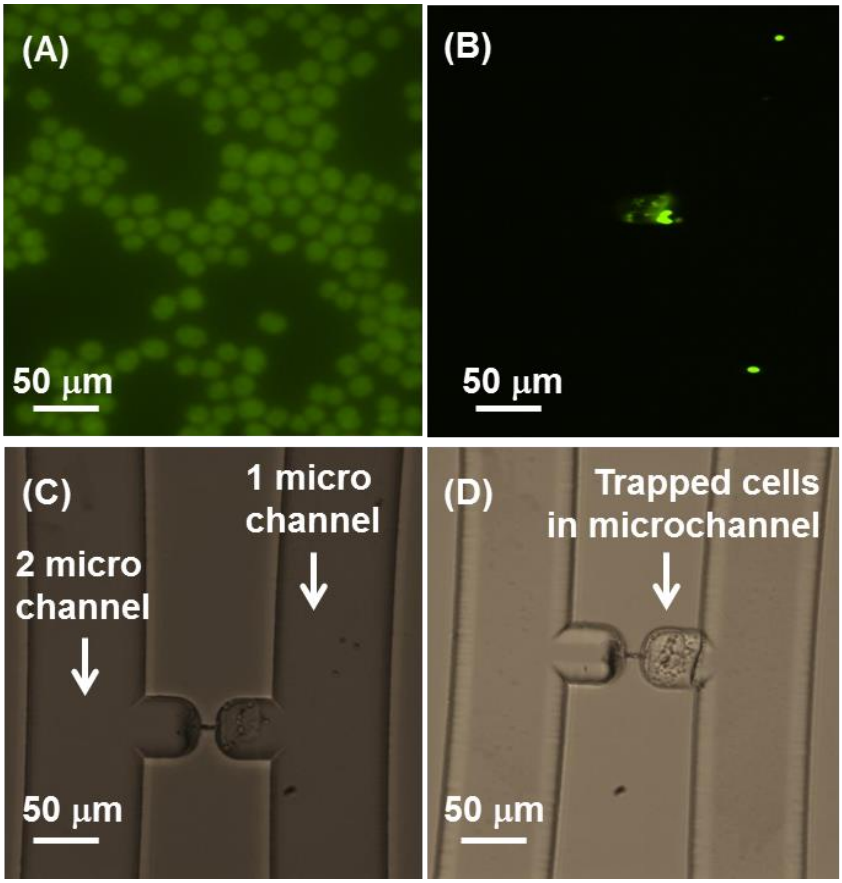

Figure 7.5: *(a) Fluorescence image of alga cells shows their circular shape and homogeneous distribution (b) Fluorescence image of trapped alga cells in the side channel (extension made using FIB) before lysis (c) optical image of the trapped alga cells (d) alga cells after the cell lysis. This experiment is performed with help of PhD student Steven Amos from School of Chemical engineering, The University of Adelaide, providing cell culture and support during cell experiments.*

7.3.3. Quantitative analysis

Quantification of DNA and RNA by absorbance and fluorescence spectroscopy is a powerful tool in life sciences. Classical methods of nucleic

acid quantification require the filling of devices, such as cuvettes and capillaries, with sample. Analysis of micro volume samples has become of paramount importance as more molecular biology techniques yield progressively smaller amounts of isolated sample and require accurate quantification of nucleic acids with minimal consumption of sample. The collected cell material after lysis was used to quantify the presence of DNA, RNA and protein with a bench-top model of Nano-Drop 1000 spectrophotometer.

Type	Conc.	Units	Factor	A260	A280	A3rd	A260/ A280
Unfiltered							
RNA	4.3	ng/µL	40	0.107	0.053	0.02	2.03
dsDNA	3.2	ng/µL	50	0.064	0.034	-0.001	1.91
Protein A280	0.044	mg/ml	10		0.044	0.046	
Filtered							
RNA	1.2	ng/µL	40	0.03	0.016	0.017	1.89
dsDNA	3.2	ng/µL	50	0.064	0.036	0.029	1.8
Protein A280	0.01	mg/ml	10		0.01	-0.023	

***Table 7.1**: Nano-Drop measurements for DNA, RNA and protein molecules in the collected sample, before and after filtration and their ratio A260/A280.*

The Nano-Drop spectrophotometer uses a patented sample retention system that holds 1µl of the sample by use of specialized micro pipette. During the measurement, the sample was analysed at 10 mm path length to report information about the available genetic material [24]. To optimize the measurement we used DI water first in the measurement and then use sample on the Nano-Drop sample holder. The ratio of absorbance at 260 nm and 280 nm is used to assess the purity of DNA and RNA [23]. A ratio of ~1.8 is generally accepted as "pure" for DNA; a ratio of ~2.0 is generally accepted as "pure" for

RNA (Table 7.1). If the ratio is appreciably lower in either case, it may indicate the presence of protein, phenol or other contaminants that absorb strongly at or near 280 nm. It is important to note that the actual ratio will depend on the composition of the nucleic acid. If the ratio is appreciably lower than expected, it may indicate the presence of contaminants which absorb at 230 nm. The collected material was also used under the UV/VIS spectrometer (Shimadzu UV-visible, UV1601) for quantification of the genetic material.

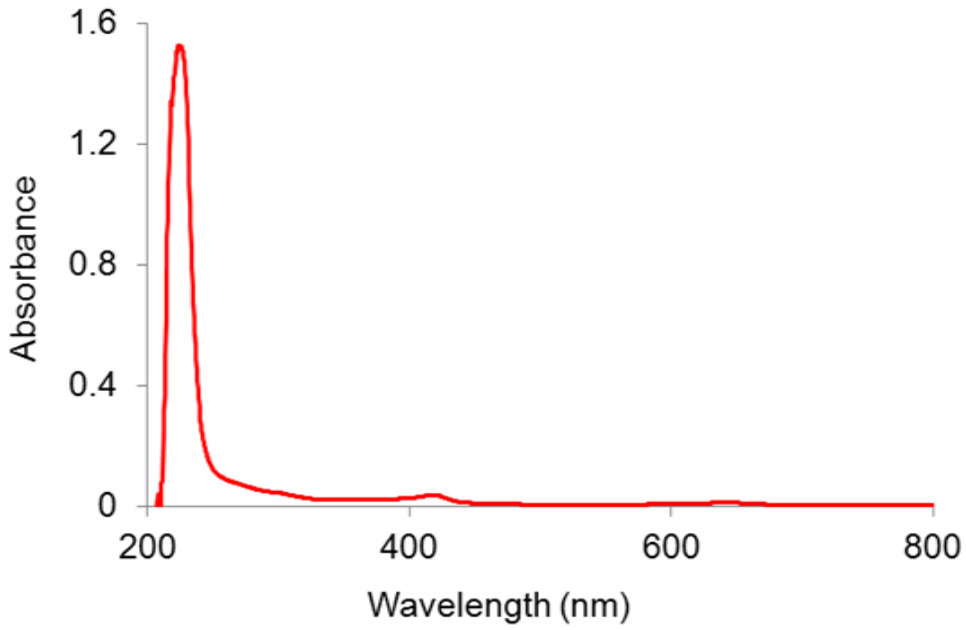

Figure 7.6: *A wide range UV/IR spectrum for the collected raw cell material shows the presence of DNA, RNA and other nucleotides peak at range of 230 – 290 also trace amount of chlorophyll molecules at 400 nm.*

The spectrum was taken on the full range from 200 – 800 nm. A strong peak was observed at the range of 230 – 290 nm, which reports the presence of molecules having double bonds in their chemical structure and are organic in nature (Figure 7.6). The DNA, RNA, other protein and nucleotides contain double bonds in their chemical structure. The small peak at 430 nm reports the presence of some chlorophyll molecules, which is present only in trace amounts.

7.4. Conclusions

We have prepared a sealed nanofluidic channel (100 nm wide, 290 nm deep, and 1 μm long) in quartz using FIB milling technique, which was integrated with wet-etched microchannels The cross-section of the channel was triangular but it is suitable for extracting cell materials from trapped cells isolated under flow. Cell lysis was carried out using NaCl solution and DNA molecules were extracted from cells and through the nanofluidic channels under positive pressure. In our experiments, sufficient DNA extraction form algal cells were achieved to analyse the small sample with a Nano-Drop spectrophotometer. The ratio of A260/A280 for the extracted material was 1.9 for DNA and more than 2 for RNA, consistent with expectations. A nanofluidic channel of this kind enables the separation of very small amounts of bio-samples [25]. Possible outcomes of this study include integration of this kind of nanofluidic channel into a biochip, investigation of the migration of single DNA or protein molecules, or studies of their interactions.

7.5. References

1. Abgrall, P.; Nguyen, N. T., Nanofluidic Devices and Their Applications. *Analytical Chemistry* **2008,** 80, (7), 2326-2341.
2. Andersson, H.; van den Berg, A., Microtechnologies and nanotechnologies for single-cell analysis. *Current Opinion in Biotechnology* **2004,** 15, (1), 44-49.
3. Hong, J.; Edel, J. B.; deMello, A. J., Micro- and nanofluidic systems for high-throughput biological screening. *Drug Discovery Today* **2009,** 14, (3–4), 134-146.
4. Cannon, D. M.; Flachsbart, B. R.; Shannon, M. A.; Sweedler, J. V.; Bohn, P. W., Fabrication of single nanofluidic channels in

poly(methylmethacrylate) films via focused-ion beam milling for use as molecular gates. *Applied Physics Letters* **2004,** 85, (7), 1241-1243.

5. Dorfman, K. D.; King, S. B.; Olson, D. W.; Thomas, J. D. P.; Tree, D. R., Beyond Gel Electrophoresis: Microfluidic Separations, Fluorescence Burst Analysis, and DNA Stretching. *Chemical Reviews* **2012,** 113, (4), 2584-2667.
6. Wang, K. G.; Niu, H., Nanofluidic Channel Fabrication and Manipulation of DNA Molecules. In *Micro and Nano Technologies in Bioanalysis*, Foote, R. S.; Lee, J. W., Eds. Humana Press: 2009; Vol. 544, pp 17-27.
7. Menard, L. D.; Ramsey, J. M., Electrokinetically-Driven Transport of DNA through Focused Ion Beam Milled Nanofluidic Channels. *Analytical Chemistry* **2012,** 85, (2), 1146-1153.
8. Klepárník, K.; Foret, F., Recent advances in the development of single cell analysis—A review. *Analytica Chimica Acta* **2013,** 800, (0), 12-21.
9. Tegenfeldt, J.; Prinz, C.; Cao, H.; Huang, R.; Austin, R.; Chou, S.; Cox, E.; Sturm, J., Micro- and nanofluidics for DNA analysis. *Anal Bioanal Chem* **2004,** 378, (7), 1678-1692.
10. Yin, H.; Marshall, D., Microfluidics for single cell analysis. *Current Opinion in Biotechnology* **2012,** 23, (1), 110-119.
11. Le Gac, S.; van den Berg, A., Single cells as experimentation units in lab-on-a-chip devices. *Trends in Biotechnology* **2010,** 28, (2), 55-62.
12. Ros, A.; Hellmich, W.; Regtmeier, J.; Duong, T. T.; Anselmetti, D., Bioanalysis in structured microfluidic systems. *ELECTROPHORESIS* **2006,** 27, (13), 2651-2658.
13. Maleki, T.; Mohammadi, S.; Ziaie, B., A nanofluidic channel with embedded transverse nanoelectrodes. *Nanotechnology* **2009,** 20, (10), 105302.
14. Hoang, H.; Segers-Nolten, I.; Berenschot, J.; de Boer, M.; Tas, N.; Haneveld, J.; Elwenspoek, M., Fabrication and interfacing of nanochannel devices for single-molecule studies. *Journal of Micromechanics and Microengineering* **2009,** 19, (6), 065017.
15. Hong, J. W.; Quake, S. R., Integrated nanoliter systems. *Nat Biotech* **2003,** 21, (10), 1179-1183.

16. Lindström, S.; Andersson-Svahn, H., Miniaturization of biological assays — Overview on microwell devices for single-cell analyses. *Biochimica et Biophysica Acta (BBA) - General Subjects* **2011,** 1810, (3), 308-316.
17. Mahalanabis, M.; Do, J.; ALMuayad, H.; Zhang, J. Y.; Klapperich, C. M., An integrated disposable device for DNA extraction and helicase dependent amplification. *Biomedical microdevices* **2010,** 12, (2), 353-359.
18. Kovarik, M. L.; Jacobson, S. C., Nanofluidics in Lab-on-a-Chip Devices. *Analytical Chemistry* **2009,** 81, (17), 7133-7140.
19. Mawatari, K.; Kubota, S.; Xu, Y.; Priest, C.; Sedev, R.; Ralston, J.; Kitamori, T., Femtoliter Droplet Handling in Nanofluidic Channels: A Laplace Nanovalve. *Analytical Chemistry* **2012,** 84, (24), 10812-10816.
20. Menard, L. D.; Ramsey, J. M., Fabrication of Sub-5 nm Nanochannels in Insulating Substrates Using Focused Ion Beam Milling. *Nano Letters* **2010,** 11, (2), 512-517.
21. He, Q.; Chen, S.; Su, Y.; Fang, Q.; Chen, H., Fabrication of 1D nanofluidic channels on glass substrate by wet etching and room-temperature bonding. *Analytica Chimica Acta* **2008,** 628, (1), 1-8.
22. Guo, L. J., Nanoimprint Lithography: Methods and Material Requirements. *Advanced Materials* **2007,** 19, (4), 495-513.
23. Triant, D. A.; Whitehead, A., Simultaneous extraction of high-quality RNA and DNA from small tissue samples. *Journal of Heredity* **2009,** 100, (2), 246-250.
24. R Desjardins, P.; Conklin, D. S., Microvolume quantitation of nucleic acids. *Current Protocols in Molecular Biology* **2011**, A. 3J. 1-A. 3J. 16.
25. Zare, R. N.; Kim, S., Microfluidic platforms for single-cell analysis. *Annual review of biomedical engineering* **2010,** 12, 187-201.

Chapter 8

GROWTH OF CONDUCTING MICROBIAL NANOWIRES THROUGH NANOFLUIDIC MEMBRANE

K. Kant, J. Rochow, C. Priest, J. G. Mitchell, J. G. Shapter and D. Losic, *'Growth of conducting microbial nanowires through nanofluidic membrane'* 4th Australia and New Zealand Micro/Nanofluidics Symposium (ANZMNF) 22-23 April **2013** Adelaide, Australia. (Oral Presentation)

8.1. Introduction

The concept of microbacterial fuel cells (MFCs) is a unique and eco-friendly approach to sustainable energy production. The *Shewanella* bacteria metabolise organic material in anaerobic conditions and produce electrons at the anode of a circuit to release their energy [1]. The mechanism of formation of conductive wires and electron transfer from bacterial cell to an electrode through these wires is not yet very clear. Most previous studies were performed using planar electrodes for the formation of conductive nanowires and MFCs [2, 3]. The long-range electron transport of electrons through the conductive biofilms and microbial to electrode interaction have potential possibilities in bioelectronics [1, 4, 5] and make contribution of microorganisms for interspecies electron transfer [4, 6]. In previous studies, bacterial biofilms were characterized as an insulating biofilm [7, 8]. However, *Geobacter* species have conductivities through its conductive *pili* and it can function as super capacitors or transistors [9]. The *pili* of these organisms enable long-range transport of electrons up to (>1 cm) with a metal like conductivity which has not been observed in any other biological materials [10].

Direct measurements of conductivity in current-producing biofilms of *Geobacter sulfurreducens* discovered high conductivities, as synthetic conducting polymers. The evidence indicates that, conductivity could be due to the network of *pili*. Multiple lines of evidence suggested that, surprisingly, the *pili* have metallic-like conductivity [2]. Metallic-like conductivity is a new hypothesis for long range electron transport in biological systems [11] and electron hopping between *c-type cytochromes* in biofilms is well known mechanism of electron

transfer [12]. Several studies have suggested that traditional electron hopping/tunneling between *c-type cytochromes* confers conductivity to biofilms transferring electrons to electrodes [13, 14]. However, biofilm conductivity was not measured in any of these studies. Instead, conductivity was inferred from measurements of electron transfer into or out of the biofilm with a single electrode using cyclic voltammetry. It is true that the *c-type cytochromes* that are often abundant in current-producing biofilms are oxidized and reduced as the electrode potential is changed [15]. The conductivity of biofilms is an important part of the conduction, which permits those microorganisms that are not in direct contact with the anode [16-18]. These types of conductive networks also help in direct exchange of electrons [19]. As we know that the *pili* of the microorganism is the main contact for electron exchange with other microorganisms, which gives idea for new approaches to stimulate and stabilize interspecies electron transfer for various applications, such as conversion of biomass or organic wastes into useful product methane. However the use of nanofluidic channels can be beneficial regarding increased surface area and improved electron transport.

This work explores the growth of microbial nanowires through nanofluidic pores of nonporous alumina (NPA). NPA is prepared with pore diameters of 60-70 nm and length of 8-10 μm. One end of the NPA nanochannel is covered with conductive silver and connected to the circuit as an anode, while other end is open for bacteria to grow nanowire (*pili)* network across the nanochannel to donate electrons at anode under anaerobic conditions as presented in Figure 8.1. The electrochemical conductivity is continuously measured under constant potential which represents the change in the resistance of the nanochannel and increase in conductivity due to electron donation by bacteria at anode. This study aims to use

nanochannel based biosensing to get a better understanding of the mechanisms by which microorganisms exchange their electrons with metallic electrodes. It has potential to help in development of new technologies as well as it will offer a better understanding for anaerobic microbial ecology.

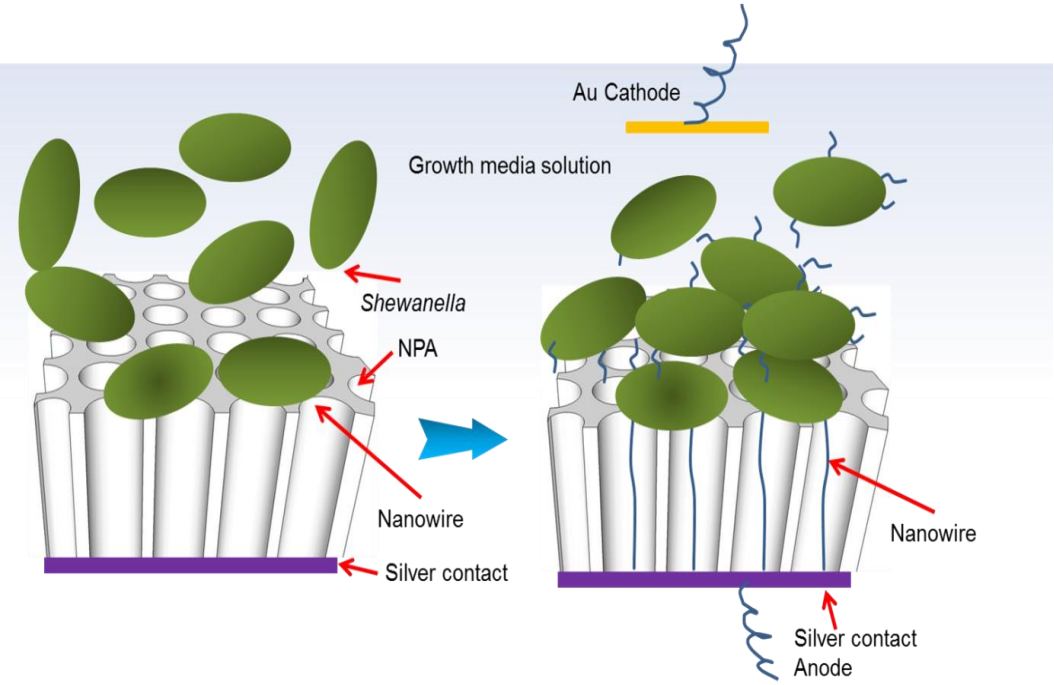

Figure 8.1: *Schematic presentation of growth of bacterial nanowire inside the nanochannels of nanoporous alumina membrane.*

8.2. Materials and methods

Aluminum foil (0.1 mm, 99.997%) was supplied by Alfa Aesar (USA). Oxalic acid, ethanol (Chem Supply, Australia), chromium trioxide (Mallinckrodt, USA), De-ionized (DI) water (ELGA) was used for preparation of all solutions. Mixed culture of *geo-bacteria species* (School of biological sciences, Flinders University) and a power supply of Keithley 2400 for electrical measurements.

8.2.1. Fabrication of ordered alumina nanopore array

NPA was prepared by a two-step anodization process using 0.3 M oxalic acid as electrolyte at 0 °C as described previously [20, 21]. Further details have been provided in Chapter 3 section 3.2.1. After removal of barrier layer a thick coating of silver is done to cover the pores from one side and provide a conductive surface for growth of bacterial growth as shown in Figure 8.1.

8.3. NPA nanopore membrane device for bacterial nanowire growth

A device with 2 cells was designed in which one of the cell containing the culture media of the bacteria and other one is used for the anode contact. NPA was sandwiched in between the two chamber cells as shown in Figure 8.2.

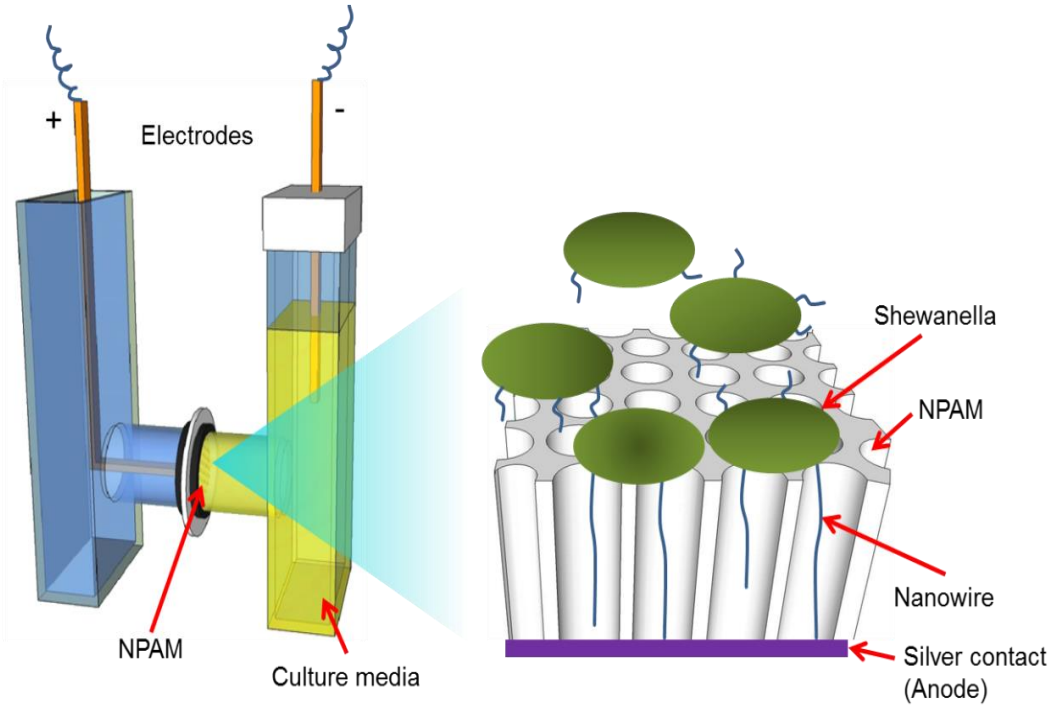

Figure 8.2: *Schematic view of the actual device and the growth of bacterial nanowire from the top through NPA nanopores towards metal electrode (silver) on the bottom of membrane.*

The NPA was coated with silver on one end of the nanochannel to make a contact for anode. During the growth of nano wires at room temperature, the bacteria tend to reach the anode by elongating their nano wires and donating electrons. The electrodes of the device are connected with a power supply (Keithley 2400) which provides a small constant voltage (1 V) at anode to direct the bacterial cell for growth of its nanowire. All data was recorded over time by use of lab view software. This growth of the nanowires took 12-18 h to reach the anode and then started to donate electron. This electron donation time is referred to as the active phase for bacteria.

8.4. Results and discussion

8.4.1. Characterization of bacterial nanowire by SEM

The diameters and length of the bacterial nanowires were determined by scanning electron microscope (SEM) (FEI Quanta 450). A 5 nm coating of platinum was used for all the SEM imaging. After the completion of the nanowire growth experiment, NPA membrane was cracked in the middle to do cross-sectional SEM imaging of nanowires. In Figure 8.3 (a) the cross sectional images of NPA nanochannels shows the presence of the bacterial nanowire. The thickness of the bacterial nano wire in the image is around 7-8 nm which is very similar to the *Geobacter* species. As it is known that the total length of the nanochannel was 4-5 μm so on average length of the bacterial nanowire achieved in our experiment is more than 5 μm.

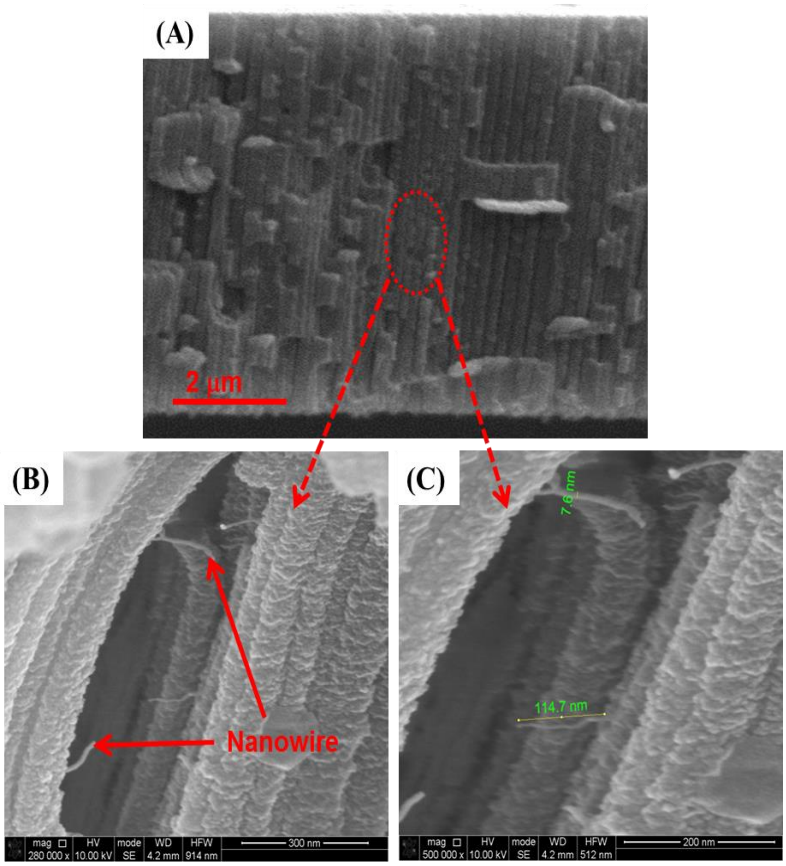

Figure 8.3: *(a) The cross sectional SEM image of the NPA taken from system with bacterial nanowire growth inside nanopores (b) Magnified view of NPA nanopores showing bacterial nanowires inside the nanopores (c) the diameter and length of the present bacterial nanowire. This work was performed in collaboration with PhD student Jacqueline Rochow from Biological Sciences, Flinders University, who supplied bacteria cells (Shewanella).*

8.4.2. Transmission electron microscopic characterization (TEM)

TEM imaging (FEI Tecnai G2 Spirit TEM) is performed on the bacterial nanowires collected using culture media in the cell after the growth of the nano wire. The negative staining on the bacterial cells is done prior to imaging to improve the imaging quality and contrast between the bacterial cell and other culture media. The length of the bacterial nanowire observed was around 10 to 15 µm with thickness of 15-30 nm. This indicates that the length of nanowires was longer than the thickness of NPA membrane and could pass through nanopore structure.

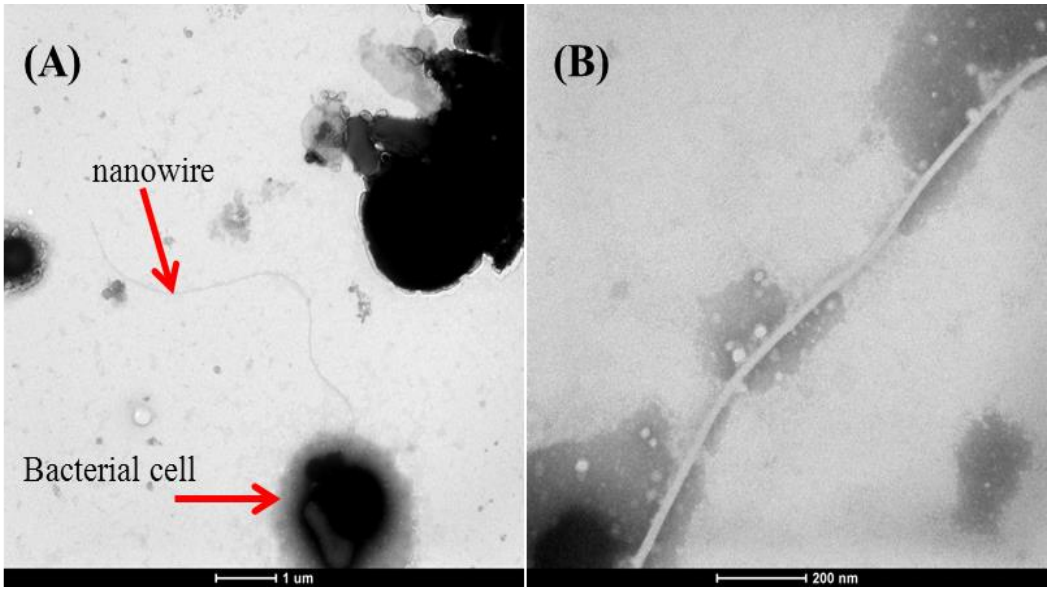

Figure 8.4: *(a) TEM image of bacterial nano wire attached with the bacterial cell (negatively stained) (b) magnified image of the bacterial nanowire.*

8.4.3. Growth of bacterial nanowires inside nanochannels

The growth of bacterial nanowire takes place inside the nanochannels as the guided growth of nano wires. The *pili* of the microbial bacteria have morphology of 10–15 nm in width and up to 10–20 μm in length. The mechanism behind the growth of bacterial nano wire inside the nanochannels is the necessity for the bacteria to donate electrons at the anode. In search of the anode in the system, bacteria grow their pili until it touches the anode and donates electrons. Figure 8.5 shows how bacterial nanowire network connects to the anode surface and is also connected to the other bacteria for communication. The results of earlier studies suggested that long-range electron transport through the biofilms could be attributed to networks of *pili* with metallic-like conductivity.

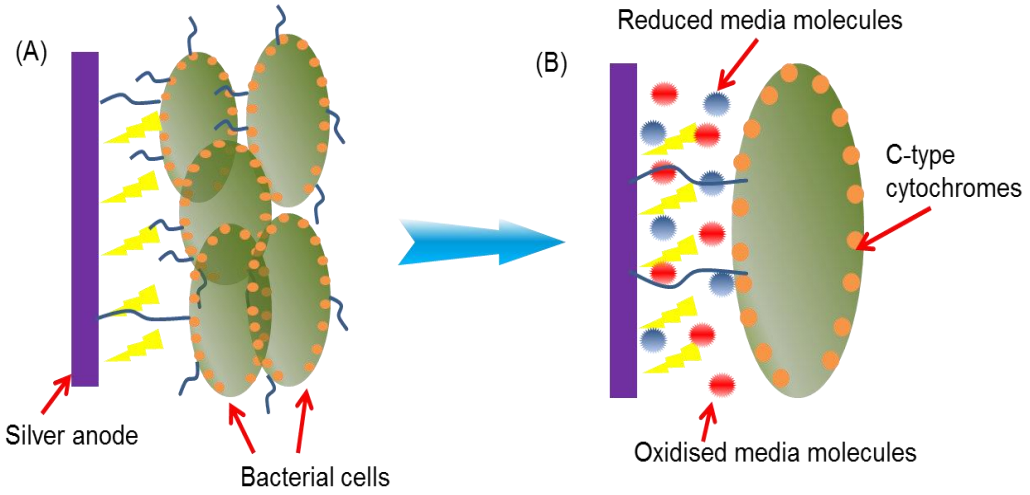

Figure 8.5: *Schematic mechanisms for micro-bacteria (Shewanella) to transfer electrons to electrodes. (a) Long-range electron transport through a conductive biofilm via electrically conductive pili, accompanied by short-range electron transfer from the biofilm in close association with the electrode surface through redox-active proteins, such as c-type cytochromes associated with the outer cell surface or in the extracellular matrix. (b) Electron transfer via reduction and oxidation of soluble media molecules [22].*

Long-range electron transport through biofilms via c-type cytochromes is physically impossible because the density of cytochromes is too low and cytochromes are spaced too far apart for electron hopping/tunneling through the biofilm. In this way the bacterial *pili* are the main source for the electron transfer. It was found in previous MFC studies that the microorganism is able to exchange their electrons with anodes to produce an electric current by consuming culture media to keep their respiration for survival. In previous studies it has been proposed that microbe-electrode exchange is an unexpected result because some microorganisms have developed effective approaches for extracellular electron exchange with insoluble/soluble mineral material [1, 22]. The microorganisms at the surface have long-term electron-accepting or donating capacity; this ability of individual microorganisms to accept or donate electrons is ultimately washed-out with time. In the mixed culture of various species including *Geobacter* species express flagella because they need to continually search for new sources of Fe(III)

to survive [23, 24]. In the same way, it is well known that electron transfer to electrodes is abiotic in microbial fuel cells which are designed to harvest electricity. In a similar way, harvesting of electricity through the nanofluidic channel may be a more efficient way of small scale energy production on nanofluidic chips.

8.5. Electrical measurements

The measurement of the electron generation at the anode of NPA channels was carried out by continuous measurements of the produced charge. A constant voltage of 1V was applied at the anode to complete the electric circuit. The output signal was recorded with Labview software over the time period microbial life time of electron production (Figure 8.6). At the initial stage of the measurement (first 1-4 hour) the stabilization of system takes place which is the initial stage of bacterial cells to start attaching on the surface of the nanochannels. Once bacterial cells start attaching to the surface of the nanochannel, the conductivity in the system reduces and the current becomes very low. Sometimes it may block the nanochannel and grow its *pili* through that channel to reach the anode. In other terms for bacteria at this stage is in its stable metabolic stage (5-15 hour). Once the bacterium begins to starve in the deficiency of the oxygen in the atmosphere and the culture media it then begins to metabolize the other organic material (e.g. sucrose, fructose) available in the culture media. Due to this metabolic process it starts to generate the electrons and tends to donate them at the anode. At this stage bacterial nanowires try to attach on the anode surface and to begin electron transfer. This termed the electroactive metabolic phase, which shows a huge jump in the electric signal with currents up to 0.7 mA generated.

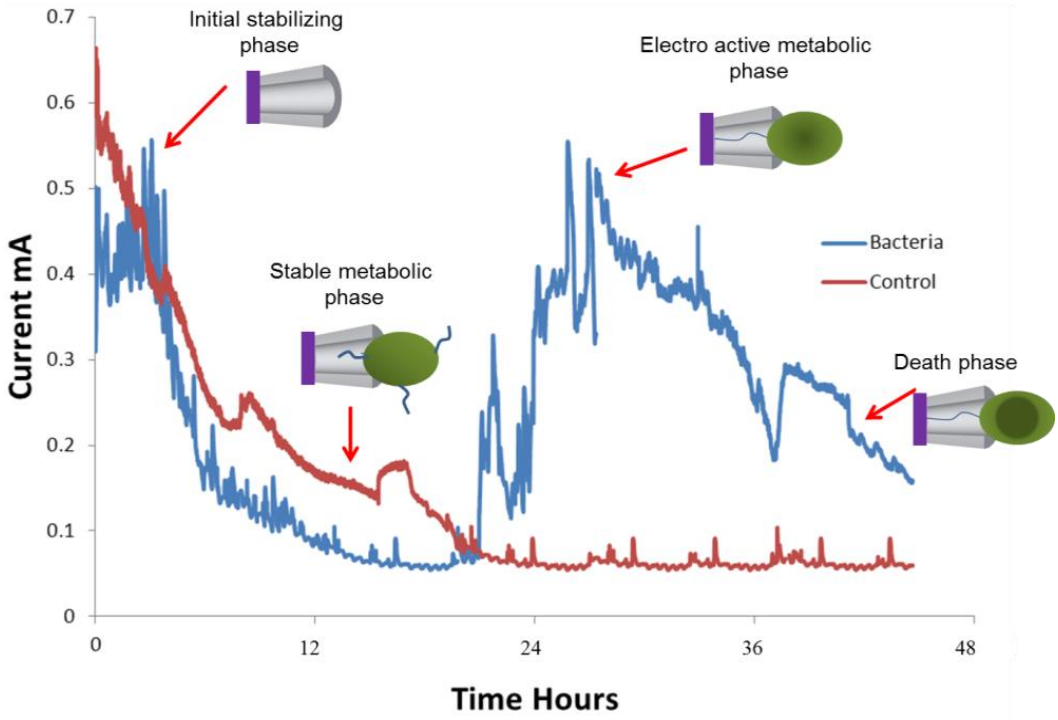

Figure 8.6: *The growth curve of bacterial (Shewanella) nanowire inside NPA nanopores through different phase of its metabolism in O_2 deficient environment. The red curve represents the control sample (aerobic condition) where no exchange of electron took place. The blue curve presents the growth of bacterial nanowires and exchange of electron at anode.*

This stage continues as long as the organic material is available to metabolize. The amount of electricity generated depends on the number of bacteria present in the culture media. In our experiments, it was observed that after the 12-18 hour of electroactive phase bacteria started to die, causing a reduction in the current. The length of the nano wire can be controlled by the elongation of the time period of the experiment by using the high amount of the culture media and also by making long nanochannels. The bacterial nanowires can also work as a prototype for electronic devices which require a high surface area. In previous mechanical studies on filaments secreted by microorganisms, researchers have shown that these filaments have high Young's modulus of 1 GPa. It may be interesting to study the mechanical rigidity of these filaments to

consider their possible applications as natural template materials [11]. Understanding the mechanisms behind metallic-like conductivity of microbial nanowires opens new possibilities for production of inexpensive, nontoxic and organic natural electronic materials. It also has potential for better design self-renewing electronic devices that can work in any natural condition like under water.

8.6. Conclusion

The growth of bacterial nanowire or *pili* was demonstrated for the first time through the nanopores where NPA is used as an electrode substrate. It is found that bacterial *pili* grow through nanochannels to reach anode. This is the first demonstration of the growth of conductive microbial nanowires directed by nanofluidic channels, which not only improves the efficiency of MFCs but also provides a new approach for synthesis of conductive nanowires using a nanopore membrane as a template. The SEM and TEM image of the nanowires and bacterial cells confirms that the nano wires formed inside the nanopores are produced by the bacteria in the period of the experiment. The length of bacterial nanowire can be controlled by varying the length of the nanochannel (4.5 μm to 20 μm). The control over the length of the nanowires and also on the production energy for long time periods provides a platform to make devices with controlled energy production. The separated bacterial nanowires have the conductive metal like properties which can be used to make metallic contacts on the nanofluidic devices.

8.7. References

1. Lovley, D. R., Powering microbes with electricity: direct electron transfer from electrodes to microbes. *Environmental microbiology reports* **2011,** 3, (1), 27-35.
2. Malvankar, N. S.; Vargas, M.; Nevin, K. P.; Franks, A. E.; Leang, C.; Kim, B. C.; Inoue, K.; Mester, T.; Covalla, S. F.; Johnson, J. P., Tunable metallic-like conductivity in microbial nanowire networks. *Nature Nanotechnology* **2011,** 6, (9), 573-579.
3. Yang, Y.; Xu, M.; Guo, J.; Sun, G., Bacterial extracellular electron transfer in bioelectrochemical systems. *Process Biochemistry* **2012**.
4. Lovley, D. R., Live wires: direct extracellular electron exchange for bioenergy and the bioremediation of energy-related contamination. *Energy & Environmental Science* **2011,** 4, (12), 4896-4906.
5. Malvankar, N. S.; Lau, J.; Nevin, K. P.; Franks, A. E.; Tuominen, M. T.; Lovley, D. R., Electrical conductivity in a mixed-species biofilm. *Applied and Environmental Microbiology* **2012,** 78, (16), 5967-5971.
6. Liu, F.; Rotaru, A.-E.; Shrestha, P. M.; Malvankar, N. S.; Nevin, K. P.; Lovley, D. R., Promoting direct interspecies electron transfer with activated carbon. *Energy & Environmental Science* **2012,** 5, (10), 8982-8989.
7. Rotaru, D. E. H.; Franks, A. E.; Orellana, R.; Risso, C.; Nevin, K. P., Geobacter: the microbe electric's physiology, ecology, and practical applications. *Advances in Microbial Physiology 59* **2011,** 59, 1.
8. Franks, A. E.; Nevin, K. P.; Glaven, R. H.; Lovley, D. R., Microtoming coupled to microarray analysis to evaluate the spatial metabolic status of Geobacter sulfurreducens biofilms. *The ISME journal* **2009,** 4, (4), 509-519.
9. Lovley, D., Long-range electron transport to Fe (III) oxide via pili with metallic-like conductivity. *Biochemical Society Transactions* **2012,** 40, (6), 1186.
10. Lovley, D. R., Electromicrobiology. *Annual review of microbiology* **2012,** 66, 391-409.

11. Malvankar, N. S.; Lovley, D. R., Microbial nanowires: a new paradigm for biological electron transfer and bioelectronics. *ChemSusChem* **2012,** 5, (6), 1039-1046.
12. Strycharz-Glaven, S. M.; Snider, R. M.; Guiseppi-Elie, A.; Tender, L. M., On the electrical conductivity of microbial nanowires and biofilms. *Energy & Environmental Science* **2011,** 4, (11), 4366-4379.
13. Fricke, K.; Harnisch, F.; Schröder, U., On the use of cyclic voltammetry for the study of anodic electron transfer in microbial fuel cells. *Energy & Environmental Science* **2008,** 1, (1), 144-147.
14. Okamoto, A.; Hashimoto, K.; Nakamura, R., Long-range electron conduction of *Shewanella* biofilms mediated by outer membrane *C-type cytochromes*. *Bioelectrochemistry* **2012,** 85, 61-65.
15. Liu, Y.; Kim, H.; Franklin, R. R.; Bond, D. R., Linking Spectral and Electrochemical Analysis to Monitor c-type Cytochrome Redox Status in Living Geobacter sulfurreducens Biofilms. *ChemPhysChem* **2011,** 12, (12), 2235-2241.
16. Torres, C. I.; Marcus, A. K.; Lee, H. S.; Parameswaran, P.; Krajmalnik-Brown, R.; Rittmann, B. E., A kinetic perspective on extracellular electron transfer by anode-respiring bacteria. *FEMS microbiology reviews* **2010,** 34, (1), 3-17.
17. Bond, D. R.; Strycharz-Glaven, S. M.; Tender, L. M.; Torres, C. I., On electron transport through Geobacter biofilms. *ChemSusChem* **2012,** 5, (6), 1099-1105.
18. Nevin, K. P.; Richter, H.; Covalla, S.; Johnson, J.; Woodard, T.; Orloff, A.; Jia, H.; Zhang, M.; Lovley, D., Power output and columbic efficiencies from biofilms of Geobacter sulfurreducens comparable to mixed community microbial fuel cells. *Environmental microbiology* **2008,** 10, (10), 2505-2514.
19. Shrestha, P. M.; Rotaru, A. E.; Aklujkar, M.; Liu, F.; Shrestha, M.; Summers, Z. M.; Malvankar, N.; Flores, D. C.; Lovley, D. R., Syntrophic growth with direct interspecies electron transfer as the primary mechanism for energy exchange. *Environmental microbiology reports* **2013**.

20. K. Kant, M. K., J. Yu, J. G. Shapter, C. Priest, D. Losic, Impedance spectroscopy study of nanopore arrays for biosensing applications *Science of advance material* **2014,** 6, 1-7.
21. Losic, D.; Velleman, L.; Kant, K.; Kumeria, T.; Gulati, K.; Shapter, J. G.; Beattie, D. A.; Simovic, S., Self-ordering Electrochemistry: A Simple Approach for Engineering Nanopore and Nanotube Arrays for Emerging Applications. *Australian Journal of Chemistry* **2011,** 64, (3), 294-301.
22. Lovley, D. R., Bug juice: harvesting electricity with microorganisms. *Nature Reviews Microbiology* **2006,** 4, (7), 497-508.
23. Mehta, T.; Coppi, M. V.; Childers, S. E.; Lovley, D. R., Outer membrane c-type cytochromes required for Fe (III) and Mn (IV) oxide reduction in Geobacter sulfurreducens. *Applied and Environmental Microbiology* **2005,** 71, (12), 8634-8641.
24. Weber, K. A.; Achenbach, L. A.; Coates, J. D., Microorganisms pumping iron: anaerobic microbial iron oxidation and reduction. *Nature Reviews Microbiology* **2006,** 4, (10), 752-764.

Chapter 9

CONCLUSION AND FUTURE DIRECTIONS

9.1. Significance of this work

This thesis outlined the development of label free affinity impedance biosensors using a nanofluidic NPA array. This was achieved by fabrication of ordered NPA array by electrochemical method and its integration in a nanofluidic device. Most of impedance biosensors are facing the difficulty of selectivity in the high concentrations of non-target material even though we know that we can overcome this problem by using labels and/or labelled secondary targets. In both situations it requires extra time and sample preparation which increases the whole system complexity. This is common to most of the label-free affinity sensors. Therefore this thesis is focused on addressing these limitations by study of the specific objectives including investigation of the geometry (diameter, length and working area of NPA) on bio-impedance measurements. Fabrication of nanofluidic devices on quartz using FIB milling approach for its application in single cell detection and manipulation was another focus area for further application and integration of nanofluidic device with NPA. These objectives were achieved through several studies including fabrication of NPA by anodization method, FIB milling, photolithography. and detailed in chapters 3-8 as listed below:

- Fabrication of NPA and its electrochemical characterization by use of EIS spectroscopy is successfully completed (Chapter 3) which provides information about the change in conductance with decreasing the nanopore size. The lengths and diameters of the nanopores is found to be crucial for their electrochemical properties.

- The fabricated NPA were further used in testing their biosensing performance (Chapter 4 and 5) with various dimension and number of nanopores to find optimised pore dimensions of NPA for biosensing applications It was observed that small diameter (25 nm) with an optimal length (5-10 μm) provide best performance to detect the lowest concentration (0.2 μM) successfully. Further reduction in the number of nanopores improves the sensitivity of the system with very small volume (10-100 μL).
- The fabrication of simplified two electrode nanofluidic device was achieved (Chapter 6) and compared with commercial four electrode system. Both the systems have its advantages and disadvantages with portability, complexity and accuracy with measurements. It was observed that newly developed miniaturized nanofluidic device perform better with use of small volume (total device volume 800 μL) in comparison with complex device with large volume (5-6 ml).
- A new kind of nanofluidic device was fabricated on quartz with the help of photolithography and FIB milling. It was a successful device having nanochannel of 1 μm length, 100 nm width and 290 nm depths. Cell was separated and lysed to obtain its genetic material by the use of fabricated nanofluidic chip (Chapter 7).
- The fabricated NPA array was also used to grow demonstrate for the first time the growth of bacterial nanowires inside its nanopores. The grown nanowires were separated and their further applications were proposed (Chapter 8).

9.2. Recommendations and future directions

The mechanisms behind the affinity interaction of bio-analytes which changes the interface impedance is not well understood and need to be further studied. This knowledge will help to optimize designing biosensing devices with advanced performances. Most of recent publications present a brief theoretical model which supports their own experimental model and observations. There are no reports which present the studies of a particular impedance change with diverse probe/target arrangements and verify expected results. The impact of electrode size, shape and essential measurement frequency range with precision mainly depends on the target molecules and instrumentation. Optimizing these parameters may allow detection of smaller changes, which may lower the detection limit. A very limited number of reports are published in implementing nanopore arrays of affinity impedance sensors (Chapter 1 [22]). However, nanopore arrays are valuable for several reasons. The increased surface area by use of nanopores for the target molecules and availability of more affinity binding sites it also help to improve reproducibility and accuracy of the sensor. This increased affinity and reproducibility will be advantageous for diagnosis, reduced cost and sample volume per data point.

After a long period of research and development there is no any biosensor available commercially, based on label-free affinity impedance biosensing. To achieve that goal, progress on reducing the sample volume and optimize existing affinity impedance biosensors is still required. As demonstrated, the greatest challenges are in optimizing the biological side (affinity step), and others are on the physical side (measurements methods). Nonetheless all need to be solved to improve entire system.

Future research in electrochemical label-free affinity biosensors should aim for better applications. The reduction of cost, size with low power consumption along with simplified sample preparation is very important for use of these types of devices. The work described in this thesis could be expanded in many ways. A small amount of significant research has been done due to the nascent field of impedance biosensors. The observation shows that changes in the impedance can indicate target binding and sample surface morphology are responsible for any changes in the sensing ability of the device. It would be interesting to study whether constant sample surface changes actually derive from target molecules with the minimum potential of the electrical double layer capacitance as it is have hypothesized in the chapters. If so, impedance may be used to detect surface changes on the sample as the ionic strength can be high during the measurement.

It is also important to understand that system can be engineered to enhance the changes measured and hence improve the detection limit. With the use of advanced electrical measurement devices, the causes of impedance change can be observed more clearly and it would improve limits of detection. At very small sensor sizes, the target binding may be detected more precisely. It would be interesting to consider electrode scaling in more detail and processing sensor data to eliminate false signals is a challenging area that merits further research effort.